U.S. DEPARTMENT OF COMMERCE
National Institute of Standards and Technology
(formerly National Bureau of Standards)

NIST Special Publication 755

The Design and Construction of a State-of-the-Art High Temperature Tribometer

Jeffrey P. Yellets, Stephen M. Hsu, and E. Erwin Klaus
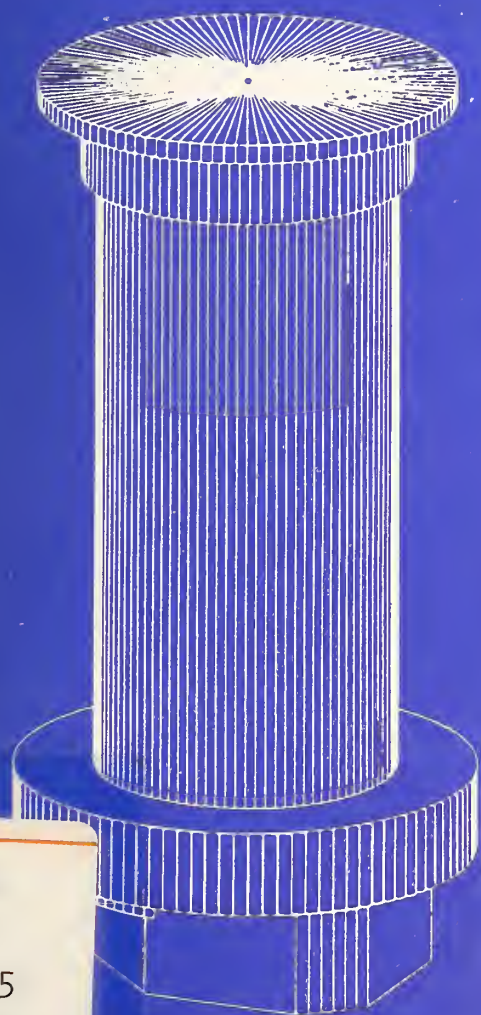
DOE ECUT Tribology Program

NIST Special Publication 755

The Design and Construction of a State-of-the-Art High Temperature Tribometer

Jeffrey P. Yellets and Stephen M. Hsu

Ceramics Division
Institute for Materials Science and Engineering
National Institute of Standards and Technology
(formerly National Bureau of Standards)
Gaithersburg, MD 20899

E. Erwin Klaus

Department of Chemical Engineering
The Pennsylvania State University
University Park, PA 16802

NOTE: As of 23 August 1988, the National Bureau of Standards (NBS) became the National Institute of Standards and Technology (NIST) when President Reagan signed into law the Omnibus Trade and Competitiveness Act.

September 1988

FOREWORD

This report is born out of a cooperative effort between the Chemical Engineering Department, at Pennsylvania State University (PSU), the Tribology Group of the National Bureau of Standards, and the partial support of the DOE ECUT Tribology Program. For years, the NBS has encouraged and sponsored graduate cooperative programs in which promising young scientists (some of them NBS staff members) come to NBS to conduct research, part of which often becomes the graduate's thesis. While it is not the objective of NBS to teach and train graduate students, such a program often furthers NBS programmatic goals by attracting high caliber scientists working on areas where NBS mission lies. Many excellent research papers have results and many students, upon graduation, have chosen to stay at NBS to continue their research careers. Such programs also draw many first rate university professors to NBS through the participation of these students in NBS research programs and projects, thus fostering NBS-university interactions and enhancing the scientific caliber of the work and reputation at NBS and the participating university. At the same time, through the frequent contacts that NBS has with industries, a natural university/government lab/industry relationship evolves, bringing a team focus on many research projects of significant economic and/or technological impacts.

In 1984, primarily through the interactions of Dr. Stephen M. Hsu of NBS and Professors Elmer Klaus and Larry Duda of PSU, a cooperative program in Tribology was started. Three graduate students: Mr. Richard Gates (a NBS staff member), Mr. Jeffrey Yellets, and Mr. Douglas Deckman were enrolled at the Chemical Engineering Department at PSU. Three reports have been prepared to describe the fruit of their relentless efforts in the last three years. These studies were conducted at NBS under the guidance of Dr. Stephen Hsu with the close participation of Prof. Elmer Klaus who visited NBS frequently.

Dr. James Eberhardt, Mrs. Terry Levinson, and Mr. David Mello of the DOE ECUT Tribology Program have at the same time sponsored a major Tribology program at NBS. That program also benefited from the studies conducted by Mr. Gates, Mr. Yellets, and Mr. Deckman. These students, while not working on sponsored projects directly, enabled NBS to explore some high risk, high pay off projects parallel to ECUT projects. When appropriate, the students were supported by ECUT for some time. To this, we gratefully acknowledge the generous support of DOE ECUT, without whose support many ideas would not be explored.

Stephen M. Hsu
Chief, Ceramics Division

ABSTRACT

High temperature ceramic tribology is one of the fastest growing and least understood areas in tribology. The need to understand the mechanisms of friction and wear for ceramic materials is critical. Ceramic materials are being utilized in tool development, bearing design, materials development for low-heat-rejection diesels, automotive gas turbines, Stirling engines, and aerospace applications. The development of a ceramics industry capable of manufacturing high technology wear resistant ceramics is essential in the United States, for if we do not develop such an industry, we will lose a substantial market to an already rapidly growing foreign technology.

This effort describes the design, development, and construction of a unique, state-of-the-art, high temperature tribometer for the mechanistic study of novel ceramic materials. An overview of ceramic tribology is included in this work as well as a review of many common wear test configurations. The final designs and the construction of the High Temperature Wear Facility is presented in this work. Recommendations for future work on high temperature wear mechanisms of ceramic materials and the tribological testing of such materials are presented at the conclusion of this work.

TABLE OF CONTENTS

Page

LIST OF TABLES

LIST OF FIGURES

LIST OF FIGURES (continued)

LIST OF FIGURES (continued)

LIST OF FIGURES (continued)

Chapter 1

INTRODUCTION

Ceramic materials are some of the oldest and most widely used man-made materials known. Evidence suggests that the use of ceramic pottery wheels began over 5000 years ago in the Near East.[1] The first tribological problems were found in the use of bitumen to lubricate potters wheels around 3250 ± 250 B.C. at Ur of the Chaldees.[2] Perhaps the earliest recorded tribologist, an Egyptian slave pouring water in front of a stone sledge that was transporting a statue of Ti (C. 2400 B.C.), was obviously intimately concerned with the friction of stone on stone.[3]

Recently, man is entering a new stage of materials development, the new stone age -- the age of advanced ceramics. These materials are currently being explored for use in a number of tribological applications.

It has been estimated that in the U.S. alone, advanced ceramic projects could add 6 billion dollars per year to the economy in 1990, 11 billion dollars in 1995, and 20 billion dollars in the year 2000.[4] If we assume linear industry growth in the periods 1990-1995 and 1995-2000 consecutively, over 135 billion dollars may be added to our economy in the coming decade. In addition to this boost to our economy, it is estimated that, in the year 2000, if we have developed wear and heat resistant ceramic materials we will save per year 1.5 billion dollars due to decrease in fuel consumption, 300 million

annually due to a reduction in maintenance costs, 530 million dollars due to tool life increase and improved machining when ceramic tools are developed, and greater than one billion dollars due to the use of ceramic related materials in integrated optics.[5]

On the other hand, the impact of <u>not</u> having a United States advanced ceramics program is great. In just the United States transportation sector in 1985, more than 8.1 million cars and 3.5 million trucks were built. Between now and 1995, 11,000 to 12,000 aircraft engines will be built.[6] If a foreign competitor was to dominate the development of a more economical and fuel efficient ceramic engine, the U.S. based transportation industry might be at a great competitive and monetary disadvantage.

Since the advanced ceramic industry seems to be an industry that <u>will</u> be developed, tribologists, scientists, or researchers should ascertain the barriers that need to be overcome in the development of the U.S. ceramics program. Many of these properties relate to tribology. According to the 1984 assessment report by the Charles River Associates, some of these barriers are standardized testing techniques, understanding and modeling of fracture behavior and time dependent properties, standard reference materials, surface and bulk chemistry, defect chemistry, and thermodynamic analysis.[7]

This report describes the systematic design and development of a state-of-the-art high temperature wear tester, the High Temperature Wear Facility. This apparatus is designed to measure friction and wear of ceramic materials at high temperatures under an

environmentally controlled condition to understand the mechanisms of wear of ceramics.

The need for such a high temperature wear tester is supported by an overview of the ceramic tribology literature. This gives guidance to the initial wear test configuration, temperature limit, speed limit, contact pressure, and environmental conditions. A review of wear test configurations also has been conducted (see Appendix A for more details) to help the initial choices.

Because of the very high temperature limits involved with ceramics, key technical challenges exist: 1) Heat Transfer, 2) Fluid Dynamics, 3) Materials Science, and 4) Mechanical and Thermo-Mechanical Design of Components. Sections on each of these areas and the final design and construction of the High Temperature Wear Facility are presented.

Chapter 2

A LITERATURE REVIEW OF CERAMIC TRIBOLOGY

2.1 Introduction

In recent years, many articles on ceramic tribology have appeared. Unfortunately, a complete tribological database does not exist. A literature survey is conducted here to: 1) assess the current status of ceramic tribology information, 2) give a broad-based information database on pre-test and post-test analysis of ceramic tribological testing, 3) establish an information base for future work, and 4) pin-point areas where improvement in methods and data analysis may improve the useability and comparability of test methods in ceramic tribology.

Since there are many potential applications for ceramics in heat engines, turbines, bearings, machine tools, etc., the review is divided into the following areas:

1)   Bearing Studies

2)   Engine Studies

3)   Tool Studies

4)   Grinding, Polishing, and Other Studies

5)   Ceramic Lubrication

6)   Conclusions

2.2 An Overview of Ceramic Tribological Literature

2.2.1 Bearing Studies

In ceramic tribology, one of the most critical applications is
the use of ceramics as bearing materials particularly rolling element
bearings. In one of the earlier studies by Sibley and Allen,[8] in
1962, a number of different ceramic materials were studied in order to
find a suitable material for high temperature bearing and seal
applications. To do this, sliding tests were conducted and several
interesting results were found. First, it was noted that thermal
streaking and hot spots occurred within the wear contact and that, in
general, the abundance of "hot spot" behavior increased the wear of
the test specimens.[9] Second, it was noted that there appeared to be a
correlation between high friction and high wear of ceramic materials
and that the formation of surface films may indeed affect the
frictional behavior of the material.[10] In a study published the
following year, Taylor, Sibley, and Lawrence[11] studied a ceramic
rolling bearing contact for three materials -- alumina, silicon
carbide, and titanium carbide. In this study it was shown that for a
standard bearing configuration, the elimination of vibration (even at
the expense of greatly increasing the load) could increase the life of
the bearing. It was also noted that superficial pitting and grain
removal occurred on the outer race of the bearing possibly indicating
that high surface stresses caused a structural breakdown of the
surface material.[12] Baughman and Bamberger[13] also studied ceramic

bearings and they found that the loss of geometrical integrity due to
wear, plastic deformation, or catastrophic cracking could cause
failure of high temperature ceramic bearings. Other more recent
studies have been conducted.[14-23] Among these, Dalal, Chiu, and
Rabinowicz[14] found that for a silicon nitride ceramic, surface cracks
seem to be responsible for spall formation at high stress levels, and
Lucek, Sibley, and Rosenleib[19] found that for silicon nitride balls,
if the surface defects could be blunted, a much better tribological
material could be obtained.

For quick reference, a list of experimental conditions and
conclusions of references [8] to [23] is given in Table 1.

From the studies done in ceramic tribological bearing testing,
several fundamental principles for the testing of ceramic materials
emerge. First, in the design of ceramic components, extreme care
should be taken in bearing configuration and design. A well designed
metal bearing may perhaps become a poorly designed ceramic bearing if
the same design is followed. Differential thermal expansion between
the ceramic bearing and metal surrounding components may cause
vibration of the bearing system. A sharp edge on a ceramic ball
bearing cage may cause extremely high surface stresses in ceramic
components. This may cause failure of the bearing system. In eight
of the thirteen studies presented, major problems were attributed to
inadequate bearing design parameters.[11,13,15,18,20-23] These problems
ranged from vibrations occurring due to inadequate design[11], to poor
mounting of the inner raceway.[20] Therefore, to design a more
effective ceramic bearing tribological test, special care should be

Table 1

Bearing Studies: A Summary of Conditions

Ref.	Speed	Load/Pressure	Temp. (°C)	Sliding/Rolling
8	3000-6100 (cm/sec)	$3.4 \times 10^4 - 3.4 \times 10^5$ Pa	500-1000	Sliding
11	27 cm/sec 5300 rpm	to 2.4N 2.5×10^9 Pa	to 800 500	Sliding Rolling
13	25,000 stress	to 2.5×10^9 Pa	to 700	Rolling
14	to 3300 rpm	to 4.7×10^8 Pa	no control	Rolling
16	1500 rpm	100N	500	Rolling
17	24,000 rpm	10N	no control	Rolling
18	to 1×10^5 cm/sec	to 780N	to 500	Rolling
19	10,000 rpm	2.7×10^9 Pa	538	Rolling
20	to 41,200 rpm	not reported	to 370	Rolling
21	10,000 rpm	2.7×10^9 Pa	538	Rolling
22	10,000-55,000 rpm	110 and 445N	to 540	Rolling
23	2000 rpm	1.9×10^9 Pa	to 800	Rolling

Table 1 (continued)

Ref.		Major Conclusions Drawn
8	1.	Thermal spots occurred in wear contact affecting wear properties.
	2.	High friction may correlate with high wear in ceramic materials.
11	1.	Elimination of bearing vibration is critical to bearing life.
	2.	High surface stresses may cause ceramic surface structural breakdown.
13	1.	Failure is due to loss of geometrical integrity.
	2.	Wear may occur by plastic deformation or catastrophic cracking.
14	1.	The structural strength of ceramic was inadequate for the bearing design and imposed loads.
16	1.	Lubricants are ineffective at test conditions used.
	2.	"Ceramic" and HP-Si_3N_4 rated poorly under large loads.
17	1.	Damage on bearing races is due to TiC particles spalling off ball.
18	1.	Properties that are important for making Si_3N_4 a viable bearing component are low elastic modulus and low density (compared to steel).
19	1.	If oxidation film can be formed and ground off, a better Si_3N_4 ball bearing with "blunted" surface defects would result.
20	1.	Primary cause of failure was due to inner race mounting inadequacy.
21	1.	Optical and SEM microscopy detected microfissuring of Si_3N_4 surface.
	2.	Extreme care must be taken in bearing and race design.
22	1.	The following factors contributed to bearing failure: a) inadequate diametrical clearance, b) thermal gradients, c) poor housing design, d) solid lubricant removal, and e) inadequate cage dampening & piloting.
23	1.	The ball retainer needs further attention in strengthening high temperature materials and reducing friction at ring lands.

taken to assure that the bearing fails due to a limitation in the ceramic bearing material and not due to poor engineering design of the ceramic components. This requires that special attention be given to seemingly trivial design parameters, but in the end, more meaningful data will result.

Second, in the testing of ceramic materials, particular attention should be given to the surfaces of the ceramic tribological components, because the surfaces are vital parts of the tribo-system. Questions like "Did I perform a process in the preparation of the component that might give rise to unusually high surface stresses?" and "Has the surface in some way altered itself such that a layer of material at the surface may have different properties from that of the bulk?" need to be asked. In the studies noted above, many of the wearing processes were thought to be initiated from high surface stresses acting at or just below the tribo-surface. In fact, the maximum shear stress in the region of a tribo-contact is often below the surface. Therefore, concern with surface and subsurface defects, inclusions, machining defects, bulk and surface porosity, and residual stresses caused by machining or processing techniques is necessary.

2.2.2 Engine Studies

Several articles dealing with the development of ceramic materials for high temperature, low-heat-rejection engine usage have been written in recent years. Unfortunately, much of the information

relating to heat engine studies is not readily accessible nor easily understood. This is true for several reasons.

First, in studies dealing with high temperature engine materials, much of the information that is discovered is proprietary and therefore not available to the general scientific community. This produces many localized databases of quantifiable information which is not accessible to the research community.

Second, it is extremely difficult to identify and measure tribologically important parameters in a ceramic engine test. For instance, what are the contact pressures of a ring on a cylinder over the stroke length? What are the velocities and accelerations along the stroke length? What are the bulk temperatures in the ceramic components along the stroke length? What are the surface temperatures along the stroke length? Is "hot-spot" behavior important in the system? These questions are not easily addressed and answers are not readily available. Therefore, interpretation of heat engine test data needs to be done carefully.

In the Highway Vehicle Systems Contractor's Coordination Meeting,[24] R. N. Katz of the Army Materials Research Center points out that the processing of ceramic materials can greatly affect their strengths. He found that for silicon nitride rotors, the sintering of the ceramic part had to be carefully compacted and sintered and that a full-density ceramic component was essential. This meant that 1) hot isostatic pressing (HIPing) should be done, 2) nitrogen over-pressures were to be used in the sintering, 3) additives which promote diffusion were to be used, or 4) the starting powder size distribution had to be

carefully controlled.[25] This problem of the careful fabrication and design of ceramic components needs to be implemented if ceramic tribological testing is to be effective. In this case, special processing techniques had to be implemented to insure that a fully dense ceramic component was produced. Katz also found that thermal cycling can greatly affect the mechanical [and perhaps the tribo-mechanical] properties of silicon nitride rotors, and under these conditions, strengths may decrease by as much as 40%.[26]

Recently, two reviews of ceramic tribology in engine development were written. George M. Thur gives a review of the Department of Energy's Heat Engine Program."[27] This review gives special insight into the wide range of national impacts of a successful low-heat-rejection engine program. Second, D. J. Godfrey, in the July 1983 issue of Materials and Design, assesses the use of silicon carbide, silicon nitride, partially stabilized zirconia, SiAlON, and SiON as candidate materials in low-heat-rejection engine design.[28]

Several studies have been conducted recently. Details and major conclusions of these studies are given in Table 2.[29-36] From these studies, three major materials emerge as potential candidates for heat engine materials. These ceramics are partially stabilized zirconia, silicon carbide, and silicon nitride. In 1982, Woods and Oda[29] looked at partially-stabilized zirconia (PSZ) for engine components. They discovered that PSZ could be useful because it has a low thermal conductivity (good insulating properties), a high coefficient of thermal expansion (which matches to metals better than some ceramics),

Table 2

A Summary of Heat Engine Studies

Ref.	Author	Organization	Material(s) Used
29	Woods	Cummins Engine Co.	Partially stabilized zirconia
30	Hannink	CSIRO Materials	Mg-partially stabilized zirconia
31	Storm	Carborundum Co.	Silicon carbide
32	Marmach	Nilsen Sintered Products	Mg-partially stabilized zirconia
33	Bryzik	U.S. Army TACOM	Partially stabilized zirconia
34	Timoney	Univ. College Dublin	Silicon carbide
35	Edwards	Sir W.G. Armstrong Whitworth and Co.	PSZ/ceramic
36	Radanovic	Cummins Engine Co.	Silicon nitride, chromium carbide

Table 2 (continued)

Ref.	Major Conclusions Drawn
29	1. PSZ is a good material because of its low thermal conductivity.
30	1. Mg-PSZ's show a wide degree of variability in many applications. 2. Mg-PSZ's properties can be tailored to many specific applications.
31	1. The attachment of the ceramic to the metal part is important. 2. Design stress analysis and interaction with manufacturers is important.
32	1. Mg-PSZ posses unique properties that make it suitable as wear resistant components for adiabatic engine applications.
33	1. The work showed dramatic results including the world's best fuel economy.
34	1. On high temperature wearing of SiC, friction is low due to either a graphite film or gas film lubrication. attachment.
35	1. A swing beam 2-Stroke diesel engine may be feasible for adiabatic diesel engine applications.
36	1. A minimum cooled engine could run as long as 1500 hours with minimum oil consumption.

and yet retains good thermal shock properties. In 1983, Timoney and Flynn explored the use of silicon carbide as "adiabatic" diesel engine components.[34] In that same year, Storm, McBeth, and Flynn found that silicon carbide components could be operated in an adiabatic diesel engine.[31] In that study, a silicon carbide rotor was 1) subjected to 800°C and 110,000 rpm, 2) mounted in a test stand for 40 hours, and then 3) put into a diesel engine tested in road service for over 8000 miles. Radovanovic, Kamo, and Dufrane explored silicon nitride as a material for high temperature engine components.[36] Also, silicon nitride already performs well as a high temperature bearing material[18,19,21,22] and therefore, it would be a primary candidate for high temperature bearings in an adiabatic diesel engine.

To conclude this brief overview of high temperature engine testing, a missing common denominator in high temperature engine testing should be examined. No laboratory simulation that effectively measures friction and wear under simulated engine conditions exists. Each of the programs referenced ran tests in different engines under different speeds, loads, environments, and temperatures, thus making results difficult to compare. Furthermore, such a wide variety of tests would not easily lend itself to a general understanding of the basic mechanisms of wear of ceramic tribological components. Therefore, it is necessary to have a high temperature tribometer that can test ceramic materials under 1) high bulk temperatures, 2) controlled atmospheres, 3) controlled loads, and 4) have the capability inherent in the design to perform mechanistic studies as well as engine simulations. Such a laboratory simulation would

further the understanding of the tribological properties of ceramic materials as candidates for low-heat-rejection engines.

2.2.3 Tool Studies

Several studies have been conducted in which ceramic materials have been used as machining and tooling materials.[37-42] Table 3 gives a summary of test conditions for these references. Bayoumi, Bailey, and Stewart[37] studied cemented carbide ceramics for use in wood machining. They found that, in the machining of materials under wet conditions, tool wear occurs by mechano-chemical removal of the binder material. Enomoto and Fujise[39] studied alumina cutting tools using cathodo-luminescence and observed that the tool tip changed both composition and structure when machining iron. Young, Becker, and Rhee[41] in 1983, studied drills coated with TiN and TiC/TiN and found that wear in their system greatly depended on how the coating was applied (i.e., Physical Vapor Deposition versus Chemical Vapor Deposition, etc.).

All of the above cited references reinforce the issue that wear of ceramics is not merely a mechanical effect, but may also include both chemical effects and tribo-chemical effects. Thus, in the design of a ceramic tribological test series, special attention to the possibility of complex chemical and tribo-chemical interactions which take place at surfaces, material-material interfaces, and solid-liquid interfaces in a tribological system need to be considered. Although tribologists know this, models which incorporate chemical,

Table 3

Tool Studies: A Summary of Parameters

Ref.	Author	Tool Speed	Feed Rate or Load	Materials Used
37	Bayoumi	42.4 m/sec	45N	A B
38	Dixon	183 m/sec (353 rpm)	0.3175 mm/rev	A B
39	Enomoto	1.5 - 1.8 m/sec	0.101 mm/rev	C
40	Chattopadhyay	1.25×10^{-3} - 5.83×10^{-3} m/sec	0.25 mm/rev	A C D E F
41	Young	1412 (rpm)	0.191 mm/rev	D F G
42	Gane	1.2 - 3.3 m/sec	0.28 mm/rev	A C H I

Key[+]

A = WC
B = (Ti, Ta, W) C
C = Al_2O_3
D = TiC
E = ZrO_2
F = Ti(CN)
G = TiN
H = Cubic BN
I = SiAlON

[+]Includes all forms and compositions of referenced material (i.e., no distinction is made between 99.5% Al_2O_3 or 85% Al_2O_3).

environmental, and mechanical effects are difficult to develop.
However, when we begin to understand these effects more fully, such
modelling will lead to a greater understanding of friction and wear in
ceramic tribological systems.

2.2.4 Grinding, Polishing, and Other Studies

Many studies have been conducted in the study of the friction and
wear of materials which find use in the grinding and polishing
industry.[43-48] Karaki and Watanabe[43] looked at zirconia as an
abrasive for the mechano-chemical polishing of crystals used in the
electronic industry, and they found that mechano-chemical polishing
can increase material removal rates several fold over chemical etching
or mechanical polishing. Komanduri, Laverty, and Shaw[44] studied
ceramic abrasives for a simulated hot grinding technique. In this
technique, either alumina or silicon carbide abrasives were used in a
grinding process at temperatures to 1000°C. Suzuki and Sugita[46]
studied polishing of MgO crystals while lubricating with water and
using a vibratory motion. They found that during the test, the pH of
the water rose because $Mg(OH)_2$ was being generated.

Other interesting studies done[49-53] include a study done by Uhrig
and Waubke[49] in which an investigation was conducted to explore the
wearing properties of a ceramic flooring material. Wallbridge and
Dowson[50] studied an alumina ceramic as a potential replacement for a
prosthetic hip joint. They found that only a marginal increase in
life was gained by using this material over other materials.

2.2.5 Ceramic Lubrication

No review of ceramic tribology would be complete without an inspection of the methods of ceramic lubrication. Traditionally, lubrication of materials for low temperature purposes has been achieved by the use of a formulated liquid lubricant package and a precisely machined bearing and lubrication system. At intermediate temperatures, more sophisticated synthetic liquid lubricants are used and sophisticated bearing lubrication systems are employed such as 1) lubricant atomization, 2) lubricant cooling and filtering, and 3) lubricant pumping.

However, at high temperatures, the above methods fail because: 1) the oxidation stability of the lubricant used is poor in high temperature oxidative environments, 2) liquid lubricant vaporization tends to cause many problems in bearing systems, 3) thermal degradation of lubricants is rapid at high temperatures, and 4) sludge formation due to increased oxidation and thermal degradation causes an increase in system wear and shortens system life.

If, however, a lubricant can be continuously replenished at a steady state level, a lubricating film can be maintained. Vapor phase deposition of lubricants is a technique which seeks to replenish a lubricant film at a steady state level. This technique shows promise and will be discussed in the following sections. However, important lubricant-ceramic chemical interactions are unknown for high temperature ceramic systems. Many of the ceramic materials may or may

not be reactive to conventional lubricants at elevated temperatures. Because of all of the above problems for ceramic lubrication at high temperatures, different approaches are being taken to solve this problem. Current efforts are divided into two major categories: 1) Solid and "self" lubrication and 2) Other techniques for ceramic lubrication.

2.2.5.1 Solid Lubrication

Solid lubrication of metals is an area that has been studied extensively for high temperature aerospace bearing studies. Recently, solid lubricants are being studied for use in high temperature engines. An excellent review of solid lubrication was written in October 1982 by H. E. Sliney.[54] Sliney separates solid lubricants into four major classes: a) layer lattice solid lubricants, b) polyimides, c) unconventional solid lubricants, and d) hard coatings.[55] Table 4 gives a summary of the lubricants examined.

Many other articles have been written that relate to solid lubrication and self lubricating composites.[56-93] For solid lubrication, many technical challenges still exist. These challenges are to describe, formulate, and verify the mechanisms for solid lubrication at high temperatures for 1) a variety of lubricants, 2) a variety of materials, 3) a variety of environmental conditions, and 4) a variety of test conditions. Such mechanisms are difficult to understand. Thus, after 30 years of intensive solid lubrication

Table 4

A List of Materials Examined from H. E. Sliney's
"Solid Lubricant Materials for High Temperatures - A Review"[54]

Layer Lattice Solid Lubricants

1) MoS_2
2) WS_2
3) Graphite
4) Graphite Fluoride $(CF_z)_n$

Polyimides

1) Polyimide Coatings
2) Polyimide - Bonded Graphite Fluoride Coatings
3) Polyimide Composites

Unconventional Solid Lubricants

1) Bonded $PbO-SiO_2$
2) LiF
3) CaF_2
4) BaF_2
5) Fluoride Metal Composites plus Coatings
6) Fluoride-Oxide Composite Coatings

Hard Coatings

1) B_4C
2) TiC
3) SiC
4) Cr_3C_4
5) WC
6) Si_3N_4
7) TiN
8) Cr_2O_3

research, the fundamental mechanisms of solid lubrication are still not well understood and characterized at extreme temperatures.

Thus, in high temperature lubrication studies, there is a need for mechanistic studies. Perhaps these tests could be most effectively conducted at high bulk temperatures while minimizing the effects of frictional heating in the tribological contact junction.

2.2.5.2 Other Techniques

Several lubrication techniques other than solid lubrication are being explored for ceramic lubrication. A method that deserves note is the use of thin gas films to lubricate tribological contact junctions. Gas supported bearings have been used for many years. Moore, Brandon, and Smyly,[94] patented the design of an alumina ceramic, gas lubricated bearing. In 1980, Zacherl patented a gas bearing design for a ceramic rotor in a gas turbine engine or turbo-machine.[95]

Several advantages and disadvantages exist for a gas bearing design. First, a great advantage of lubricating a bearing using a thin gas film is that, if the bearing operates in an ideal fashion, tribological surfaces do not contact but a thin gas film maintains separation of the surfaces. However, problems could exist with gas bearing designs if 1) a stable and pure constant pressure gas supply is not maintained for a pressurized hydrostatic gas bearing, or 2) a certain speed and load regime is not maintained for a hydrodynamic gas bearing. Thus, designs of this type represent challenges in design

but opportunities if these designs can be perfected. For instance, hydrostatic 'assist' on a hydrodynamic bearing could improve greatly the performance of such a bearing.

A second, technique for high temperature lubrication of ceramic materials is the Chemical Vapor Phase Deposition of Lubricants. This technique, pioneered by Dr. E. E. Klaus of the Pennsylvania State University, involves 1) vaporizing a lubricant at relatively low temperatures in the presence of a carrier gas (which may or may not contain oxygen), and 2) contacting this carrier gas with a hot substrate. When the vaporized lubricant contacts the hot substrate, the lubricant oxidizes or thermally degrades forming a thin lubricant coating on the surface of a component. This coating then provides lubrication for a limited period of time and, if replenished at a steady state level, can provide continuous steady state lubrication.

This process is encouraging for high temperature tribology because it relies on the thermal degradation of a material. In 1974, Lai studied such a vapor phase lubrication system for stainless steel die casting.[96] Min, in 1980, conducted a limited study of vapor deposited films[97] while Pinto, in November 1982, studied high temperature vapor phase lubrication for organic liquid lubricants.[98] These studies show promising results for Chemical Vapor Phase Deposition of Lubricants as a method for high temperature lubrication of metals in low-heat-rejection engines. Feasibility of this concept on ceramic surfaces has not been demonstrated. Research in this area is continuing.

2.3   Summary/Conclusions

Tribology of ceramic materials is an interdisciplinary science involving materials science, physics, chemistry, and the engineering sciences. To fully understand ceramic tribology, engineers, materials scientists, ceramists, and tribologists need to work together to understand tribological processes in ceramic wear contacts. A first step towards that goal was to review the work done in the area of ceramic tribology, for in reviewing the work several conclusions can be made:

1. In many cases, materials parameters are not sufficiently described or reported. Therefore, effective comparisons between data sets simply cannot be made. For example, let's look at the aluminum oxide ceramic system. If a researcher reports that he is working with an "alumina" powder, question such as, "Is this alumina an alpha, chi, delta, eta, gamma, kappa, iota, theta, or xi alumina?"[99] might be asked. Furthermore, if it is reported that gamma alumina is used, is the gamma alumina really gamma alumina, eta alumina, delta alumina, or a mixture of chi and gamma alumina? Which conventions were used when samples were received? Was the conversion Alcoa's or was it Haber's? Was the convention British or French?[100]

Apart from general nomenclature challenges, commercial materials should be specified carefully. If a ceramic is reported as "company X's alumina" and a researcher wants to follow up on another's research, then the questions, "How was the processing done? What was

the purity of the alumina? What was done in finishing the components after fabrication? What batch number was used? Is that material still available?" can be asked. These questions require answers before a researcher can duplicate another's experiment.

In addition to the key parameters mentioned above, it is necessary to report materials parameters when working with ceramic materials. Charles F. Bersch, in "Properties of Ceramics for Structural and/or High Temperature Use: Need for Control, Measurement, and Compilation",[101] states that several parameters are needed to specify the mechanical properties of a ceramic.[102] These are given in Table 5. Furthermore, to describe the tribological properties of the ceramic material, the processes involved in machining of the ceramic surface are important. For instance, was grinding used, and was the surface subsequently polished or lapped? Are the surfaces stressed? Are there surface defects? If the above properties were reported, a better understanding and comparison of ceramic tribological tests could be realized.

2. In many cases throughout the tribological testing community, different loads, speeds, temperatures, and materials are tested. This variation in load, speed, temperature, and materials is to be expected. Every application is not the same. Every wear tester is not the same. However, within a data set, batch to batch variations in materials may cause problems in internal consistency. Thus, there is a need for a ceramic standard reference material. If experimenters were to compare their results relative to a given ceramic material an internally consistent data set might result. In addition to this, it

Table 5

Ceramic Mechanical Characterization Parameters

Conventional Characterization:

composition (1 percent level)
average grain size
density

Augmented Conventional Characterization:

crystalline and amorphous phases
grain shape
grain size distribution
degree of preferred orientation
distribution of porosity
surface roughness

Fine Microstructure and Other Characteristics:

trace impurities, amount and state of aggregation
dislocation concentration
twin concentration
point defect concentration
residual stresses
ambient atmosphere
radiation field
state of temper (glass)

would be convenient to have an industry wide standard wear reference material. If this material is characterized and tested as a reference material with ceramic test materials, a measure of consistency for external comparison can be attained.

3. Better temperature control and measurement systems are needed to effectively test ceramic materials. In many cases, contact temperatures far exceed bulk temperatures in the ceramic material. This factor alone may be critical to the wear of the ceramic material. J. E. Hines, Jr.,[103] reported that for an alumina based ceramic material in a "room temperature" test, a phase transformation of the wear tip to delta alumina occurred. This indicates that surface temperatures were 1100°C or higher.[104]

Two solutions exist to the above problem. First, it is necessary to develop adequate temperature modeling. Then, for a given ceramic material in a given configuration and subjected to certain loads and speeds, a reasonable prediction of the surface temperatures can be made. Second, if an apparatus could measure the surface temperature directly at high bulk temperatures and low frictional heating rates (i.e., low loads and/or speeds), then surface activities and reactivities of ceramics might be found. Finally, it would be useful to measure the temperature of the ceramic contact at low bulk temperatures taking into account the surface activities of ceramic materials as well as temperature differences between the contact and the bulk ceramic (i.e., differential expansion and thermal shock properties may be important).

4. Tribological testing of ceramic materials for use in engine applications has increased rapidly in recent years. Unfortunately, mechanisms of wear of ceramic materials in engine applications are not generally understood. Temperatures in an engine test are not easily measured or controlled and the engine tests themselves are usually very time consuming and expensive. Therefore, a technology gap exists in the area of heat engine technology. To bridge this gap, wear test facilities should be developed that can test ceramic materials at conditions in which high temperature mechanisms of friction and wear can be studied. This may require high temperatures and conditions which minimize frictional heating. As an added capability, it would be useful if such a facility had the capability for modification to simulate high temperature engine tests and to control, measure, and intentionally induce vibrational transients that may cause other modes of wear in ceramic systems.

Chapter 3

DETERMINATION OF DESIGN PARAMETERS AND SPECIFICATIONS

Ceramic tribological research is being conducted for ceramic bearing research, tool studies, low-heat-rejection engines, and several other critical wear processes. In designing a wear tester for ceramics, the end use applications should be considered. However, to design a wear tester that will be able to test all materials at all conditions of speed, load, temperature, atmosphere, and lubrication is impossible. In trying to design a tester that can operate under all loads, speeds, and temperatures, precision and sensitivity would be sacrificed. This tester might operate under a very wide range of conditions, but might produce high quality data only in a narrow range. This is not acceptable in wear tester design. For any apparatus, the researcher desires that the wear tester would:

- o   be as frictionally sensitive as possible so that low frictional levels might be detected.
- o   maintain contact alignment so that anomalous wear problems are not encountered.
- o   minimize machine vibrations so that anomalous friction and wear can be avoided.

Therefore, the major usage of the apparatus being designed as well as desirable secondary usages for the equipment should be

determined. Once these uses are determined, tester configuration, temperatures, loads, speeds, and environments for the primary and secondary applications can be specified.

The development of the design parameters and specifications for the High Temperature Wear Facility was approached accordingly. The purpose of this facility is to gain a basic understanding of the mechanisms of friction and wear of ceramic materials at high temperatures. This fundamental purpose spans a number of technical application areas such as ceramic materials for low-heat-rejection engines, tools, and advanced bearings. If a basic understanding of the mechanisms of friction and wear for a number of ceramic systems could be unraveled, then the design of materials which would minimize friction or wear in a given application would result. Furthermore, since many of the materials to be studied may be used as advanced heat engine materials, it is desirable to have the future capability to simulate motions which occur in a piston ring-cylinder liner contact or a cam and tappet contact. This would enable the tester to test research samples as well as to test leading ceramic candidates for engine applications. To summarize, the major purpose of the High Temperature Wear Facility is to effectively test ceramic materials for friction and wear in order to gain insight into the fundamental mechanisms of wear in ceramic-ceramic tribo-systems. A desirable future capability would be the ability to simulate conditions in which an advanced heat engine might operate.

3.1 Wear Test Configuration

The choice of wear test configuration is fundamental to wear tester design. Many wear test configurations are used throughout the tribological community, and each is designed for a specific application. Appendix A provides a careful analysis of several major wear test configurations. For a comprehensive review, ASLE[105] provides a summary of over 230 wear test devices.

For the High Temperature Wear Facility, a ball-on-disk configuration was chosen. This configuration is commonly used and is adaptable to a number of different specimens such as pin-on-disk, button-on-disk, pin-on-flat, and ball-on-flat without compromising geometric integrity.

3.2 Temperature Limit

To determine the temperature ranges that are necessary to study the mechanisms of wear of ceramic materials, the temperatures encountered in the wear testing of ceramic materials should be ascertained. Enomoto and Fujise,[106] in 1983, found in an alumina tool study with cathodo-luminescence that the tool tip temperature was nearly 1000°C for a room temperature test. Munro[107] found that temperatures in a four ball contact could be higher than 800°C for a sintered alumina material. Burton[108] found "red hot" hot spots in a "room temperature" steel wear test. Winer[109] found that in a 20°C bulk temperature system, flash temperatures could raise the

temperature for 8 μs up to 1100°C at asperity contacts. Earles,
Hayler, and Powell[110] found that surface temperatures could rise to
650°C in a room temperature test. In an advanced heat engine, we find
that temperatures at a thermal barrier pistons may be in excess of
800°C.[111] If we were to study what might happen in a tribological
contact junction at high temperatures, a tester that has temperature
capabilities of 1450-1500°C is desireable.

3.3 Environment and Lubrication

In order to examine the wear mechanisms of materials for advanced
heat engines, the capability to test these materials under similar
conditions is necessary. Usually, the material is tested in the
presence of oxygen and oxidative atmospheres. In addition, it is
necessary to operate such an apparatus under inert gases such as
argon, helium, or nitrogen to establish an oxidation baseline. For
future studies in which the effect of water vapor on the friction and
wear of ceramic materials is to be examined, the capability to
introduce water vapor into the system is required. To summarize, the
atmospheres which may be used are argon, helium, or nitrogen as an
inert, and oxygen, air, or a mixture of oxygen and an inert might be
used as a test atmosphere. It would also be convenient to be able to
introduce water vapor into the wear tester for future studies.

In lubrication, it would be desirable to have the capability to
perform solid and vapor phase lubrication studies at high
temperatures. Material-material and material-lubricant interactions

are important and should be studied. In vapor lubrication, the effectiveness of vapors on various materials combinations under a wide range of conditions should be investigated to prove concept feasibility. Current wear testers are not capable of operation under high temperatures and vapor lubrication conditions.

3.4 Speed Ranges

In the study of surface transformations and reactions which occur in high speed contacts, it is important to know accurately the surface temperature at the tribological contact. This may be approached in two ways.

The first approach is to run the system at any speed and to accurately measure the surface temperature in the tribological contact. In practice this is a difficult task to perform. If this approach is taken the questions "How will I measure temperature in the wear contact?", "What will I use?", and "How can I be sure that I am really measuring the temperatures in the contact?" arise.

The second approach in accurately determining the contact junction temperature is to minimize the effects of frictional heating. This requires very accurate, low speed control so that no appreciable frictional heat will be generated. In this way, the assurance that the contact temperature is very close to the bulk temperature of the ceramic material is possible. This approach will be taken with the High Temperature Wear Facility. With a 1750 rpm motor which has 100

rpm as a minimum speed, if 100:1 reduction in speed is used, then a speed range from 1 rpm to 17.5 rpm is accessible.

Conversely, if the apparatus is to be used for the secondary purpose of engine simulation, then much higher linear speeds are desired. For instance, operating with a ball on a two inch disk apparatus contacting at a radius of one inch, 1000 rpm would give a linear speed of 8.7 ft/sec. This is closer to cam and tappet speeds in an engine than 0.008 ft/sec (1 rpm) would be.

Therefore, the speed range is chosen to be 0 to 50 rpm with the capability of in the future of higher linear speeds.

3.5 Load Range

For mechanistic studies, the load range needs to be versatile. For chemical reaction/surface reaction studies at high temperatures, low loads are desirable. In this case, a 0-20 kg load range would be more than sufficient. For simulatory motions, the average Hertzian contact pressures need to be compared with piston ring/cylinder linear pressures and cam/tappet pressures. In a cam and tappet contact, the peak pressure is about 8×10^8 Pa.[112] In a piston ring/cylinder liner, a maximum pressure of 3.44×10^7 Pa for an engine operating at 136 bmep, 2200 rpm, and 2000-4000 psi cylinder pressure[113] is generated. If we take the very simple formula for Hertzian contact radius for a ball on a flat disk:

$$a = \left[\frac{3LR(1-\nu^2)}{2E} \right]^{1/3} \qquad [1]$$

where L = load (in N)

     R = radius of ball (in m)

     ν = Poisson's ratio for material under study

     E = modulus of elasticity (in N/m^2) (Pa)

     a = Hertzian contact radius (in m)

For alumina ceramic material, the modulus of elasticity is 393×10^9 Pa, and the Poisson's ratio is 0.21. Therefore for a ball radius of 6.35 mm (1/2" dia.) we have a Hertzian contact radius of (for a 10 kg load) $a = 9.113 \times 10^{-5}$ m. The mean Hertzian stress would be $98N/\pi(a^2)$ $= 3.7562 \times 10^9$ Pa. This is above the needed contact pressure by an order of magnitude. However, at high temperatures, Hertzian contact stresses may be less than those at low temperatures and larger loads may be necessary.

3.6 Summary of Specifications

Table 6 presents a summary of the design parameters and specifications for the High Temperature Wear Facility. Both needed and desired load ranges are given in the compilation.

In addition to the above, future modification for reciprocating motions should be possible for engine simulations.

Table 6

High Temperature Wear Facility Design Specifications

Design Target: Versatility

Configuration:	Ball-on-disk
Modification for:	Pin-on-disk Ball-on-flat Pin-on-flat
Temperature:	Ambient to 1500°C Control capabilities for room temperature to 1500°C.
Load:	0-40 kg (0-394.4N) Capability for modification to higher loads.
Atmosphere:	Oxygen Argon, Nitrogen, Helium Mixture of Argon, Oxygen, Nitrogen, or Helium Addition of Water Vapor
Lubrication:	Solid Lubrication Vapor Deposition of Lubricants
Motion:	Unidirectional Capability for modification to reciprocating motion.
Gas Flow Rates:	0-0.15 ℓ/min

3.7 Introduction to Design

A unique set of design and performance criteria exists for the High Temperature Wear Facility. Special care should be taken in materials selection because of the high temperature and loading requirements of the facility. For many materials, the high temperature strength capabilities are exceeded. These materials cannot be used. Oxidation and environmental control at high temperatures presents many unique design challenges. Sensitivity, precision, and accuracy of frictional measurements coupled with high temperature machine and contact alignment, vibration control, and provisions for lubrication further complicate already complex design issues.

Novel approaches to design are necessary because of the unique design specifications for the facility and the design challenges which accompany them. Key technical challenges occur in heat transfer of the system, materials selection for the facility, fluid dynamics, and mechanical design of components. Chapter 4 describes the challenges which occur with the heat transfer of the High Temperature Wear Facility Furnace. Chapter 5 examines materials selection for the facility, while Chapter 6 deals with fluid dynamics and the design of a frictionally sensitive, high temperature alignment system. Finally, Chapter 7 addresses several challenges which occur in the mechanical design of components to account for differential thermal expansion, design of a drive mechanism, and selection of materials for frame design.

Chapter 4

HEAT TRANSFER

The design of a system to accommodate 1500°C temperatures
presents several complex technical challenges. Conductive, convective
and radiative heat transfer should be accounted for because of the
extreme temperature testing. The basic heat transfer equations for
such a process are quite complex and are given below as

$$\frac{\partial}{\partial t} \rho U = - (\nabla \cdot \rho U v) - (V \cdot q) - p(\nabla \cdot v)$$

$$- (\tau : \nabla v) - (E - A) \qquad [2]$$

where t = time

ρ = density

U = internal energy per unit mass

v = mass average velocity

q = energy flux relative to mass average velocity

τ = viscous stress tensor

E = local rate of photon emission per unit volume

A = local rate of photon absorption per unit volume

and

$$\frac{\partial}{\partial t} U^{(r)} = -(\nabla \bullet q^{(r)}) + (E - A)$$ [3]

where $u^{(r)}$ = charge of radiant energy density

$q^{(r)}$ = radiant energy flux

The operator

$\nabla \bullet v$ is defined as the divergence of a vector field

$$\nabla \bullet v = \sum_i \sum_j \frac{\partial}{\partial x_i} v_j = \sum_i \frac{\partial v_i}{\partial x_i}$$ [4]

where v is a vector function of x_1, x_2, and x_3 and x_1, x_2, and x_3 are the spatial variables for a given coordinate system.

Similarly

$$\tau : \nabla v = \sum_i \sum_j \tau_{ij} \frac{\partial}{\partial x_j} v_i$$ [5]

where τ_{ij} are the components of the stress tensor field and x_j's are the space variables for a given coordinate system.

Such equations are difficult (at best) to solve. Therefore, a number of simplified heat transfer models should be systematically examined.

4.1   Heat Transfer Calculations

There are several different methods of heating a sample to very high temperatures.   One method would be to locate a "space heater" in near a ceramic test sample and to radiate energy directly to the surfaces of the specimens.   Initially, this type of heating was considered.   Figure 1 shows the general schematic of such a heating system for a ball-on-disk configuration.

In this system, radiative heat transfer to heat the surfaces of the wear test specimens is important.   Therefore, to determine the energy requirement necessary for such a system, the radiative heat transfer equation is used:

$$Q(\text{Energy/Time}) = \sigma(\epsilon_1 A_1 F_{12} T_1{}^4 - \epsilon_2 A_2 F_{21} T_2{}^4) \qquad [6]$$

where σ = Boltzmann's constant

ϵ_1 = Emissivity of specimen holder

ϵ_2 = Emissivity of chamber

A_1, A_2 = Respective surface areas

F_{12} = View factor from holder

F_{21} = View factor from chamber

T_1 = Temperature of holder
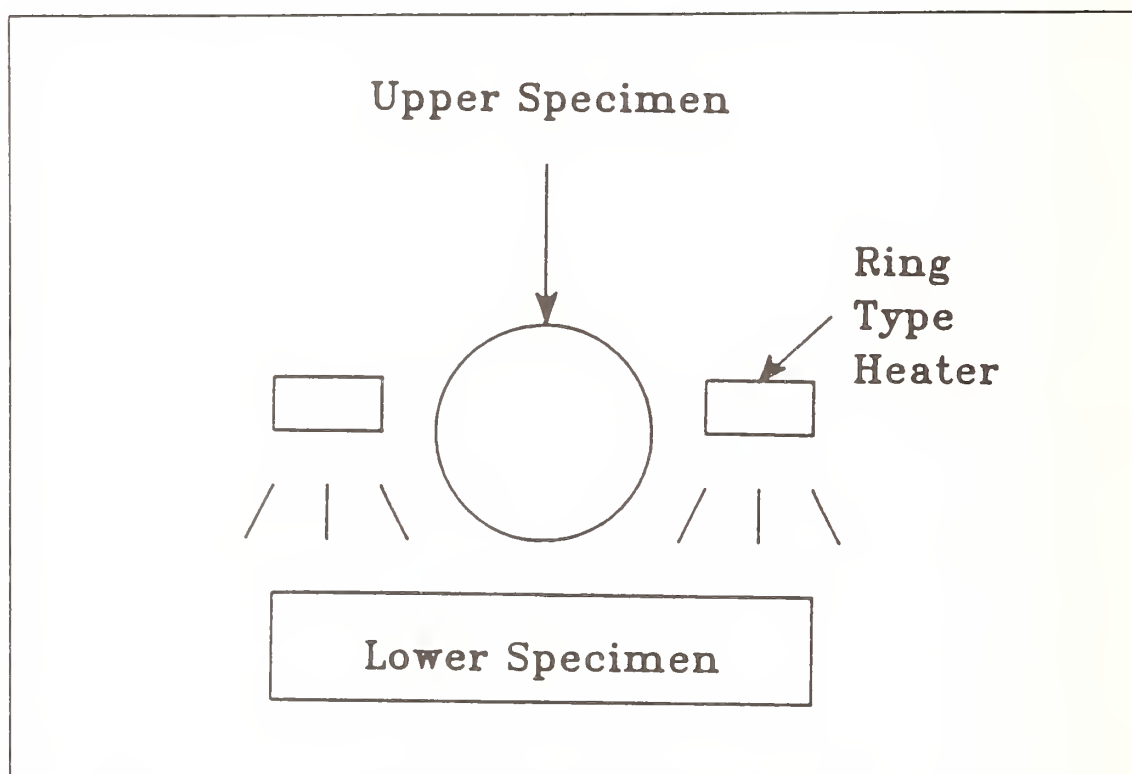
T_2 = Temperature of chamber

Figure 1. General Schematic of Space Heater System

Furthermore, assume total enclosure ($F_{12} = F_{21} = 1$), good radiators (ϵ_1, $\epsilon_2 = 0.8$), specimen temperature of 1500°C, and surrounding temperature of 20°C. If the area of a specimen is $A_1 = 155$ cm^2 (24 in^2), the heat needed to maintain the surface is approximately

$$Q = 6000 \text{ W/specimen}$$
$$\approx 23,679 \text{ BTU/hr/specimen} \qquad [7]$$

Assuming that the space heater used would be a common molybdenum disilicide space heater which has a heat flux density at 1500°C of 11.6 W/cm^2 (75 W/in^2), a surface area of 516 cm^2 (80 in^2) is needed to provide adequate heating. This is virtually impossible in a wear tester, because samples need to be in close proximity.

Furthermore, to complicate this problem, large thermal stresses would be caused in this system because of very large thermal gradients in the low conductivity ceramic materials. If this type of system were used, thermal shocking of both specimens and sample holders might occur.

Therefore, an alternate approach to heating the High Temperature Wear Facility is considered. A logical choice would be to heat the whole specimen holder and chamber to 1500°C and to maintain the temperature at this limit. The major technical challenge in this type of design is the thermal insulation of the heated chamber. To obtain a rough idea of what would be necessary for thermal insulation of such a system, the following assumptions are made:

o   cubic heating chamber with dimensions 15.2 cm x 15.2 cm x

15.2 cm (6" x 6" x 6")

o   6 heaters, 161 cm² (25 in²) each

o   heaters can supply 11.6 W/cm² (75 W/in²)

Figure 2 gives a general schematic of radiation heat shielding

necessary for this design.

Assuming that the heat stages are close together and the area of

each stage is approximately constant, the radiative heat transfer

equation reduces to:

$$Q_{heater} = \epsilon\sigma A(T_1{}^4 - T_2{}^4) \qquad\qquad [8]$$

If the radiation shields are blackbodies themselves, $\epsilon = 1$, and

$$T_2 = \sqrt[4]{T_1{}^4 - A/\sigma A} \qquad\qquad [9]$$

If:

$$T_{wall} = 1500°C \qquad\qquad [10]$$

A = 216 in² (4 walls)

Q = 75 W/in² x 100 in² (4 walls)

the following temperatures for each radiation stage result:
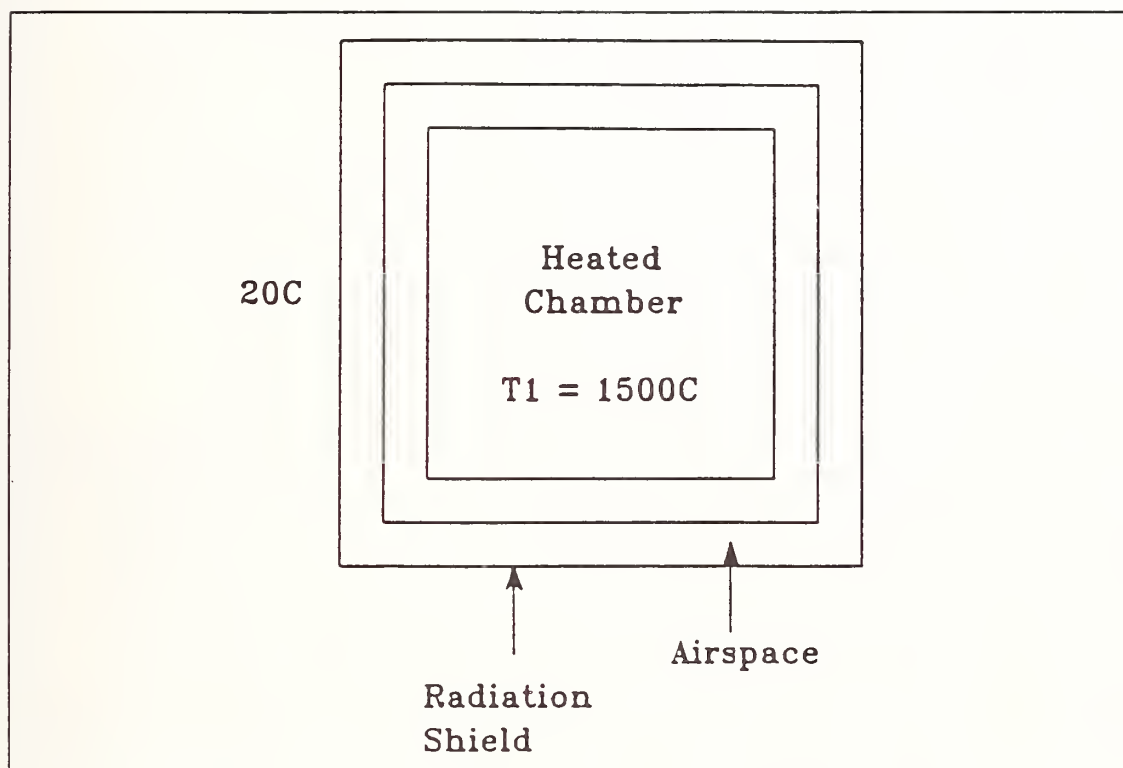
Figure 2.   Heat Staging Scheme

T (chamber wall) = 1500°C

Stage 1   = 1455°C

Stage 2   = 1407°C

Stage 3   = 1356°C

Stage 4   = 1297°C

Stage 5   = 1232°C

Stage 6   = 1157°C

Stage 7   = 1068°C

Stage 8   = 957°C

Stage 9   = 803°C

Stage 10   = 531°C

If 500°C is the maximum allowed attachment point temperature for a metal to ceramic interface, a minimum of 10 heat stages is needed. This is too many stages for conventional staging.

Another approach to insulation was considered. If a porous ceramic material were used for insulation, a greater heat insulation would result due to multiple radiation shielding by the many pores in the material. One side of the pore can radiate to the other thus making each pore a radiation shield. This is illustrated in Figure 3.

If the pores are small in such a material, then many radiation stages may be supplied per unit thickness of material. Such a material will maximize structural strength and insulation capacity.

A configuration for the calculation needs to be specified. Top and side views of the original high temperature wear facility furnace
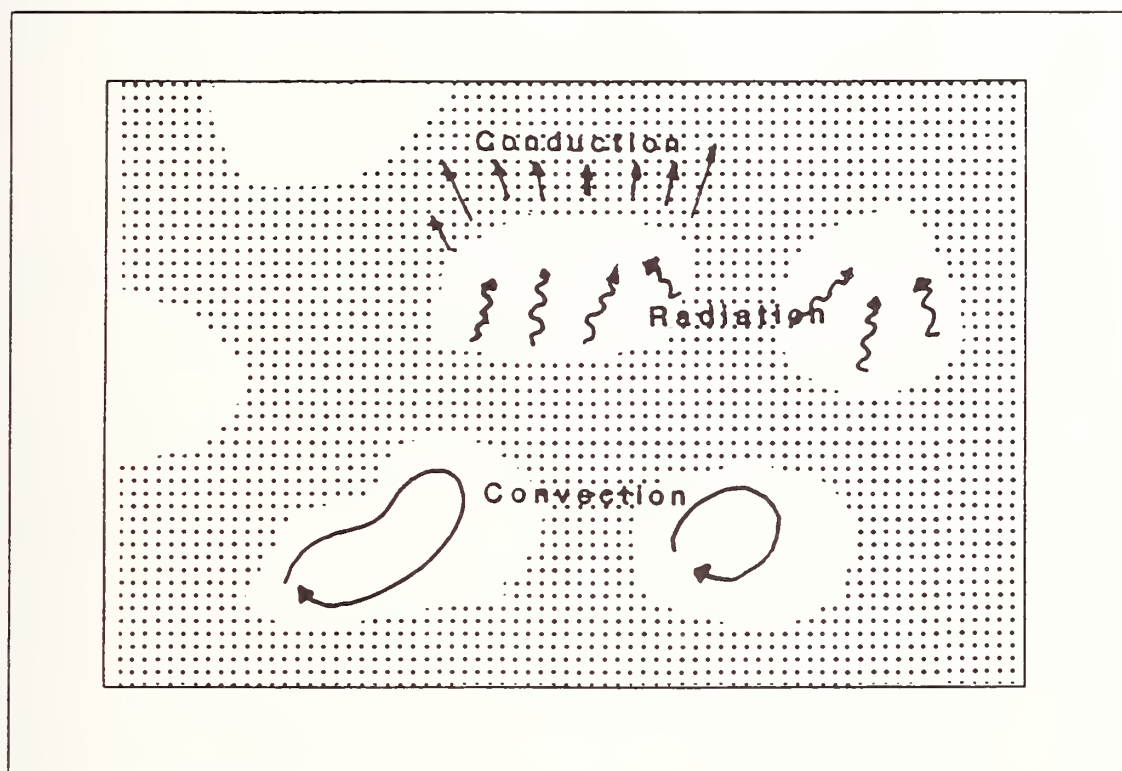
Figure 3.   Porous Insulators as Radiation Shields

design are given in Figures 4 and 5. If we assume uniform heat flux in the angular (θ) direction, the steady state energy transport becomes:

$$\frac{1}{r} \frac{\partial(rq_r)}{\partial r} + \frac{\partial(q_z)}{\partial z} = 0 \tag{11}$$

where $q_z = - keff\ \partial T/\partial z$

$q_r = - keff\ \partial T/\partial r$

k_{eff} = effective combined thermal conductivity taking into account conduction, convection, and radiation throughout the insulation material under examination.

$$k_{eff} = k_{eff}(T). \tag{12}$$

and

$$T = T(r,z) \tag{13}$$

To summarize, we have a 2-dimensional, cylindrical, steady state heat transfer equation with a temperature dependent thermal conductivity (keff).

Boundary conditions may now be specified for the system. Since we have specified that no θ variations in heat flux, the smallest symmetric element can be extracted from the furnace. This is shown in Figure 6.
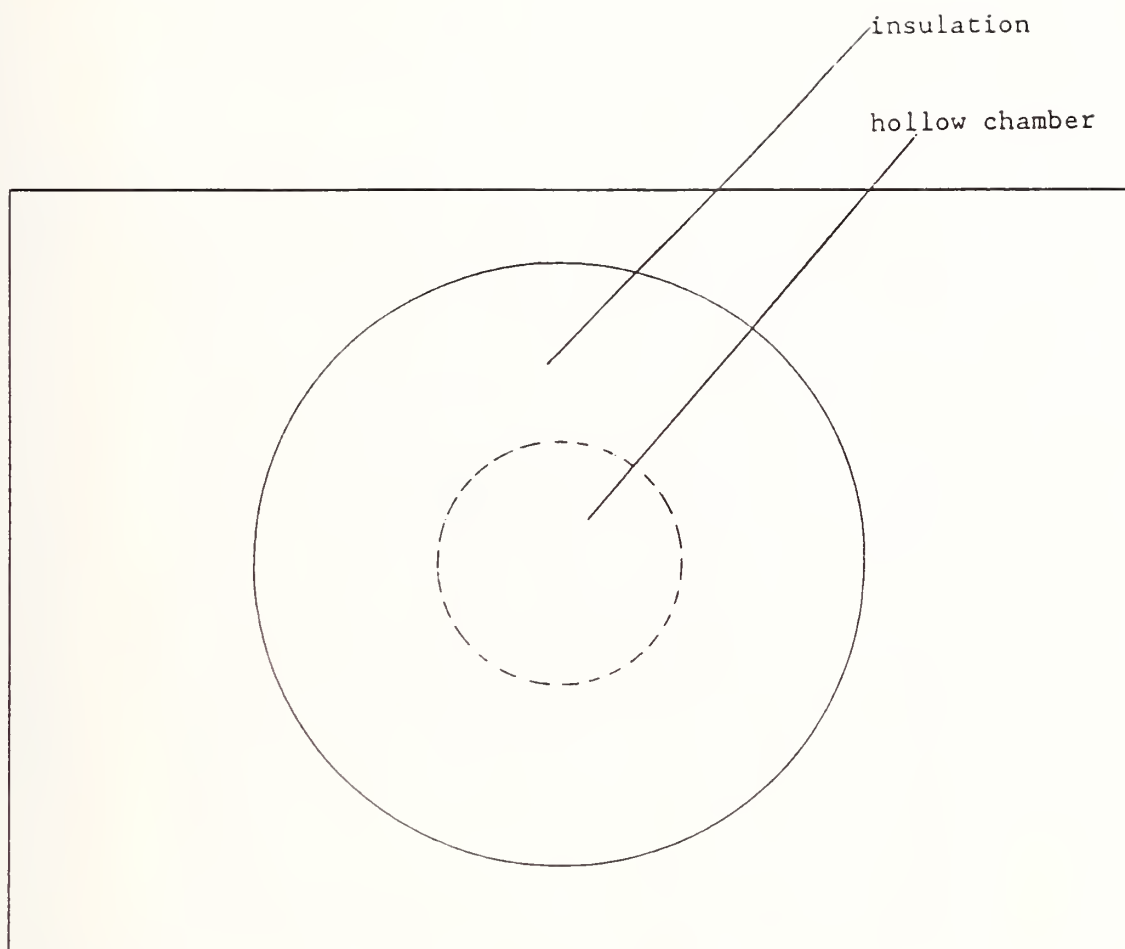
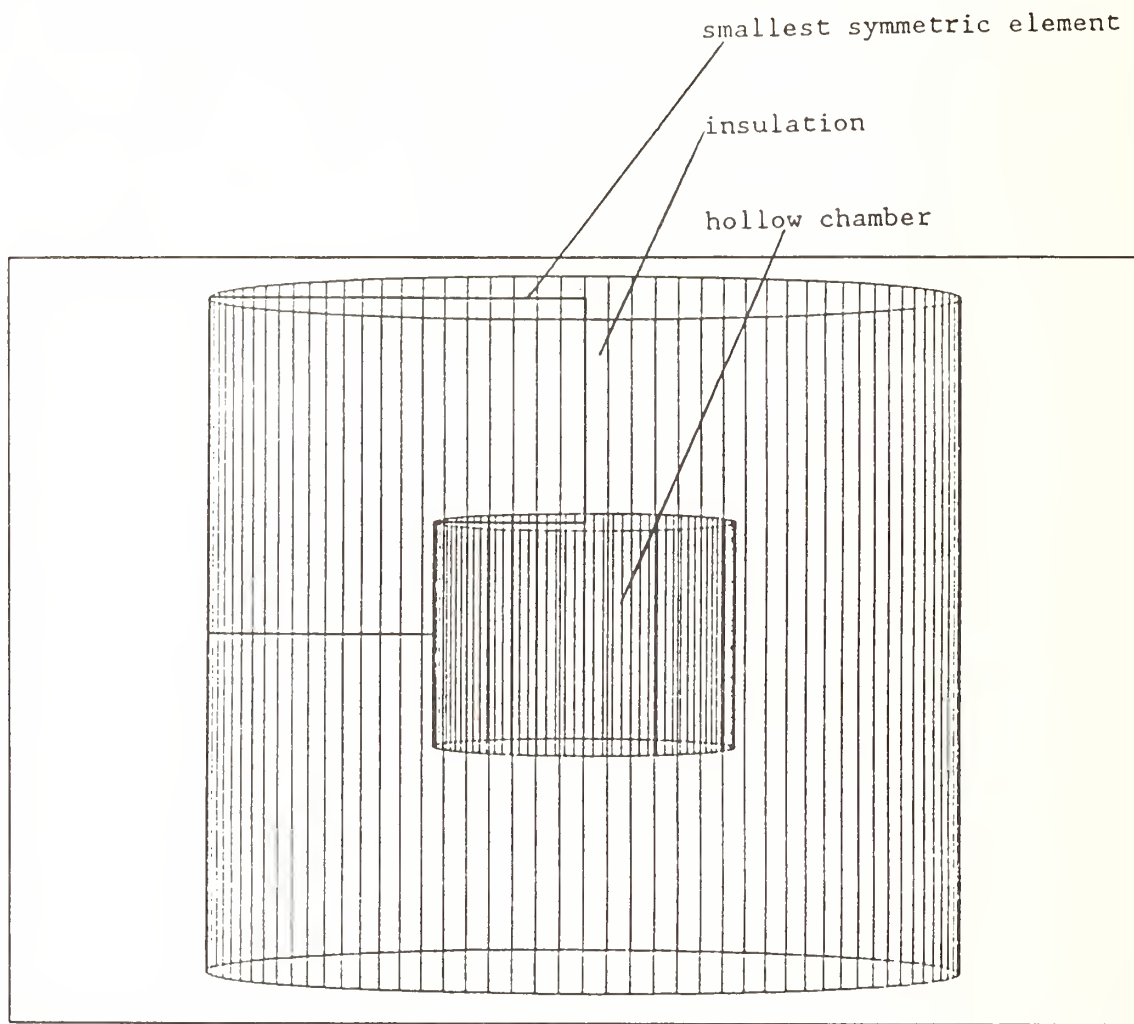Figure 4. Top view of High Temperature Furnace Design

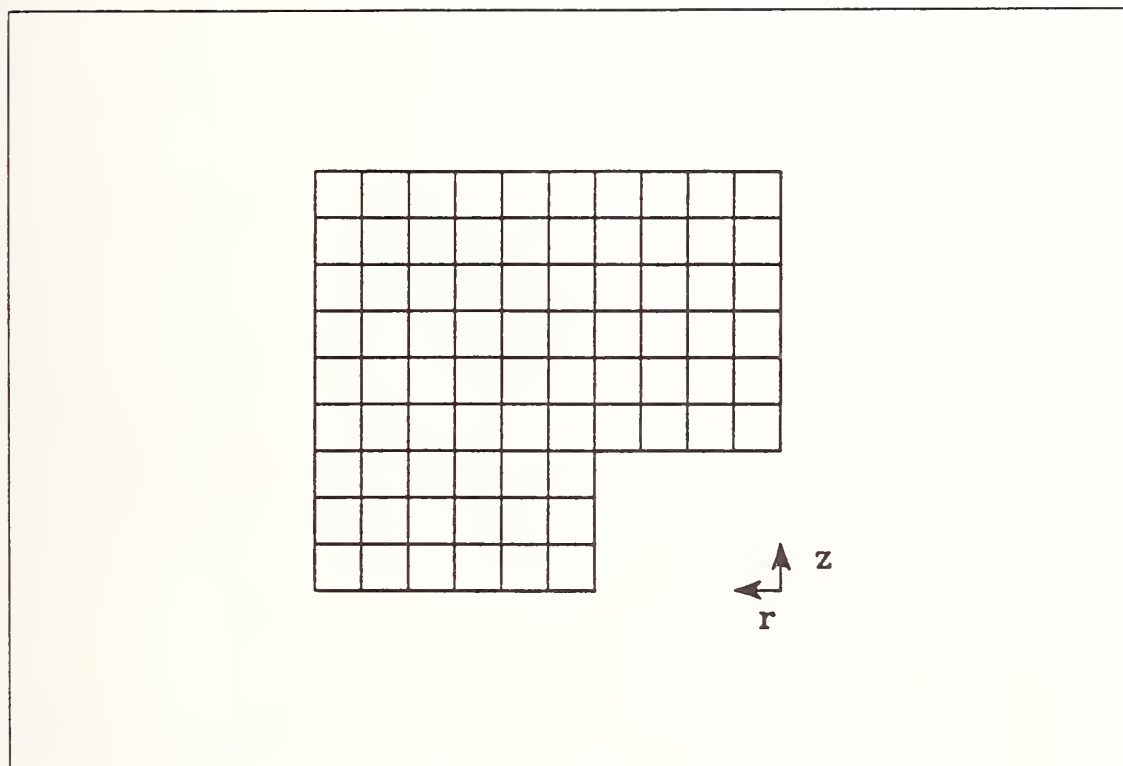Figure 5. Side View (3-D) of Insulation

Figure 6.   Smallest Symmetric Element for High Temperature
            Furnace Design

If the width of a square is one unit (arbitrary units), the boundary conditions become:

@ r = 4, 0 ≤ z ≤ 3, T = 1500°C

@ 4 ≤ r ≤ 10, z = 0, $\partial T/\partial z$ = 0 (symmetry)   [14]

@ 0 ≤ r ≤ 4, z = 3, T = 1500°C

@ r = 0, 3 ≤ z ≤ 9, $\partial T/\partial r$ = 0 (symmetry)

Now, specify the boundary conditions on the outer surface of the furnace. We assume that the room temperature is 20°C (68°F) which is typical of a laboratory. Since free convection dominates heat transfer to the laboratory at the outer surface of the furnace, we will assume a heat transfer coefficient of 20 kcal/m^2 hr °C (~4 BTU/hr ft^2 °F)[114] from the outer wall to the 68°F room. Therefore the outer wall boundary conditions become:

@ r = 10 0 ≤ z ≤ 9 q_r = h(T_{wall} - T_{room})   [15]

@ 0 ≤ r ≤ 10 z = 9 q_z = h(T_{wall} - T_{room})

where T_{room} = 20°C (68°F)

    h = 20 kcal/m^2 hr °C (~4 BTU/hr ft^2 °F)

T_{wall} = T_{wall}(r,z).

Figure 7 summarizes the boundary conditions for the given configuration. To simplify the problem, assume that the thermal conductivity (k_{eff}) of the insulation is constant at its highest value
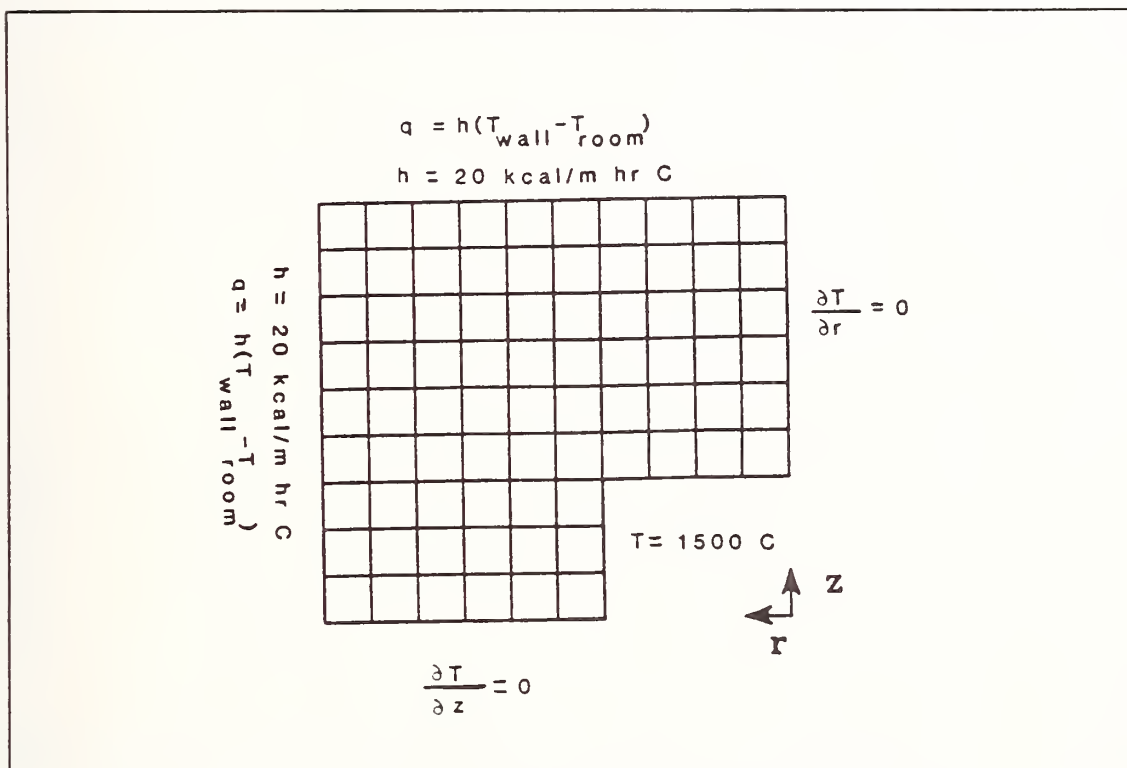
Figure 7. Summary of Boundary Conditions for High Temperature
Wear Facility Furnace Design

of 0.4 BTU/ft hr °F. Also, assume that one arbitrary unit of distance

is equal to 2.54 cm (1 inch). This gives a minimum of 15 cm of

insulation on all sides of the high temperature chamber. Now a finite

element analysis can be conducted. Such an analysis is still quite

complex and requires computer methods. A pre-developed program for the

given configuration was supplied by the Statistical Analysis Division.

For the given configuration under specified boundary conditions, outer

wall temperatures are calculated at r=0, z=0, and at maximum r and z.

This provides centerline and extremity temperatures. For 15 cm of

insulation, it was found that at:

r=0, z=9 (arbitrary units), T = 100°C

r=10, z=0 (arbitrary units), T = 70°C   [16]

r=10, z=9 (arbitrary units), T = 20°C

These results are shown in Figure 8. If interested in temperature

distributions, Appendix B provides a finite difference analysis for the

given configuration. This analysis can be used to develop a computer

program that will provide temperature distributions. For the purpose

of feasibility analysis, centerline temperatures (maximum temperatures)

and extremity temperatures (minimum temperatures) were sufficient.

Based on the above analysis, the use of a high temperature porous

zirconia insulation such as that used by the space shuttle is viable

for furnace design. The High Temperature Wear Facility Furnace was

designed in this manner.
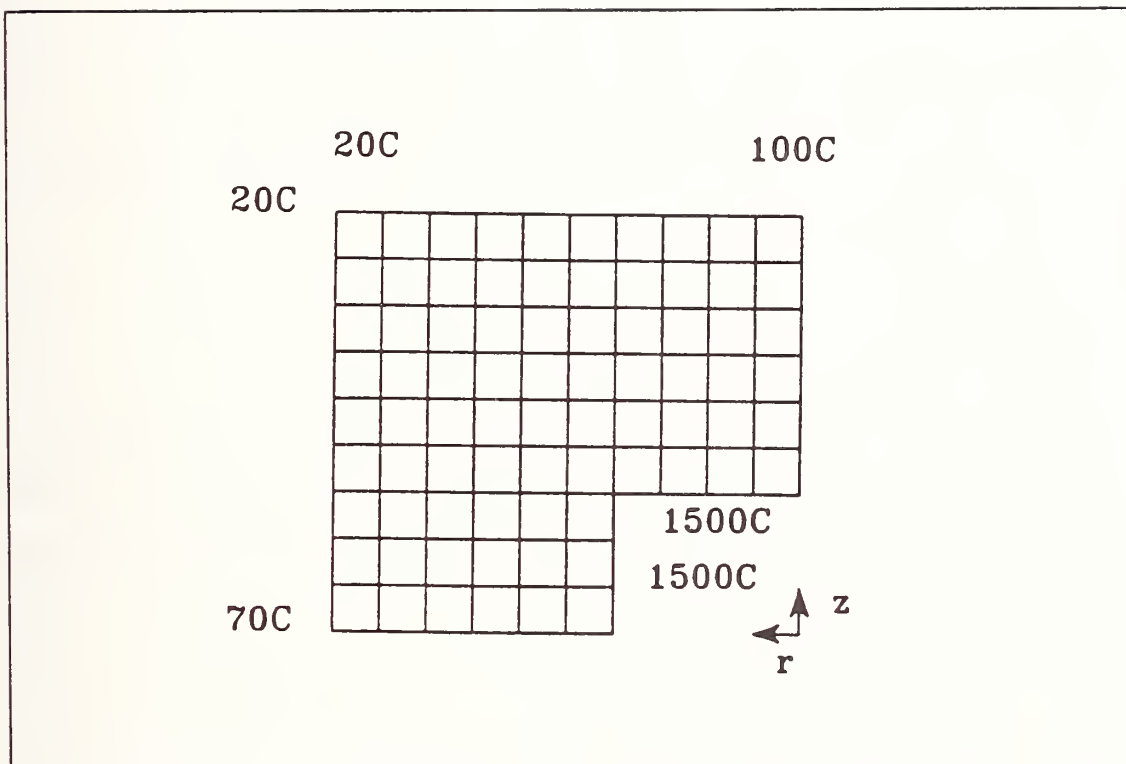
Figure 8. Results of Finite Element Analysis
(Courtesy of Statistical Analysis Division)

Chapter 5

MATERIALS SELECTION FOR THE HIGH TEMPERATURE WEAR FACILITY

5.1 Introduction

Materials selection for wear test equipment is a complex and difficult process. In selecting a material for a given application, several factors are important such as:

o   strength of the material

o   chemical reactivity of the material the simulated environments

o   fabrication technology

o   fabrication cost of the material and the final machined
    component

For the design of a high temperature wear tester, design is much more complex. Components made from the materials need to maintain mechanical stability from room temperature to 1500°C. Furthermore, additional considerations are required such as:

o   thermal expansion of materials,

o   differential thermal expansion of mating materials,

o   oxidative and thermal stability of materials,

o   dimensional stability (shape retention) of materials,

o   surface reactions and phase transformations of materials

There are several potential candidates from these considerations. They are:

- o   Partially Stabilized Zirconia (PSZ)

- o   Silicon Nitride (Si_3N_4)

- o   Silicon Carbide (SiC)

A typical properties table for these materials is given in Table 7.

5.2   Partially Stabilized Zirconia

PSZ is a ceramic which is based on zirconium oxide stabilized with magnesia or yttria. The crystalline matrix consists of cubic zirconia with residual tetragonal and monoclinic structures at grain boundaries and within the cubic grains. When this material is stressed, the tetragonal phase transforms to the monoclinic phase causing a 4% volume increase. This volume increase causes a compressive stress to be formed at crack tips. Thus Partially Stabilized Zirconia has a fracture toughness of 8 MPa $\sqrt{m}$ at room temperatures.

Another property which makes PSZ attractive as a structural material is PSZ's coefficient of thermal expansion. The coefficient of thermal expansion of PSZ is $10.1 \times 10^{-6}/°C$ while that of silicon nitride is $2.3 \times 10^{-6}/°C$. For a ceramic, zirconia has a high coefficient of thermal expansion, and thus can mate to steels much

Table 7

Properties of Selected Ceramic Materials

		Ceramics[1]		
Material →		α-SiC	Si₃N₄	PSZ
Manuf. →		Carborundum	GTE	Nilsen
Identifi. →		Hexaloy	SNW1000	TS
Density	g/cm³	3.1	3.3	5.8
Thermal Conductivity	w/m K	126	27	1.8
Heat Capacity	J/kg K	2803	810	400
Thermal Expansion Coefficient	10^{-6}/K	4.0	2.3	10.1
Electrical Resistivity	Ω-cm	0.2-300	$>10^{14}$	$>10^{11}$
Hardness Knoop	GPa	27.4	12.7	10.0
Brinnell	#	- -	- -	- -
Elastic Modulus	GPa	410	276	205
Tensile Strength	MPa	- -	- -	- -
Compressive Strength	MPa	- -	- -	1850
Flexural Strength	MPa	550	665	690
Yield Strength	MPa	- -	- -	- -
Elongation	%	- -	- -	- -
Fracture Toughness	MPa√m	4.6	4.5	9.5
Maximum Service Temp. (Air)	°C	1650	~1200	950
Melting Point	°C	~2700	~1900	- -

-- indicates data not available.
(1) Source: Compiled from company literature.
(2) Source: Perry (25).

better than other ceramics. The coefficient of thermal expansion of a typical carbon steel is ~12 x 10^{-6}/°C.[115]

However, because of the materials transformations in PSZ, several problems are encountered. First, at 1240°C, all residual monoclinic zirconia will transform to tetragonal zirconia. Accompanying this transformation is a sudden 4% decrease in the volume of the transforming zirconia. Thus, if components are overheated during testing, phase transformations occur which change the microstructure and density of the PSZ permanently. Figure 9 shows a typical expansion curve of PSZ from 0 - 1500°C. Upon heating, expansion follows the solid line. Since the microstructure has been changed, however, the thermal contraction of the material follows the dashed line.

To compound the problem, upon cool down between 500 and 600°C, metastable tetragonal zirconia reverts to the monoclinic phase. This causes an ~0.4% expansion and possible failure of the bulk component. Thus, PSZ was ruled unacceptable as a 1500°C structural material.

5.3 Silicon Nitride

Silicon nitride is widely used as a high temperature bearing material. Table 7 shows that silicon nitride can have a hardness of 91 R45N compared to 83 R45N of alumina. Furthermore, silicon nitride also shows no loss of flexural strength up to 1000°C. Thus, this material is ideal for a structural material because of its high strength and good shape retention properties.
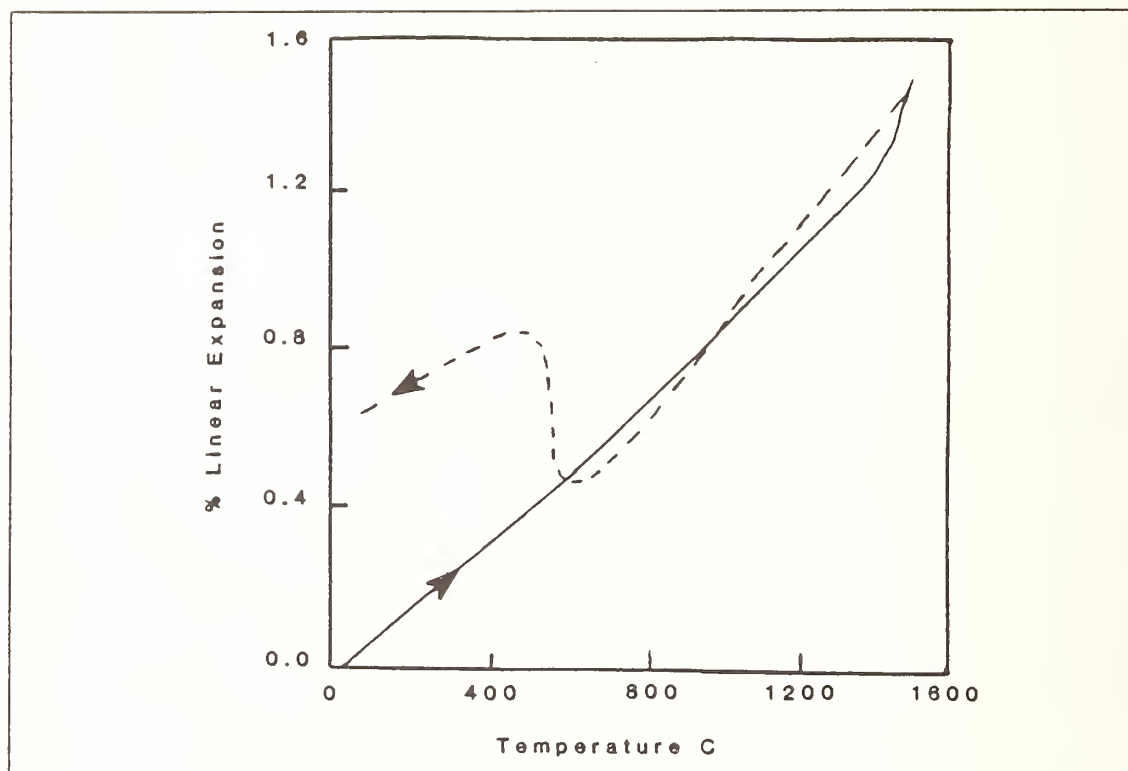
Figure 9.   Linear Thermal Expansion Curve of PSZ from 0-1500°C
(Source: Nilsen, Inc. Literature)

However, for 1500°C operation, silicon nitride is also unacceptable. Above 1000°C, silicon nitride rapidly loses strength. Also, oxidation of silicon nitride causes loss of nitrogen and silicon segregation in the ceramic.

5.4 Silicon Carbide

Several different silicon carbide materials exist. These can be divided into two categories: 1) cubic silicon carbide, and 2) hexagonal (α) silicon carbide. Table 7 shows a comparison between these materials. The hexagonal silicon carbide (Sohio Engineered Materials) has a higher hardness (27.44 GPa) than any other ceramic shown in Table 7 and has approximately double the hardness value of alumina. The flexural strength of this material is high (550 MPa) and this material has the highest elastic modulus (410 GPa) and shear modulus (178 GPa) of the materials shown. The tensile strength of α-SiC relative to other ceramics is shown in Figure 10. At 1500°C, α-SiC is the strongest material selected and has strengths higher than silicon nitride, partially stabilized zirconia, or alumina. Also, the tensile strength of α-SiC increases with temperature to ~1200°C. Furthermore, α-SiC unlike other silicon carbides has no free silicon and is extremely oxidatively and chemically stable to temperatures over 1650°C. To summarize, α-SiC has:

   o   the highest hardness of the ceramics selected
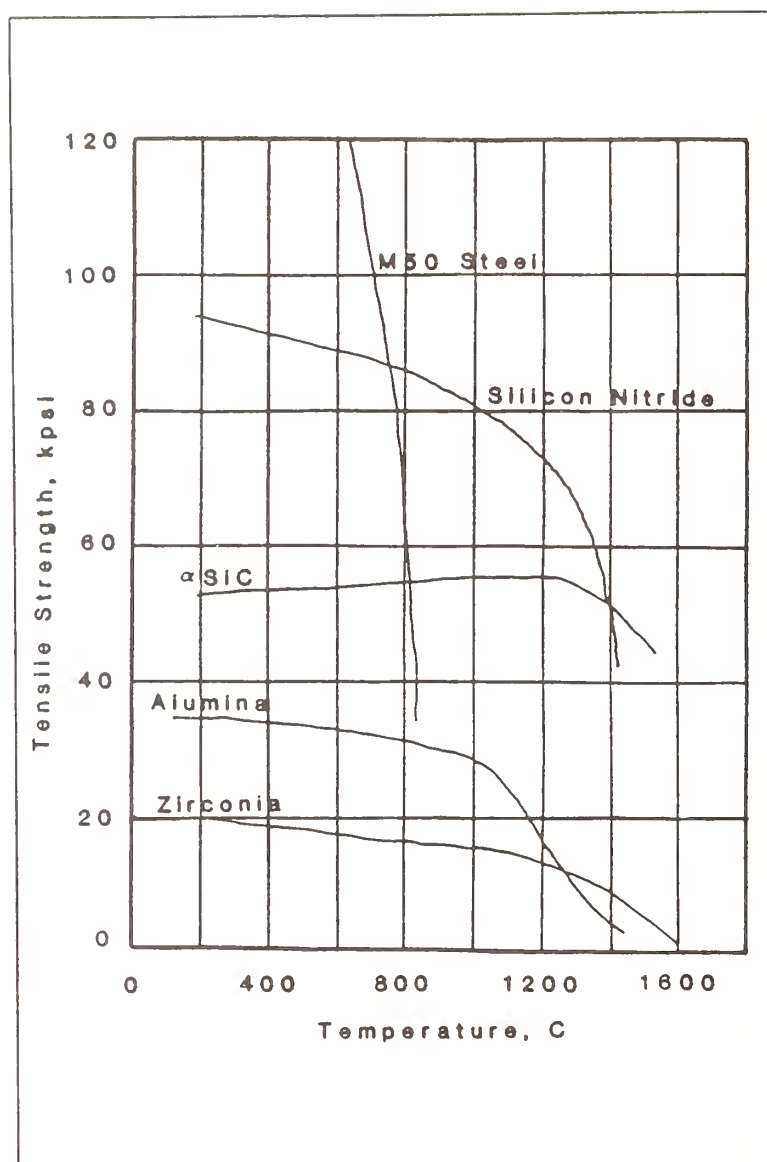
   o   excellent oxidation stability

Figure 10.   Tensile Strength of Materials to 1500°C

o highest elastic modulus of materials selected

o best 1500°C tensile strength of materials selected

A typical properties compilation for this material is given in Table 8. This material was therefore chosen for the 1500°C structural components of the High Temperature Wear Facility.

Table 8

A Typical Properties Table of α-SiC

Dissociation/Melting Temperature

Property	Units	RT	200°C	400°C	600°C	1500°C
Thermal diffusivity (laser flash)	cm²/sec	0.413	0.230	0.185	0.140	
Specific heat (drop calorimeter)	cal/g °C	0.160	0.220	0.252	0.268	0.334
Thermal conductivity	cal/cm² sec °C	0.208	0.160	0.147	0.118	

Thermal-Shock Resistance Parameter

Property	Units
Thermal-expansion coefficient	10^{-6}/°C RT - 700°C $\sim$ = 4.02 700°C - 2000°C $\sim$ = 5.32

Chemical Stability

Material			Chemical Agent			
	HC1	H_2SO_4	HNO_3	H_2S	HF	NaOH
Hexoloy™ SA			Excellent			
99% Al_2O_3	Fair	Good	Good	Good	Fair	Fair
Tungsten Carbide -6% Cobalt	Poor	Fair	Very Poor	Fair	Fair	Fair
Stainless Steel	Very Poor	Very Poor	Poor	Poor	Poor	Good

Source - Sohio Engineering Materials Company.

Table 8 (continued)

Properties

Property	Units	RT	1000°C	1200°C	1400°C	1500°C	1650°C
Hardness (Knoop)	kg/mm^2	2800					
Wet abrasion (Riley-Stoker)	---	3.4					
Density	g/cm^3	3.1					
Young's modulus	Mpsi	58.9	54.9				
	(GPa)	(406)	(378)				
Shear modulus	Mpsi	25.8	24.5				
	(GPa)	(178)	(169)				
Poisson ratio	---	142	.118				
Flexural strength (4 pt.)							
Air	kpsi	66.6	64.1	65.3	62.7	58.6	
	(MPa)	(459)	(442)	(450)	(432)	(404)	
Argon	kpsi	64.8					71.6
	(MPa)	(446)					(494)
Weilbull modulus (2 parameter) -		12.3					
Fracture toughness (double torsion &	kpsi in$^{\frac{1}{2}}$	4.2	5.8				
SENB)	(MPa m$^{\frac{1}{2}}$)	(4.6)	(6.4)				
Oxidation	---	---	---	---	---	---	not detectable

Source - Carborundum Resistant Materials Company.

Chapter 6

FLUID DYNAMICS

In wear tester design, two important design considerations are the precise alignment of test specimens and the control of machine/contact vibrations under the full speed range. Test specimen alignment is important in wear rate measurements and uniform contact pressure throughout the test. Misalignment during the wear test could cause premature surface damage and change the wear mode. Friction and wear results are dependent on the machine vibration frequency and amplitude to a certain extent. Under excessive vibrations at a particular sliding speed, wear mode could change due to fretting wear.

Therefore, in the design of a wear test apparatus, the designer seeks to 1) maintain test alignment, 2) minimize vibration, 3) be sensitive for friction measurements, and 4) maintain the structural integrity of shafts and holders.

Traditionally, for low temperature wear test devices, the above four conditions are satisfied by conventional methods. A precision bearing with a lubrication system is used to control the stiffness of the shafts. The whole system mating is controlled by high precision machining on the rotating shafts, on the bearing packs which mate to the shafts, and on specimen holders and other structural components. Self-aligning contact geometry is often designed to maintain alignment throughout the test.

For high temperature wear tester design, traditional methods of maintaining test alignment and controlling vibration are no longer effective. Conventional lubricants fail to lubricate at high temperatures. The lubricants may thermally degrade or oxidize causing catastrophic failure of the bearing system. Apart from lubricant reactions, high temperature surface reactions may cause components to fuse together. Even if parts did not fuse together, standard bearing materials become much too soft at high temperatures causing deformation of bearings, bearing races, shafts, and specimen holders. This will cause loss of test alignment and will introduce vibration into the system.

To overcome these difficulties, externally pressurized gas film bearings were chosen because they provide:

o   no contact between stationary and moving surfaces,

o   good stiffness,

o   good alignment capabilities,

o   maximum sensitivity for friction measurements

Externally pressurized bearings of this type represent 3-dimensional compressible fluid flow problems. The basic equations for this type of system are, in rectangular coordinates:

Equation of continuity:

$$\frac{\partial \rho}{\partial t} + \frac{\partial}{\partial x} (\rho v_x) + \frac{\partial}{\partial y} (\rho v_y) + \frac{\partial}{\partial z} (\rho v_z) = 0 \qquad [17]$$

Equation of motion:

x-component

$$\rho \left[\frac{\partial v_x}{\partial t} + v_x \frac{\partial v_x}{\partial x} + v_y \frac{\partial v_x}{\partial y} + v_z \frac{\partial v_x}{\partial z} \right] =$$

$$\frac{\partial p}{\partial x} - \left[\frac{\partial \tau_{xx}}{\partial x} + \frac{\partial \tau_{yx}}{\partial y} + \frac{\partial \tau_{zx}}{\partial z} \right] + \rho g_x \qquad [18]$$

y-component

$$\rho \left[\frac{\partial v_y}{\partial t} + v_x \frac{\partial v_y}{\partial x} + v_y \frac{\partial v_y}{\partial y} + v_z \frac{\partial v_y}{\partial z} \right] =$$

$$- \frac{\partial p}{\partial y} - \left[\frac{\partial \tau_{xy}}{\partial x} + \frac{\partial \tau_{yy}}{\partial y} + \frac{\partial \tau_{zy}}{\partial z} \right] + \rho g_y \qquad [19]$$

z-component

$$\rho \left[\frac{\partial v_z}{\partial t} + v_x \frac{\partial v_z}{\partial x} + v_y \frac{\partial v_z}{\partial y} + v_z \frac{\partial v_z}{\partial z} \right] =$$

$$- \frac{\partial p}{\partial z} - \left[\frac{\partial \tau_{xz}}{\partial x} + \frac{\partial \tau_{yz}}{\partial y} + \frac{\partial \tau_{zz}}{\partial z} \right] + \rho g_z \qquad [20]$$

where ρ = density of gas

v = velocity

x,y,z = spatial coordinates for the system

g_z = component of gravitational force in the z direction

τ = stress tensor

Such calculations are quite complex in that we have 4, 3-dimensional, coupled, partial differential equations to solve in conjunction with the appropriate boundary conditions.

Furthermore, several other design challenges in a bearing of this sort need to be addressed.

The first challenge in any design of this type is to design a bearing that maintains side-to-side alignment while still allowing freedom of movement in the other directions. Initially, the general layout given in Figure 11 of such a self-aligning hydrostatic bearing was considered.

Several advantages of the layout given in Figure 11 can be seen. First, in a "U" shaped bearing design of this sort, both horizontal and vertical stabilizations occur independently. This means that only side to side vibrations will be compensated in the horizontal direction, and only load variations will be compensated for in the vertical direction. This is an ideal situation, but unfortunately, this preliminary design had to be rejected. Because hydrostatic bearings of this type have to be machined to very tight tolerances to maintain stiffness, it was found that bearing designs of this type would be very unforgiving to temperature variations between the gas supply surface and the specimen
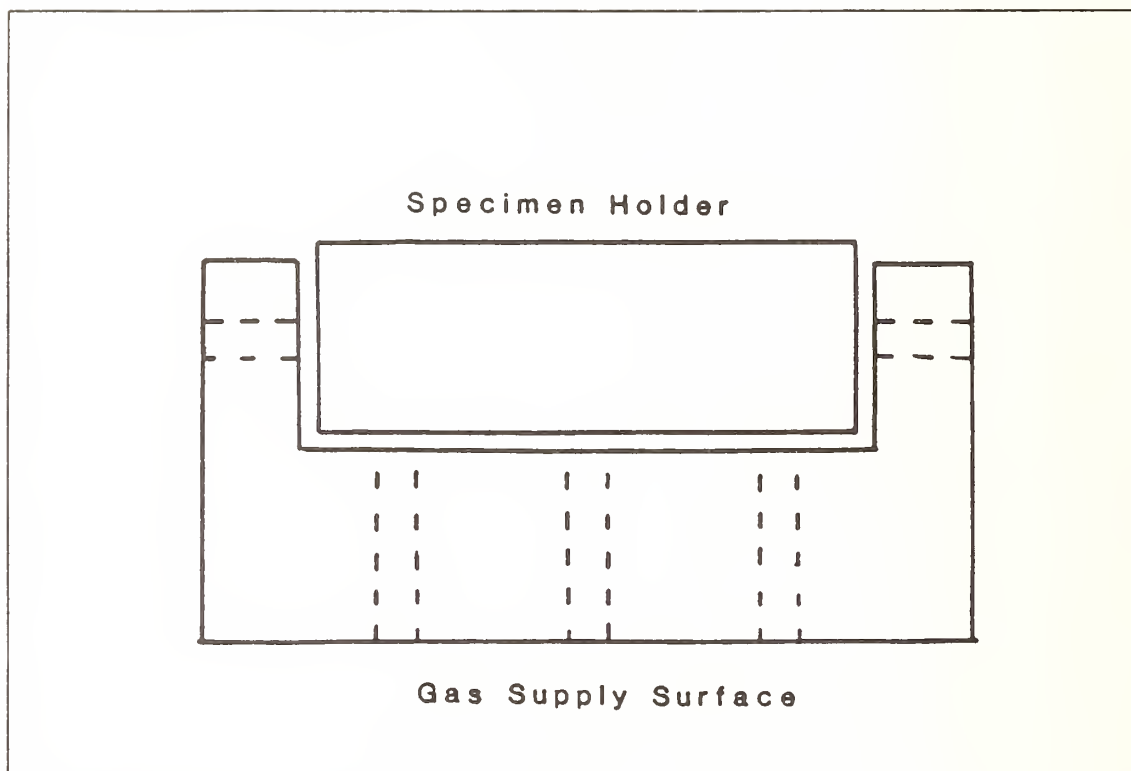
Figure 11. Original Preliminary Hydrostatic Gas Bearing Layout
(Side View)

holder. A slight temperature rise in the specimen holder without a
rise in the gas supply surface would cause total bearing failure,
because of the steep angled walls (90°). The sides of the bearing
would meet due to differential thermal expansion if it occurred.

Therefore, to increase the tolerance for differential thermal
expansion, a "V" shaped bearing was next considered. This is shown in
Figure 12.

This "V" type design has the advantage of allowing for small
differences in thermal expansion that may occur between the specimen
holder and the gas supply surface. Unlike the "U" shaped bearing,
these small temperature differences will not cause bearing failure.
Unfortunately, the "V" type layout also has some strong shortcomings.
Compensation for forces in the vertical direction and the horizontal
direction are not independent. If a load on the bearing surface of F_y
is applied as shown in Figure 12, an equal and opposite force of F_y in
the vertical direction is required to keep the bearing afloat.
However, gas bearings always exert forces which are normal to their
surfaces, so the gas bearing exerts a normal force of N. Resolving N
into its component horizontal and vertical forces, for the bearing to
stay afloat:

$$|F_y| = |N| \cos(\theta) \qquad\qquad [21]$$

However, a side force is also generated,

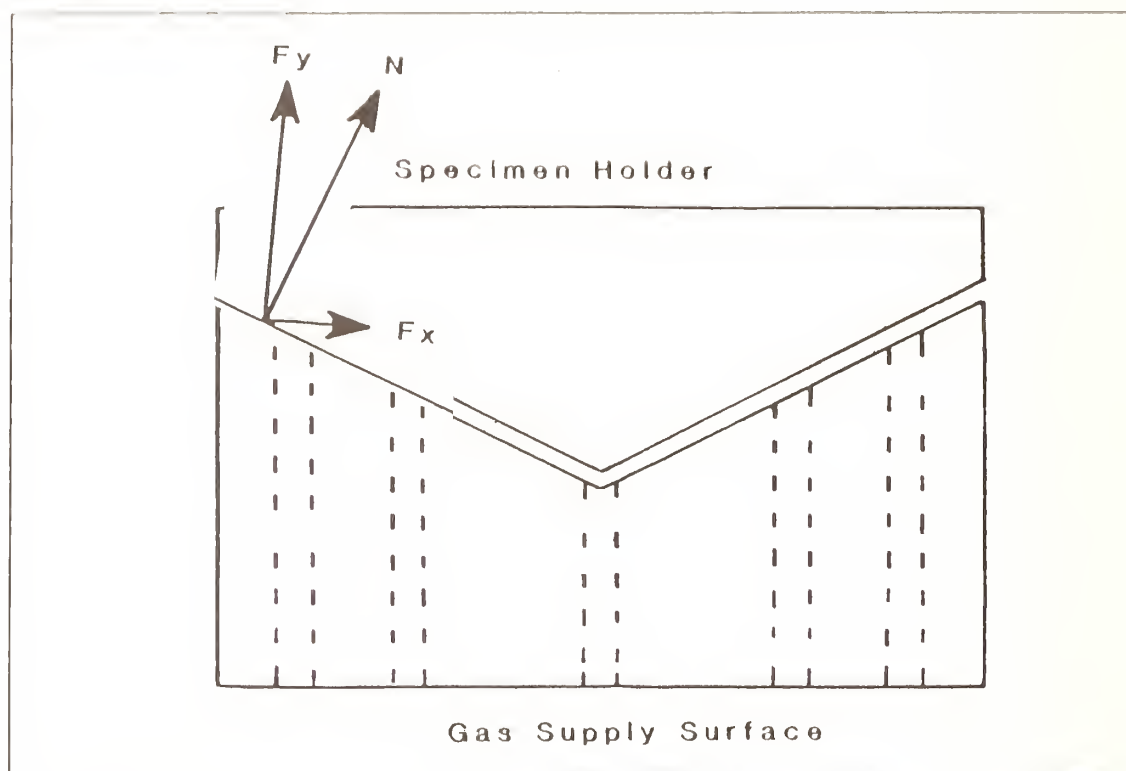$$|F_x| = |N| \sin \theta \qquad\qquad [22]$$

Figure 12. "V"-shaped Hydrostatic Gas Bearing Layout

Since these side forces are needed to maintain stiffness against vibration, stiffness will depend upon the load applied and on the tilt of the bearing supply surface. Table 9 gives F_y/F_x ratios for a number of given angles.

If an angle of 45° were used in design and a load of 10N were applied in the y direction, a reaction of 10N in the x direction would also occur. Thus, in not having a horizontal surface to independently compensate for load, side to side instability might occur for the bearing. The "V" shape bearing would not be acceptable because independent compensation in the load from a horizontal surface is not present.

Finally, after careful design considerations, the advantages of both the "U" and "V" shaped bearings were combined into a new design. Figure 13 gives top and side views of the hydrostatic bearing layout.

The next task is to design gas supply hole shape. There are two main types of hole shapes: inherently compensated and orifice compensated. An orifice compensated bearing and an inherently compensated supply hole are shown in Figure 14.

The difference between these two types of designs is that in an inherently compensated supply, the major restriction to gas flow occurs at the bearing surface, while in an orifice compensated supply, the major restriction to gas flow is away from the bearing surface. This difference allows the orifice compensated bearing to be as much as 20% more stiff, but the orifice compensated bearing may, depending on transient gas pressures, experience a dynamic instability called

Table 9

F_y/F_x Ratios for "V" Shaped Bearing Design

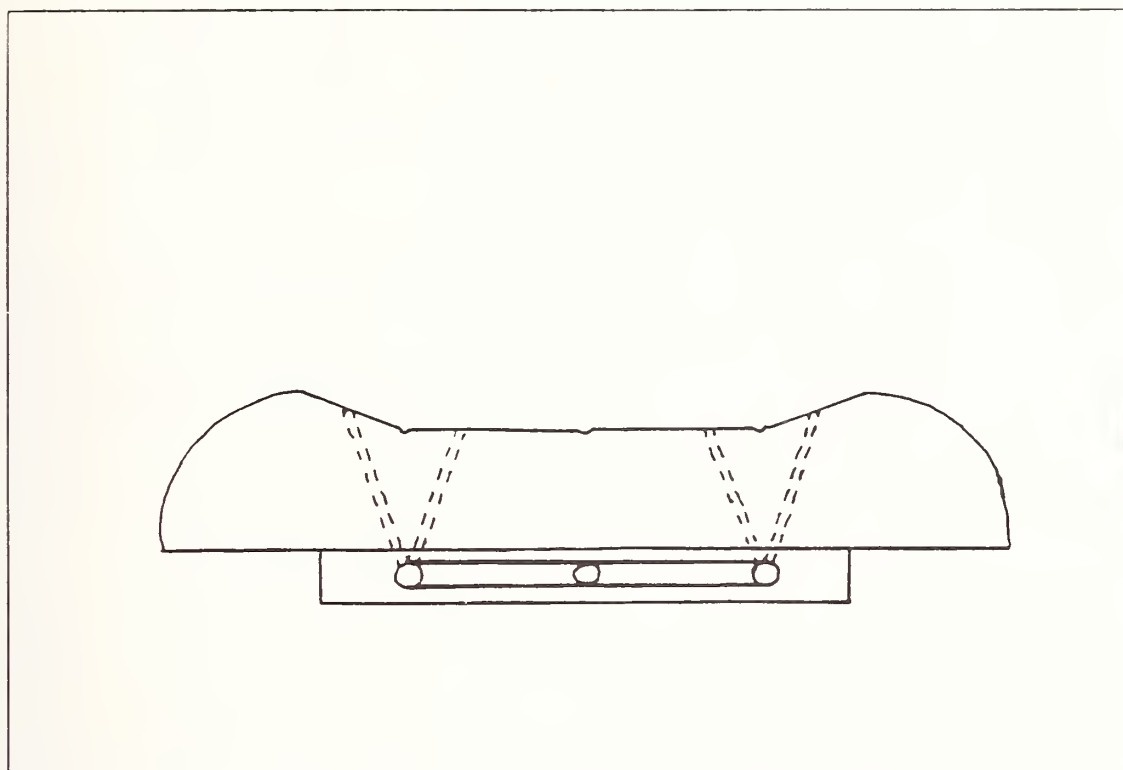| θ (degrees)	F_y/F_x
0	∞
5	11.43
10	5.67
15	3.73
20	2.74
25	2.14
30	1.73
35	1.43
40	1.19
45	1

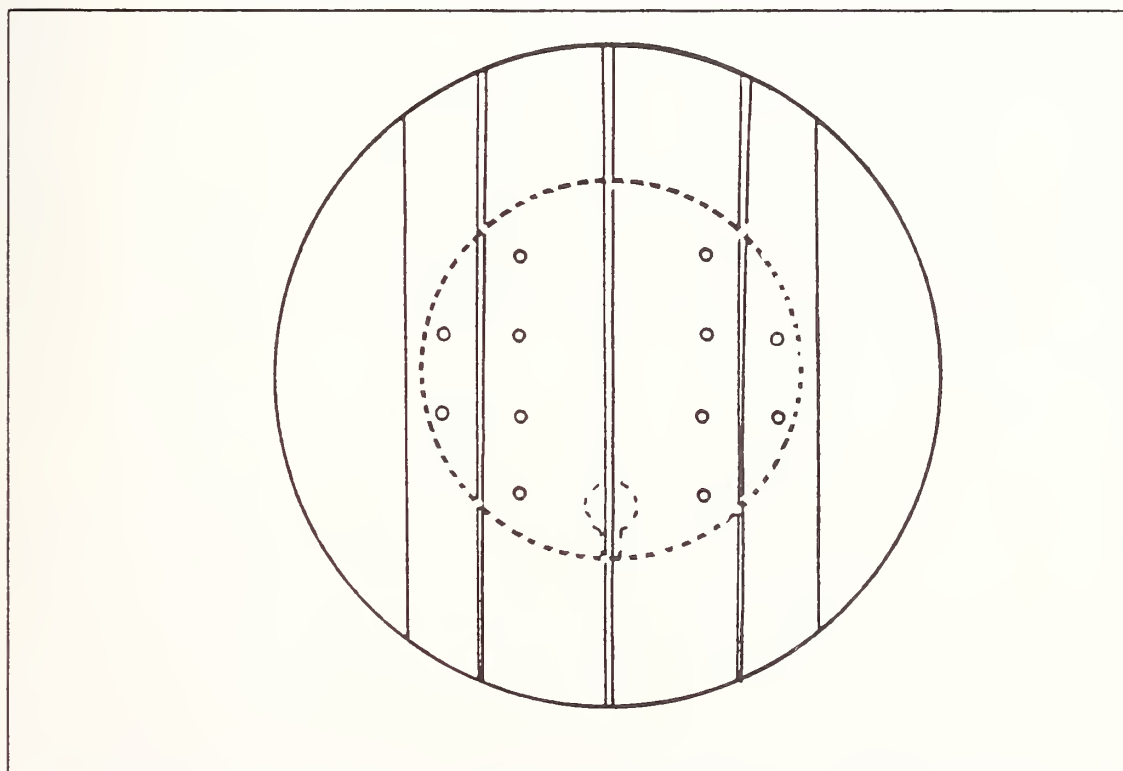Figure 13(a).   Side View of Hydrostatic Bearing

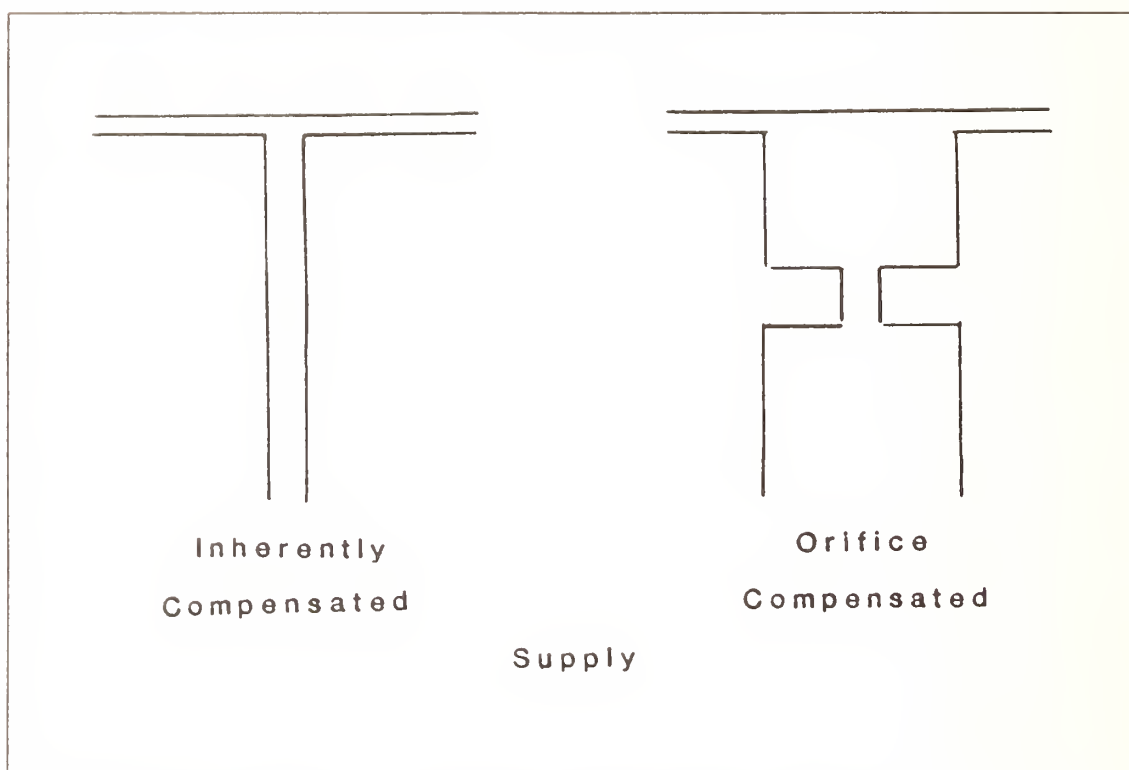
Figure 13(b).   Top View of Hydrostatic Bearing

Figure 14.   Inherent and Orifice Compensated Supply Holes
(Sectional View)

pneumatic hammer (i.e. a series of high frequency surface contacts causing bearing damage). Theoretically, inherently compensated gas bearings should not hammer. Therefore, an inherently compensated bearing is chosen.

For the hydrostatic bearing a three-dimensional, compressible, unsteady state fluid flow calculation was performed. Appendix C gives the full design calculation for the hydrostatic bearing. For this hydrostatic bearing, the Mechanical Technology Incorporated Gas Bearing Design Manual was used as a design guide.[116]

To summarize the design given, it was originally decided that at least 8 holes of 0.050" diameter should be used with argon gas. In the calculation, worst case conditions were used. For a gas which increases its viscosity with temperature, room temperature argon provides the lowest load carrying capabilities. Therefore, the room temperature properties of argon were used in the design calculation.

Since the hydrostatic bearing was to be made of an expensive material and, since the approximation of a standard configuration allows the design of a bearing for a non-standard configuration, it was decided that a brass bearing prototype would be built to test the bearing design.

Fortunately, this approach was taken in the design of this critical component, for several interesting results emerged. The hydrostatic gas bearing (which was inherently compensated) pneumatically hammered. Theoretically, this should not have happened. After contacting the author of the gas bearing design manual for thrust gas bearings, the following was found: 1) it was assumed that for an

inherently compensated bearing that the bearing would not hammer and 2) for strange configurations, a small region of instability could develop if the wrong hole size was chosen.

Therefore, the hole size was decreased from 0.050" to 0.021". It was found that the smaller hole hydrostatic bearing <u>did not</u> experience pneumatic hammer. Therefore, in specifying 0.050" dia. holes (which normally would be better than 0.021" dia. holes) we were merely unfortunate in hole size selection. However, the machining of 0.021" dia. holes of the length necessary would not be possible for current state-of-the-art ceramic machining. The hole size had to be changed to 0.040". This was the smallest hole possible for ultrasonic machining of the component. Another prototype bearing was made and finally an acceptable bearing design was found. The 0.040" dia. holes did not cause pneumatic hammer, so the bearing could be designed.

Chapter 7

MECHANICAL DESIGN OF COMPONENTS

There are several technical challenges in high temperature wear tester design. They are: 1) design of ceramic/metal components to accommodate differential thermal expansion of pieces, 2) design and selection of drive mechanism, and 3) design of machine framework for a high temperature facility. Each of these areas will be briefly addressed in this section.

7.1 Design of Ceramic/Metal Components to Accommodate Differential Thermal Expansion

Thermal design of ceramic-ceramic and ceramic-metal interfaces is critical in wear tester design. Both interfaces have unique properties, and both require special design.

In the design of the High Temperature Wear Facility, the following was required of ceramic-ceramic and ceramic-metal interfaces at high temperatures:

o   interfaces cannot slip, move, or readjust themselves at high temperatures.

o   ceramic-ceramic interfaces should remain permanent after attachment.

To meet these requirements, two approaches were considered. Ceramic-ceramic and ceramic-metal interfaces could be attached through the use of a high temperature refractory cement. However, refractory cements lose bonding strength at high temperatures. For ceramic-ceramic interfaces which would be in the 1500°C furnace, pieces could slip, move, and possibly mis-align themselves. Also, small particles are usually present in high temperature refractory cements. If these particles become entrapped between a tight fitting ceramic-ceramic or ceramic-metal interface, high point stresses could result. This may cause the cracking of a ceramic component.

A second way to assure that interfaces do not move is to design ceramic-ceramic and ceramic-metal interference fits. Traditionally, with metals, interference fitting and compression fitting are considered to be synonymous terms. The inner component is forced, by compression, to fit inside the outer piece, and the outer piece is deformed elastically to make a permanent fit.

To design an interference fit, stress calculations for ceramic materials are conducted. There are two types of stresses that may be considered in the design of a ceramic tube to metal and/or ceramic interface. They are tensile hoop stress on a tube (Figure 15a) and compressive hoop stress on the tube (Figure 15b).

The basic design criteria for such interference fits are that if the tube is put in tension, then the hoop stress cannot exceed the tensile strength of the tube material, or if the ceramic tube is put in compression, the hoop stress due to the interference fit cannot exceed
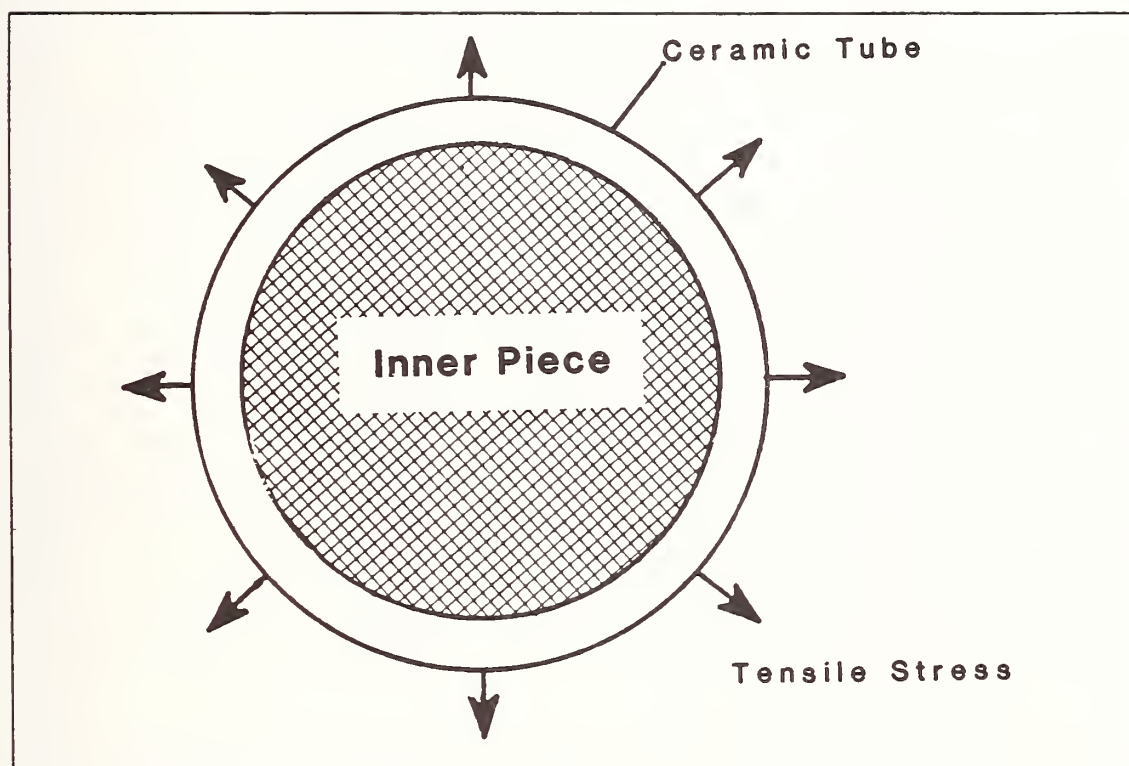
Figure 15(a). Tensile Hoop Stress on a Ceramic Tube Interference Fit (Top View, Sectional)
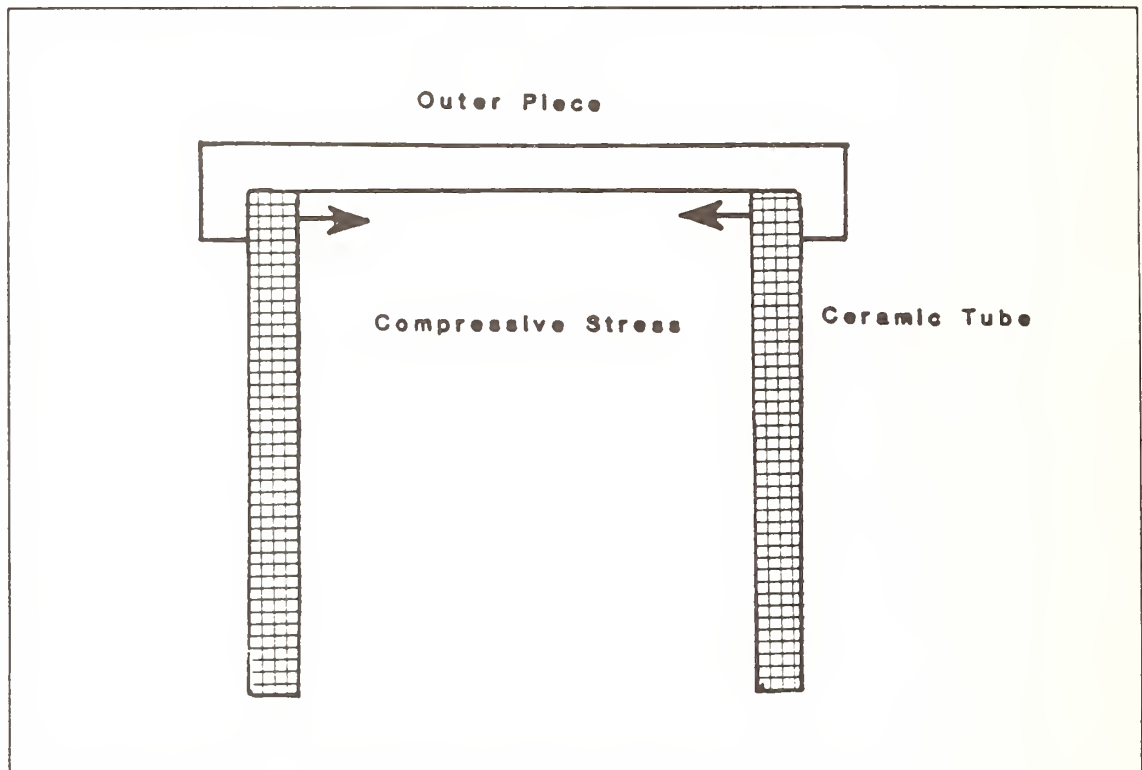
Figure 15(b).   Compressive Hoop Stress on a Ceramic Tube Interference
                Fit (Side View, Sectional)

the compressive strength of the tube materials. For ceramic materials, the compressive strength is usually 1-2 orders of magnitude higher than the tensile strength.

For Carborundums' Hexoloy α-SiC:

Tensile Strength:	350 MPa
Compressive Strength:	3900 MPa

Hoop Stress Calculations:

The general configuration of the hoop stress calculation is shown in Figure 15(a):

$$\sigma_h = \frac{qr}{A} \hspace{4cm} [23]$$

where σ_h = hoop stress

q = unit loading per length of tube

r = radius of tube assuming thin wall tubes

A = area of contact of interference fit.

The hoop strain is related to the hoop stress and design parameters as follows:

$$\epsilon = \frac{\Delta d}{d} = \frac{\sigma}{E} \hspace{4cm} [24]$$

where ϵ = hoop strain

Δd = maximum diametrical interference

d = nominal diameter of tube

σ = hoop stress

E = modulus of elasticity of material

For compressive stress on the tube:

$$G_{max} = 3900 \times 10^6 \text{ Pa (compressive strength of } \alpha\text{-SiC)} \qquad [25]$$

$$E = 410 \times 10^9 \text{ Pa (modulus of elasticity)} \qquad [26]$$

$$\epsilon_{max} = \frac{\Delta d_{max}}{d} = \frac{\sigma_{max}}{E} = \frac{3900 \times 10^6 \text{ Pa}}{410 \times 10^9 \text{ Pa}} \qquad [27]$$

$$\frac{\Delta d_{max}}{d} = 9.512195 \times 10^{-3} \qquad [28]$$

If the nominal outside diameter of the tube is 100.95 mm (3.9746"), then

$$\Delta d_{max} = 9.6 \times 10^{-1} \text{ mm } (3.78 \times 10^{-2} \text{ in)} \qquad [29]$$

However, if the contact is not perfect and only 1/10 of the area contacts, then

$$\Delta d_{max} = 9.60 \times 10^{-2} \text{ mm } (3.78 \times 10^{-3} \text{ in)} \hspace{2cm} [30]$$

Finally as an added measure of safety, an engineering safety factor is added to insure that parts do not crack. Therefore for a tube in compression $\Delta d_{max} = 7.06 \times 10^{-2}$ mm $(2.78 \times 10^{-3}$ in).

Similarly, for tensile stress on the tube:

$$\sigma_{max} = 350 \times 10^6 \text{ Pa} \hspace{2cm} [31]$$

$$\epsilon = 410 \times 10^9 \text{ Pa} \hspace{2cm} [32]$$

$$\epsilon_{max} = \frac{\Delta d_{max}}{d} = \frac{\sigma_{max}}{E} = \frac{350 \times 10^6}{410 \times 10^9} \hspace{2cm} [33]$$

$$\Delta d_{max} = 8.10 \times 10^{-2} \text{ mm } (3.19 \times 10^{-3} \text{ in.) if all area contacts.} \hspace{0.5cm} [34]$$

If 1/10 of the area contacts, then $\Delta d_{max} = 8.05 \times 10^{-3}$ mm $(3.17 \times 10^{-4}$ in).

Another technical challenge arose in assembling the ceramic components. With ceramic materials, the concept of compression fitting needs to be modified because they are much more brittle than metals and would fracture rather than elastically or plastically deform. Therefore, the concept of shrink fitting rather than the concept of compression fitting is used. In shrink fitting, the outside component is heated until there is clearance between components. The components are then assembled. Once the outer component cools, clearance will no

longer exist. Precise alignment of components is required so that misalignment and fracture of components does not occur.

7.2 Design and Selection of the High Temperature Wear Facility Drive Mechanism

In the design of a drive mechanism for the High Temperature Wear Facility, two important factors are to minimize machine vibration and to maintain overall machine alignment. The drive motor and alignment system should be chosen so that vibrations are minimized and alignment is maintained.

7.2.1 Selection of a Drive Motor

Several types of motor drives are commonly available: gear drive, direct motor drive, toothed belt drive, v-belt drive, O-ring drive, and several other drive motor types. Geared drives transmit vibration because of the engagement and disengagement of gear teeth. Toothed-belt drives produce vibrations from the engagement and disengagement of belt teeth. Direct drive assemblies transmit motor and line vibrations throughout the wear test assembly. Therefore, the drive that produces the least amount of vibration, the O-ring drive was chosen. Drives of this type are used in precision grinding processes in which vibrational transients are minimized.

7.2.2   Selection of an Alignment System

Again in this area, the maintenance of precise alignment without the transmission and introduction of vibration is essential.   In the precision grinding industry, air bearing spindles which maintain both precise alignment and frictionless contact are utilized.   Such a precise spindle was used in the High Temperature Wear Facility.   A general schematic of the drive system is presented in Figure 16, and a more complete description of this part of the apparatus is given in the Overall Design Presentation portion of this work.
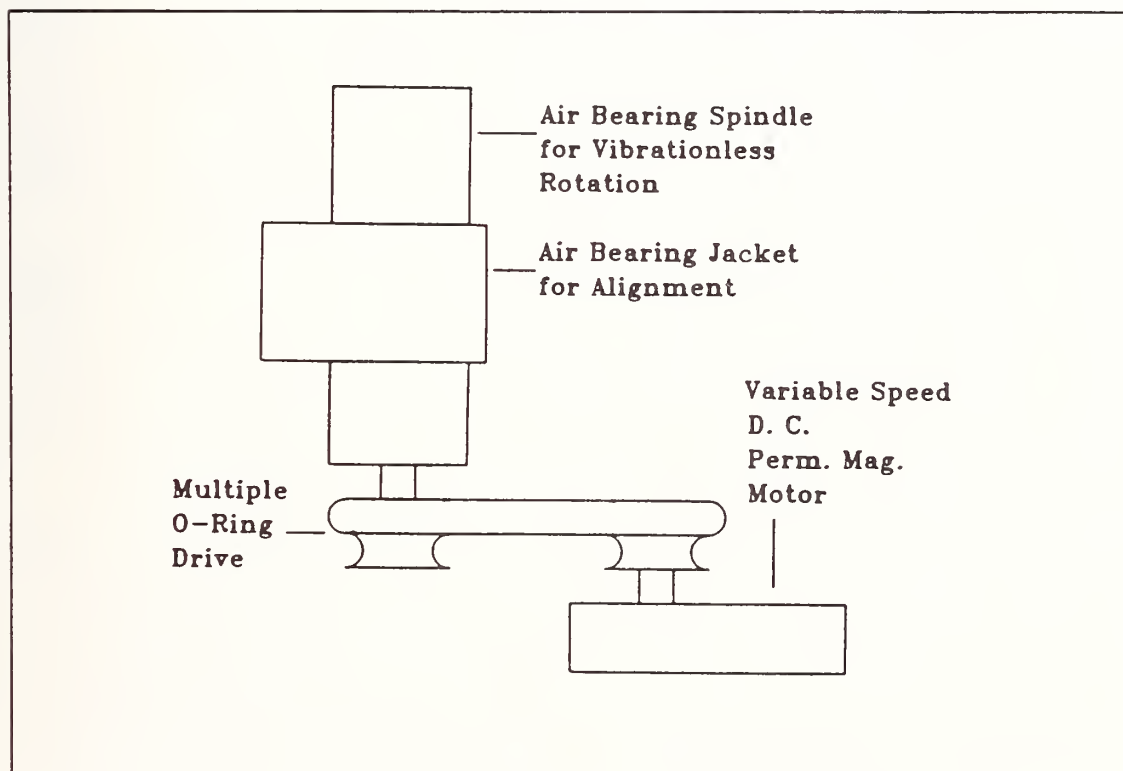
Figure 16.   General Schematic of Drive System

7.3 Design of the High Temperature Wear Facility Machine

Framework

Several basic criteria dictated the design and materials selection
for the High Temperature Wear Facility. High strengths, thermal
stability, machinability, and availability were necessary for the frame
material. Two common structural materials are aluminum and steel. The
strengths properties of aluminum and steel are given below:[117]

Material	Yield Strength (kpsi)	Tensile Strength (kpsi)	Brinell Hardness	Density (lb/in^3)	Melting (°F)
Aluminum	5	13	23	0.098	1190
Steel	38	65	130	0.284	2760

Steel was chosen as a structural material because steel has a
higher strength, hardness, and melting point than aluminum. Thus,
steel provides better protection in the event of a failure in the
system insulation. To assure that the frame would provide safe and
secure support, square steel tubing and multiple design redundancies
were designed into the framework.

Chapter 8

DESCRIPTION OF THE HIGH TEMPERATURE WEAR FACILITY

This chapter describes, in simple schematics, the design of the High Temperature Wear Facility. Overall schematics of the wear tester are shown in Figures 17 to 19. This can be divided into the following components/assemblies. They are the: 1) lower ceramic specimen holder assembly, 2) upper ceramic specimen holder assembly, 3) high temperature furnace, 4) air bearing spindle and loading mechanism assembly, 5) unidirectional motor assembly, and 6) frame assembly. Finally, after showing each of the assemblies separately, the major assemblies will be placed into the frame of the High Temperature Wear Facility to give the reader some sense of spatial relationships.

Figure 20 gives a general schematic of a pin-on-disk configuration. In the High Temperature Wear Facility, a similar configuration exists in which a rotating disk contacts a stationary pin or ball specimen.

The disk specimen is held by the lower ceramic specimen holder assembly. This assembly consists of 3 major components, A) a metallic arbor which fits into a rotating spindle, B) a ceramic tube which is connected to the arbor, and C) the ceramic disk specimen holder. Figure 21 describes the lower assembly in a three-dimensional view. The arbor connects a rotating spindle with the high temperature components which protrude into the high temperature zone of the
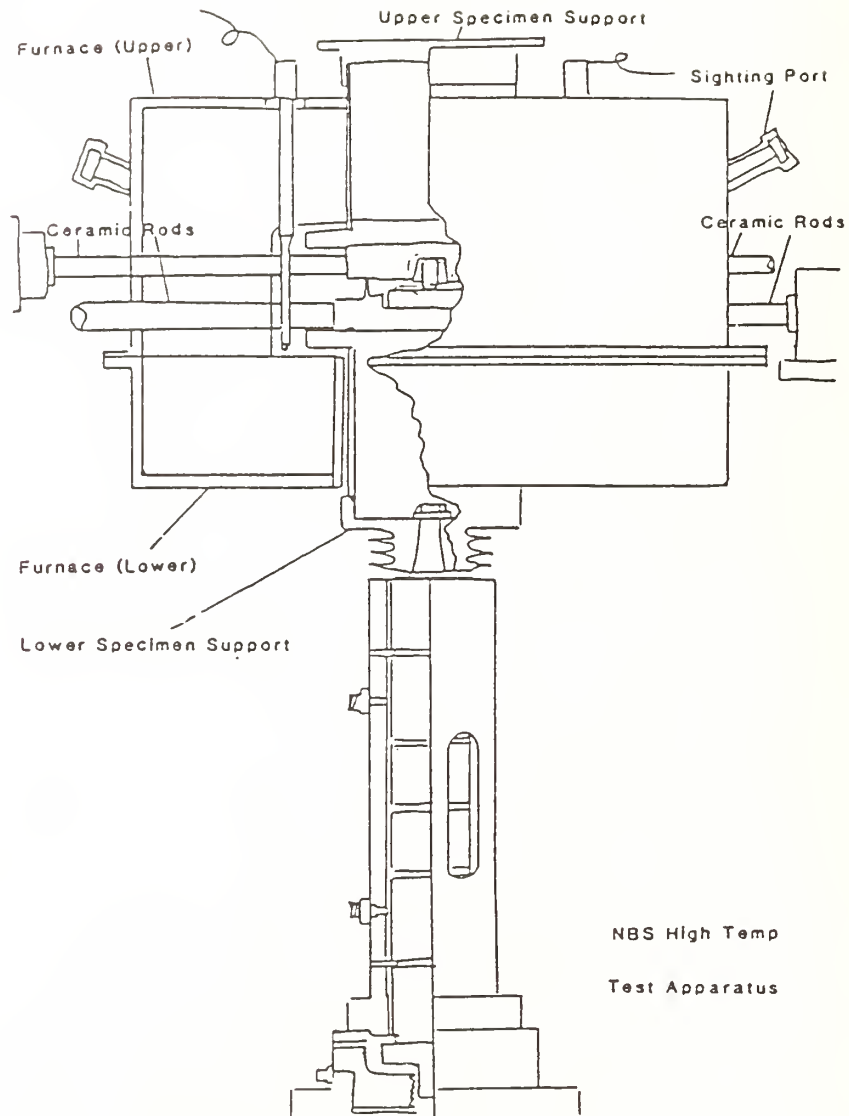
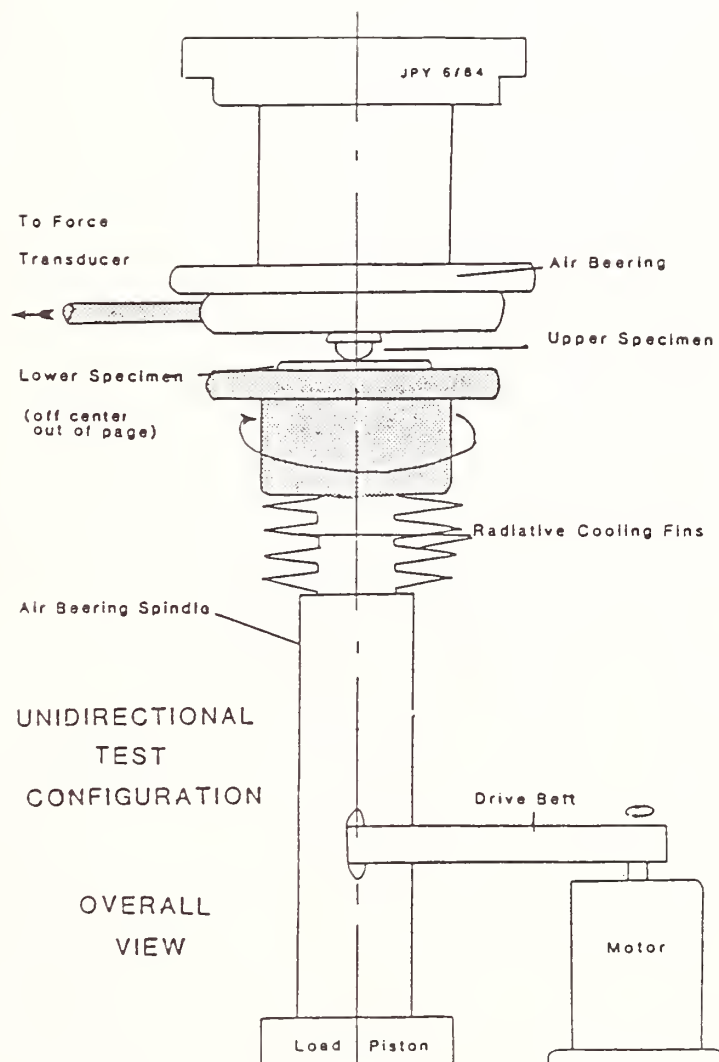Figure 17.   Overall Schematic Diagram of the Wear Tester

Figure 18.   Unidirectional Test Configuration
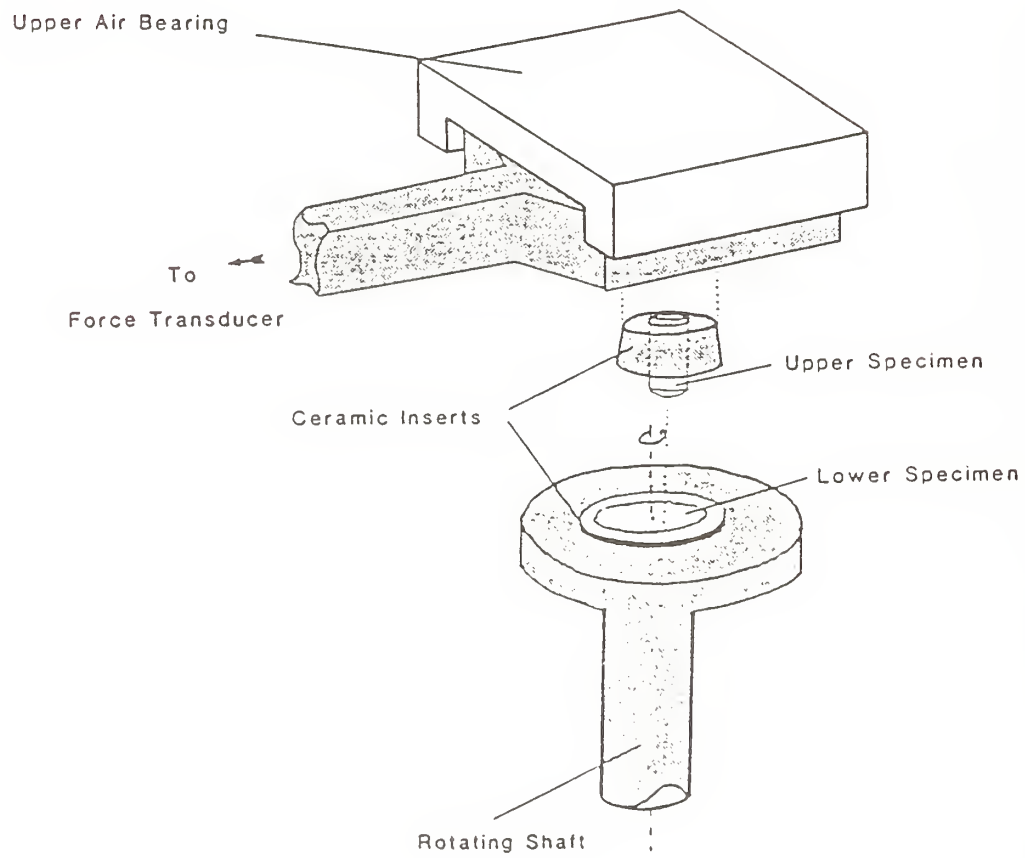
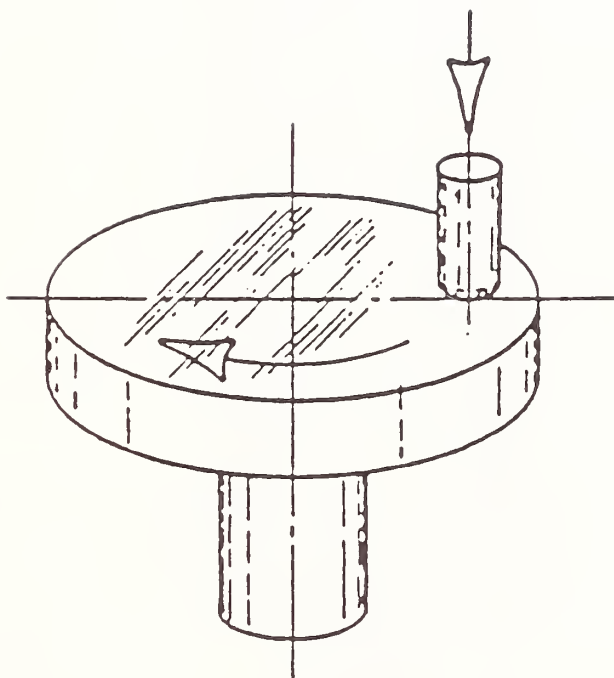Figure 19. Unidirectional Wear Test Configuration
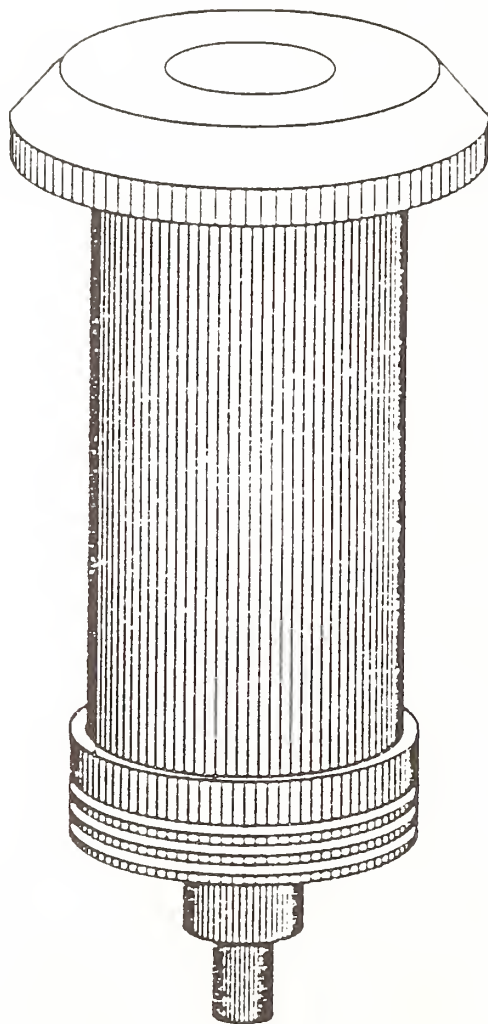
Figure 20. Pin-on-Disk Configuration

Figure 21.   Lower Ceramic Specimen Holder Assembly

facility. Connected to the arbor at the upper surface is a ceramic tube. The arbor and tube are joined through careful design of an interference fit between the tube and the arbor. Connected to the top of the ceramic tube is the disk specimen holder. This specimen holder is constructed out of a ceramic material and will be placed in the high temperature zone of the facility. To connect the specimen holder to the ceramic tube, a very carefully designed ceramic-ceramic interference fit was designed.

The upper specimen holder assembly, which holds the pin or ball specimen, consists of four major components. These are a) the upper specimen sample holder (Figure 22), B) the hydrostatic bearing mount (Figure 23), C) the ceramic tube, and D) the Inconel topcap. The upper specimen holder is constructed out of a ceramic material and is the riding piece in the hydrostatic gas bearing. This bearing was designed to maintain a frictionless contact within the high temperature zone of the facility. Connected to the upper specimen holder is a ceramic rod which extends outside of the high temperature zone so that friction can be measured.

The upper surfaces of the sample holder are machined to ultra-high precision to match the mating surface of the hydrostatic gas bearing mount. This mount is made of the same material as the sample holder so that the effect of differential thermal expansion is minimized. Connected to the hydrostatic bearing mount is a ceramic tube. This ceramic tube is designed to have an interference fit with the hydrostatic bearing mount. Finally, to complete the upper assembly, an Inconel topcap is connected to the tube by means of a ceramic-metal
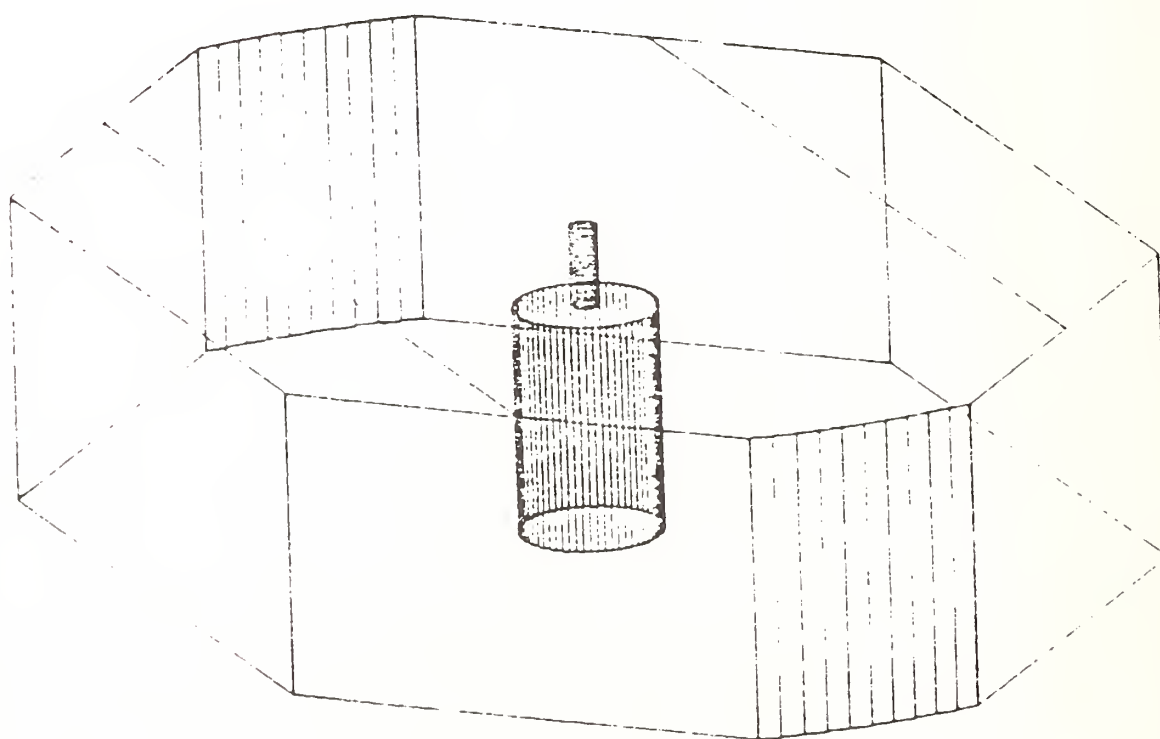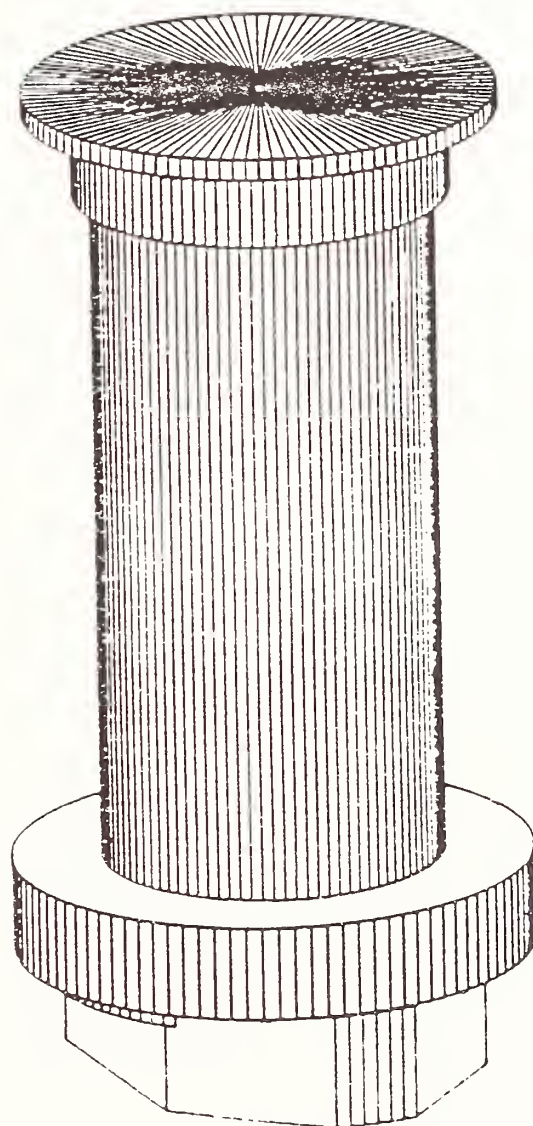
Figure 22. Upper Sample Holder Diagram

Figure 23. View of Complete Upper Assembly

interference fit. The upper assembly is bolted to a plate which is connected to a translation weigh which is, in turn, bolted to the frame of the facility.

The high temperature furnace is another major component of the facility. The ceramic upper and lower assemblies fit into the specially designed furnace. This furnace, which can be split into left and right halves for specimen access, was specially designed and consists of two major components: A) the main furnace and B) the furnace annex. The furnace contains several bayonet type SiC heating elements specially designed to operate at temperatures to 1500°C. Figure 24 gives a front on view of the furnace chamber, furnace annex, and heating elements. A distinction should be made between the main furnace chamber and the lower furnace annex for the following reason: The furnace annex, which is located below the main furnace chamber, remains fixed to the frame directly and cannot traverse side to side. The main furnace chamber is attached to the translation weigh along with the upper ceramic assembly. This allows side-to-side translation so that off center testing can be done for the pin-on-disk configuration.

Next comes the air bearing spindle and loading mechanism assembly. Below the Inconel arbor in Figure 25 is the air bearing spindle and loading mechanism assembly. This assembly allows rotation of the lower (disk) assembly as well as applies a normal load to the specimen contact. The assembly consists of three main parts: A) the linear air jacket, B) the air bearing spindle, and C) the loading piston. The linear air jacket provides an air film which maintains precise spindle
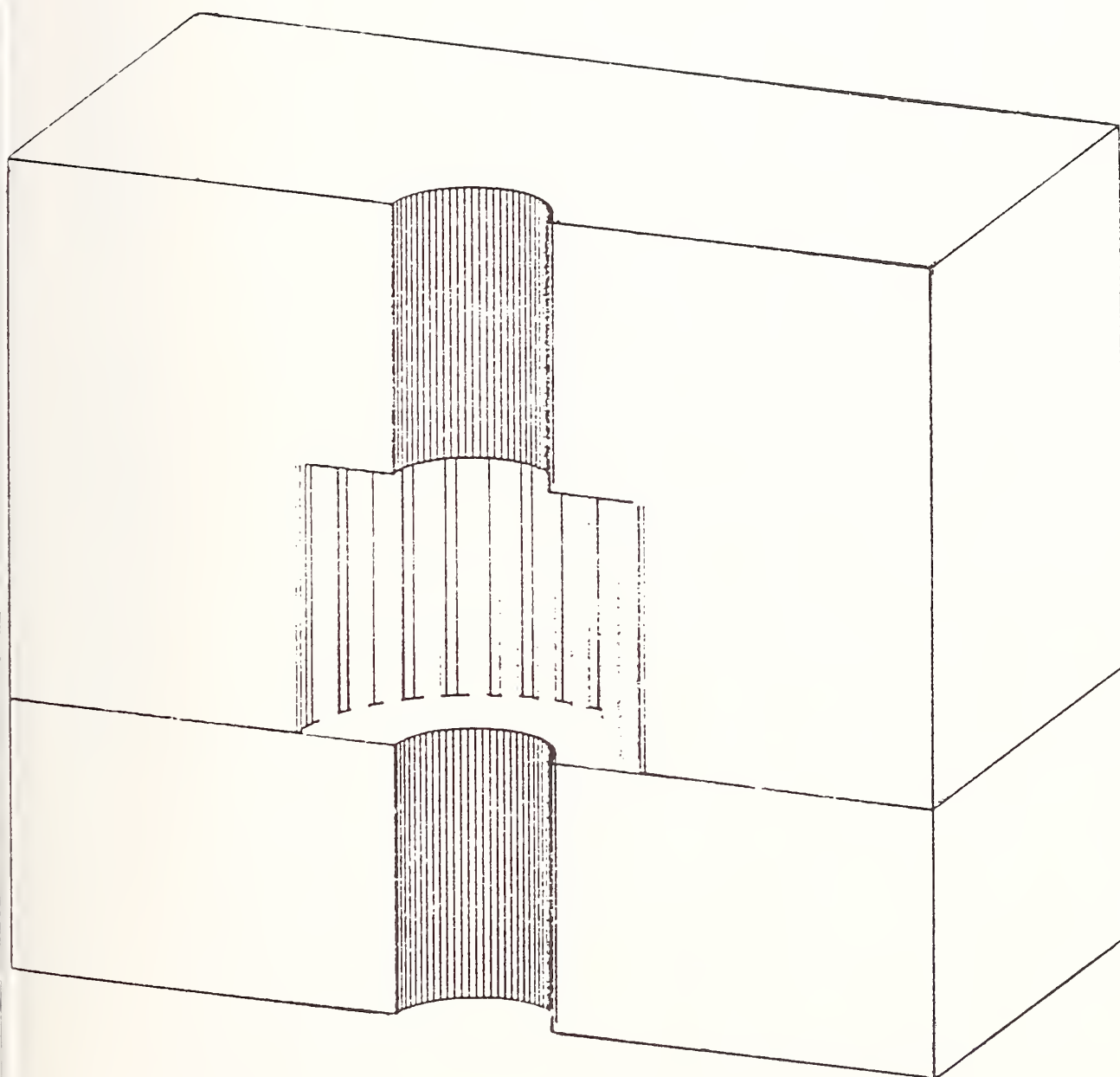
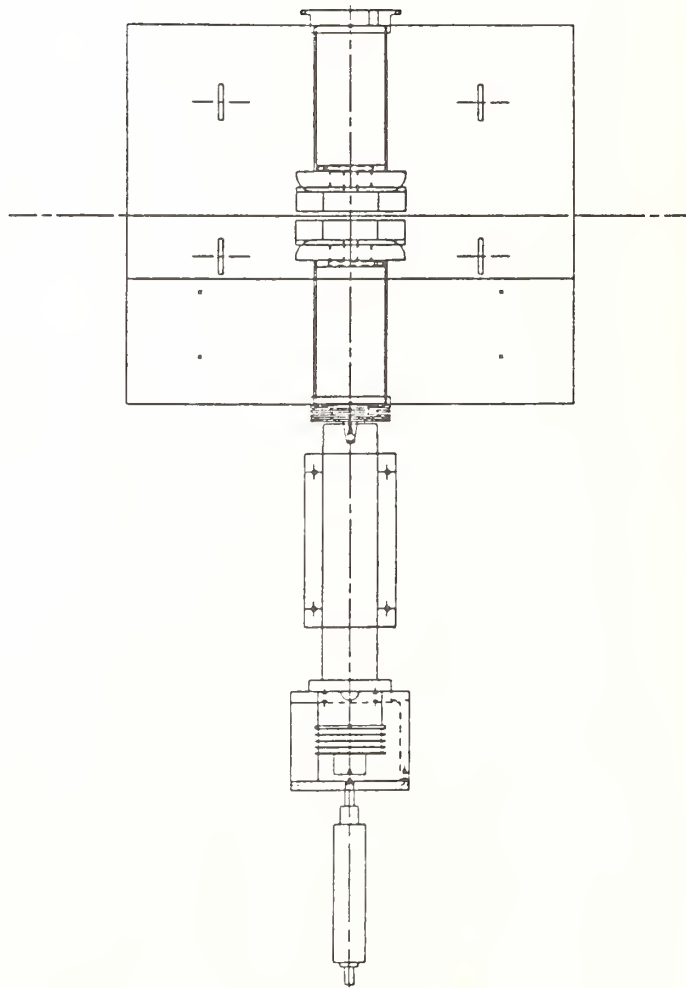Figure 24.   Furnace Chamber and Heating Elements

Figure 25. Design Layout - Upper and Lower Assemblies and Furnace

alignment while allowing vertical and frictionless translation of the spindle. The air bearing spindle can rotate and has several internal thrust and journal air bearings. This allows frictionless rotation of the spindle shaft, and, since the spindle is connected to the lower assembly, easy rotation of the disk specimen. An O-ring drive pulley is attached to the lower end of the spindle shaft to allow the driving of the spindle. To facilitate vertical translation of the spindle a pneumatic piston is attached to the bottom of the specially designed spindle extension. This allows an axis loading of the test specimens. Figure 26 shows the complete air bearing spindle assembly.

The unidirectional motor assembly drives the air bearing spindle through the O-ring drive consists of several components. These are: A) the motor, B) speed reducer, C) O-ring drive, D) O-ring belts, and E) base plates. To keep the High Temperature Wear Facility as free from vibration as possible, the motor is mounted on its own base plate and vibrationally isolated from the surroundings through the use of vibration feet. A general schematic of the drive and spindle system is given in Figure 27. A 3-D visualization of the front and side views of the motor and spindle system are given in Figures 28 and 29.

The frame is presented in Figure 30 together with the furnace, motor, and lower drive assembly.
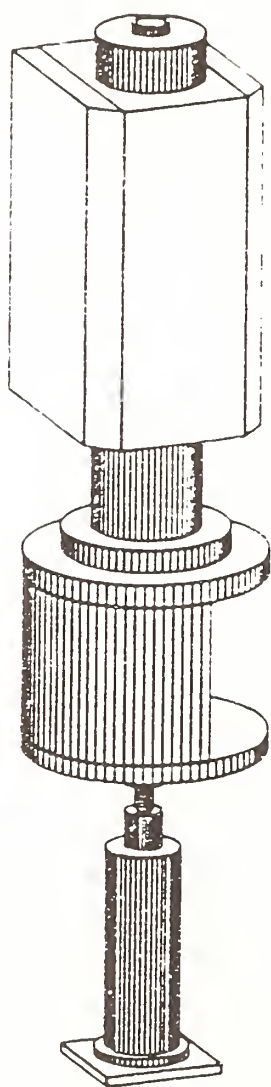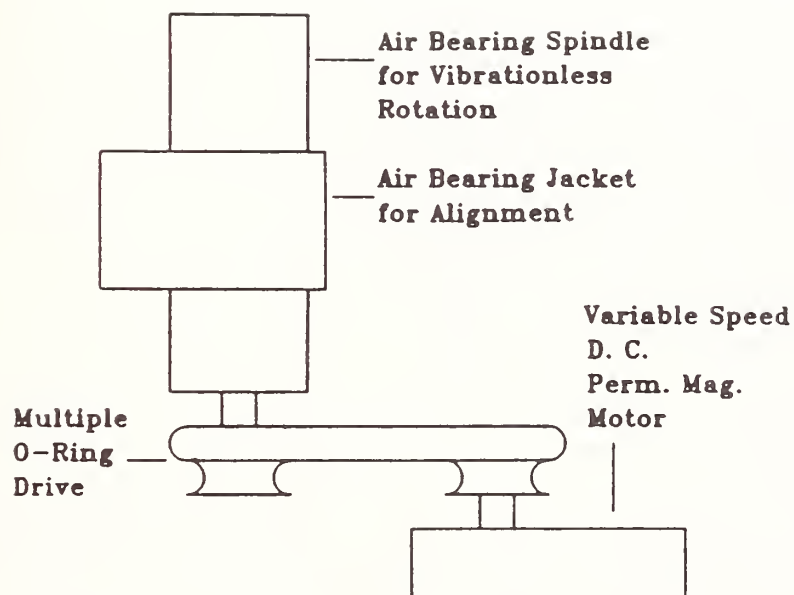
Figure 26.   Air Bearing Spindle Assembly

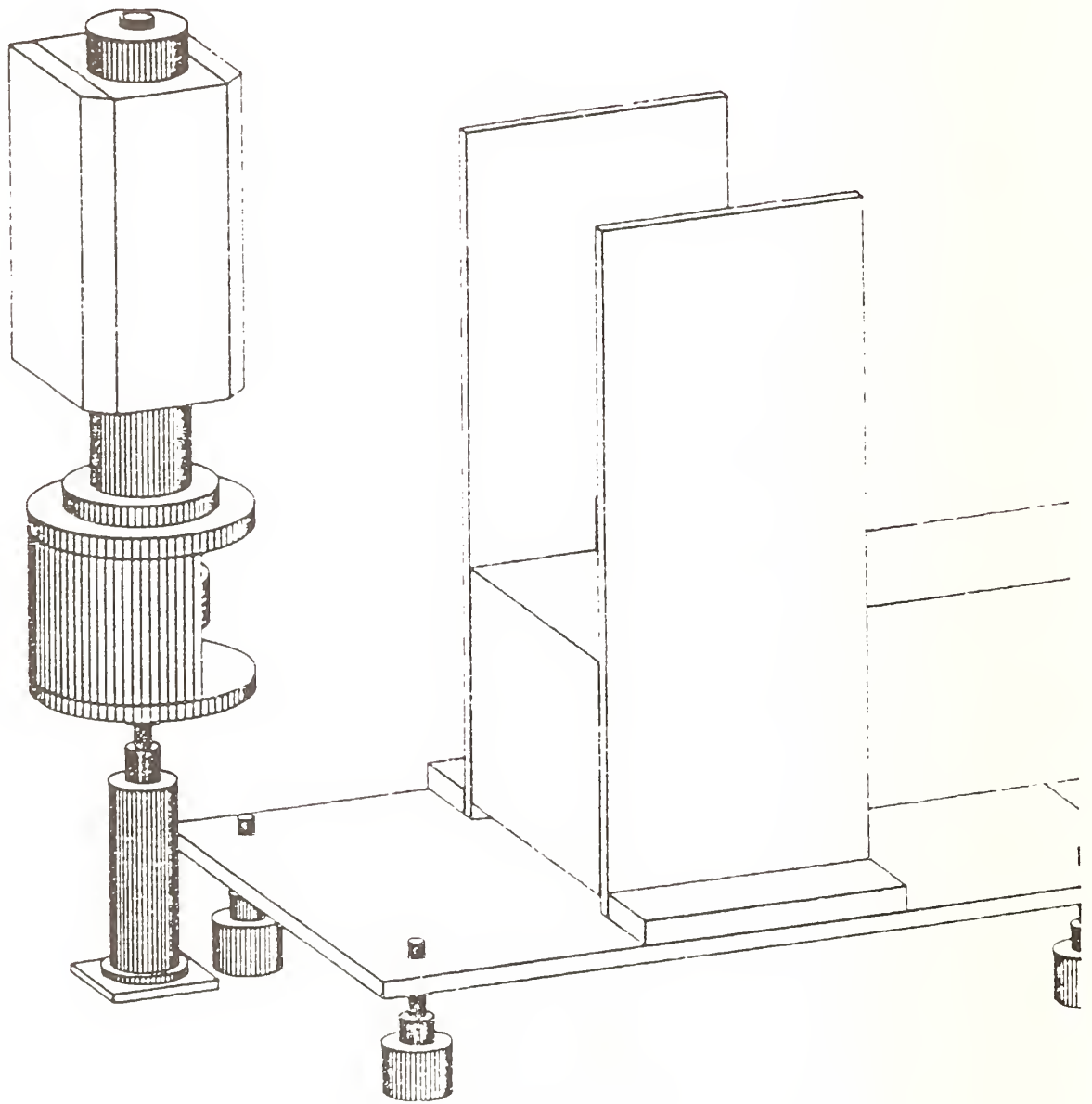Figure 27.   General Schematic of Drive and Spindle System

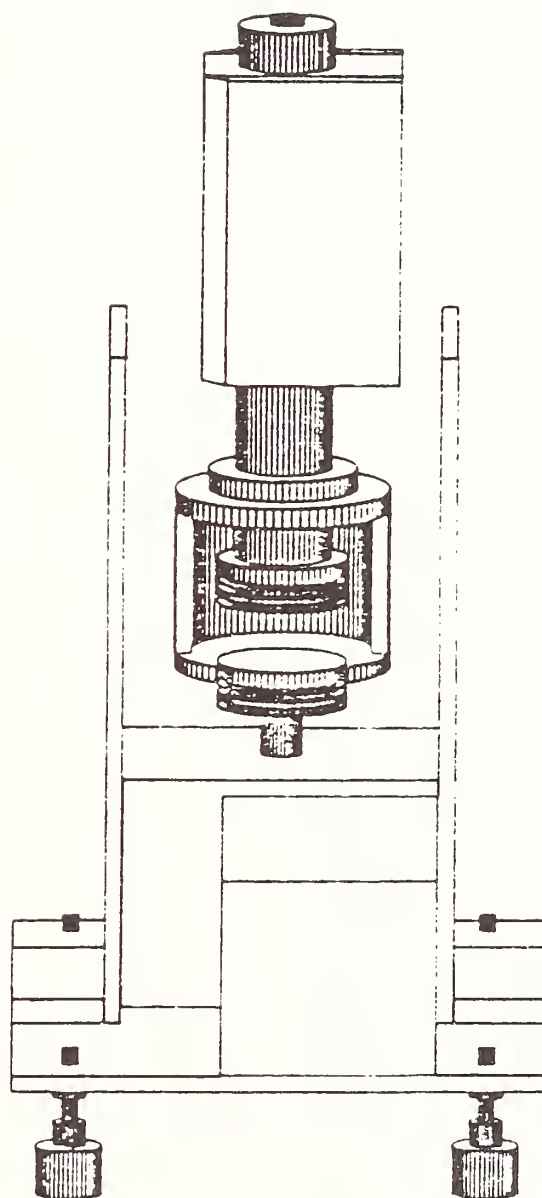Figure 28.   Front View - Motor Spindle System

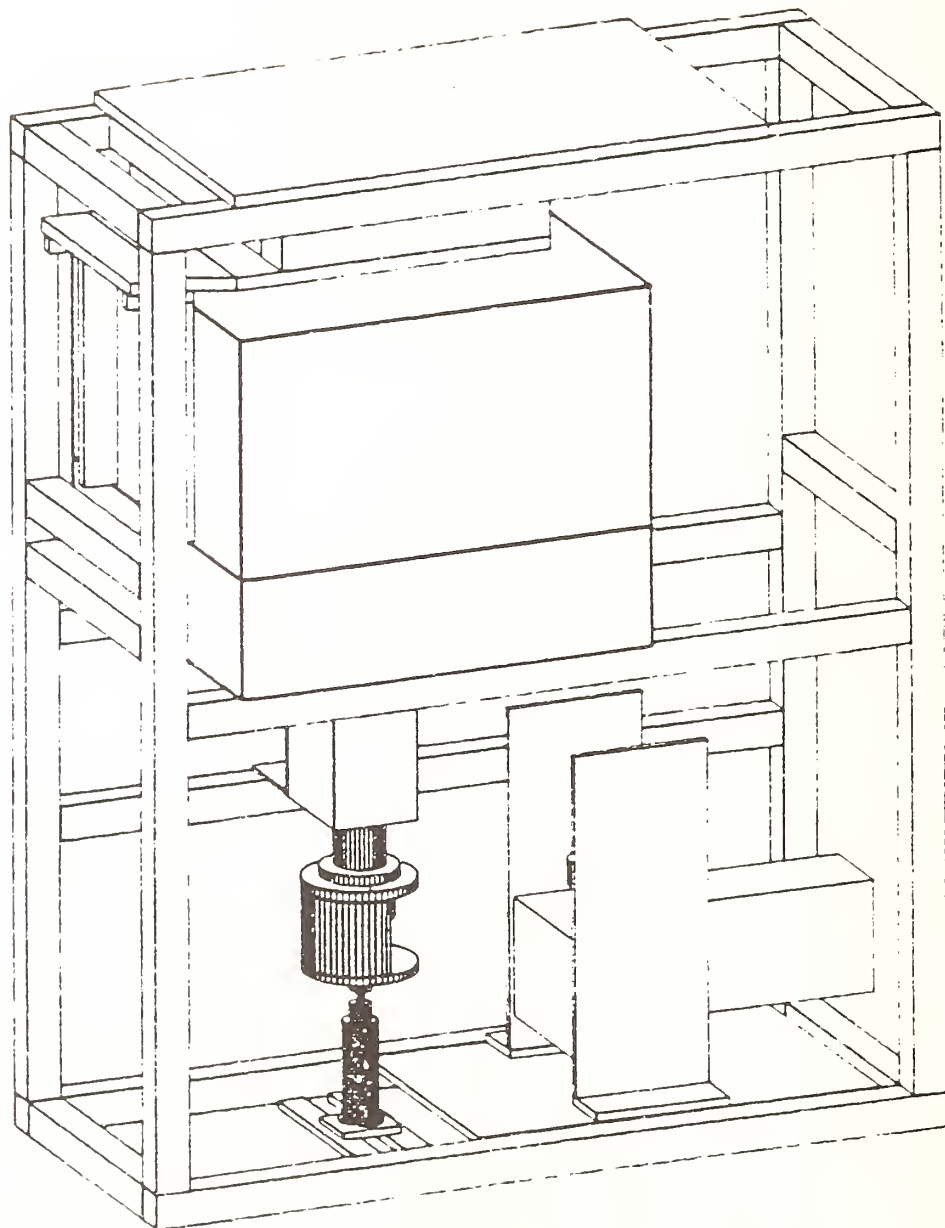Figure 29. Side View - Motor and Spindle System

Figure 30. Addition of Motor Assembly - Front View

Chapter 9

INSTALLATION AND INITIAL TESTING

Equipment installation and demonstration of the High Temperature Wear Facility has been carried out. Because of the number of components and the complexity of installation a summary checklist of the components is given below. Initial experimental results were presented to demonstrate the design integrity.

This section is divided into the following subsections for convenience:

9.1 Installation of Equipment

9.2 Testing of Equipment

9.2.1 Preliminary Testing

9.2.2 Friction Testing - Integrated Mechanical Wear Facility Testing

9.1 Installation of Equipment

Item	Installation Completed (mo/yr)
General	
High Temperature Wear Facility Mounting Feet	5/86
Setco M-50 Dovetail Slide	5/86

Item	Installation Completed (mo/yr)
Heating System/Temp. Meas.	
SiC Helical Heating Element	6/86
Mellen 1500°C Furnace	6/86
Mellen 1500°C Annex	6/86
Eurotherm Furnace Controller	9/86
Mellen PS400 SCR Power Supply	9/86
Omega Engineering DP900 Temp. Meas. Device	10/86
Type S Pt Rd Temp. Meas. Device	12/86
Mikron M6T Infraducer	9/86
Protective Cooling Jacket	9/86
Air Purge Assembly	9/86
Mikron 60TS Digital Temp. Indicator	10/86
Motor Assembly	
Motor Base Plate Assembly	7/86
Motor Leveling Brackets/Side Assembly	7/86
MWU 6 Oil Reducer	7/86
Fincor #9037509 TF	7/86
DC Permanent Magnet Motor	
Motor Controller-Fincor	10/86
10 Turn Potentiometer	10/86
Assembly/Run Stop	
Switch Assembly	

Item	Installation Completed (mo/yr)
Air Bearing Spindle Assembly	
Westwind Air Bearing	10/86
Spindle Model 107	
O-Ring Pulley	
Linear Alignment Air Block	10/86
Loading Modification	9/86
O-Ring Drive	9/86
Accushnet O-Ring EPDM	10/86
Loading Assembly	
ARO Low Friction Cylinder	12/86
0415-1204-030	
Entram ELF-100 Load Button	12/86
Cylinder/Horseshoe Load Connector	12/86
Ceramic Assemblies	
Spindle/Arbor Connector Rod	12/86
Arbor To Tube Assembly	11/86
Zirconia Foam Insulation Lower Assembly	11/86
Lower Sample Holder/Tube Assembly	11/86
Topcap To Tube Assembly	12/86
Tube TO Hydrostatic Mount Assembly	12/86
Gas Supply Tube & Seal System	12/86
Zirconia Foam Insulation Upper Assembly	12/86
Friction Measurement System	

Item	Installation Completed (mo/yr)
Specimen Holder/Ceramic Rod Assembly	12/86
Accelerometer/Force Transducer Bracket	10/86
Ceramic Rod/Radiation Shield Assembly	11/86
Shield Force Transducer Assembly	11/86

Laboratory Modification

Install Water Cooling Lines	2/86
Modify Existing Counter Space	2/86
Special Designed Canope Hooding Installation	3/86
Electrical Modification/Power Supply Installation	3/86
Canope Hood Folding Doors	7/86
Installation of 100 psi Air Lines	3/86
Installation of Argon/Compressed Air Gases	9/86

9.2 Testing of Equipment

9.2.1 Preliminary Testing (OK-√)

Furnace System		Motor System	
Furnace	√	Motor	√
Controller	√	Controller	√
Power Supply	√		
Temperature Measurement System		Loading System & Spindle	
Pyrometer & Supply	√	Pneumatic Cylinder	√
Independent Temp. Meas.	√	Load Cell	√
		Linear Block	√
		Air Bearing Spindle	√
Ceramic Components		Force Transducer System	
Lower Assembly	√	Force Transducer	√
Temp. Ramp-Lower	√	Upper Sample Holder	√
Upper Assembly	√		
Temp. Ramp-Upper	√		

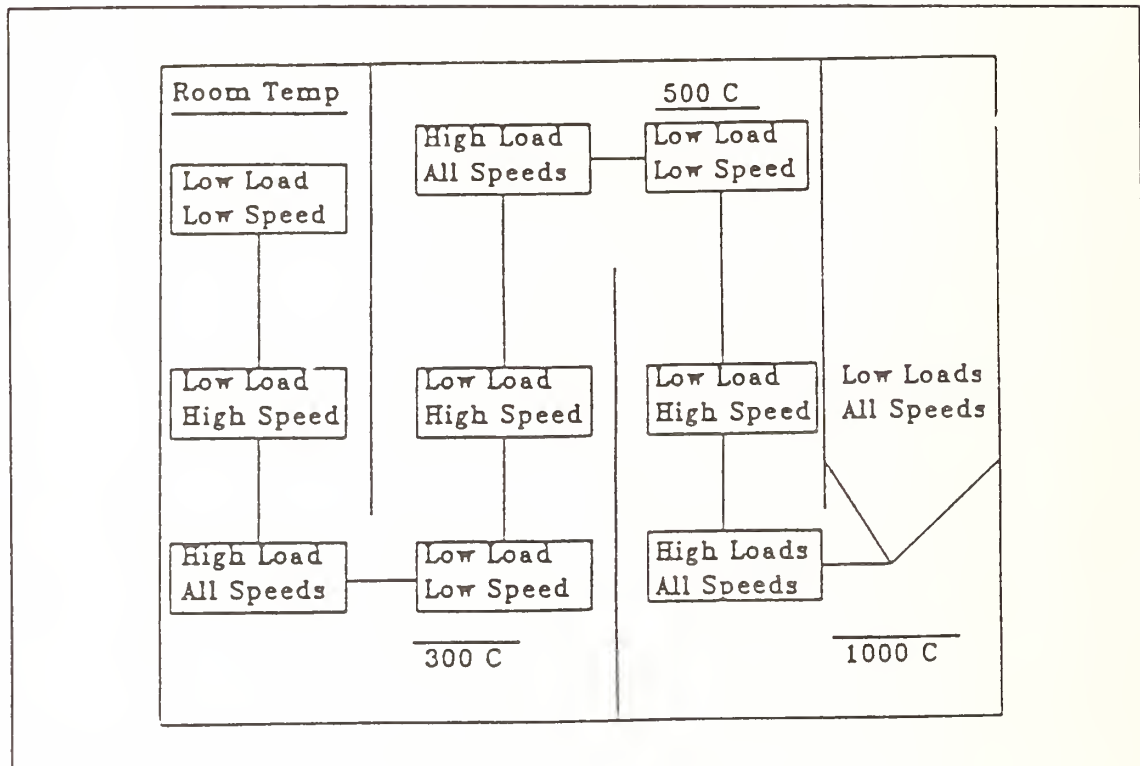9.2.2 Friction Testing - Integrated Mechanical Wear Facility
Testing

Figure 31. Frictional Testing Plan

The overall frictional testing plan for the high temperature wear
facility is shown in Figure 31. Initial testing occurs at room
temperature followed by elevated temperature tests. The friction test
presented consists of a 0.5" diameter, 99.8% sintered aluminum oxide
ball contacting a 99.8% sintered alumina 2" diameter disk. Each of
these specimens were mounted in a ceramic insert which accommodates
differences in thermal expansion between the specimens and the ceramic

specimen holders. To facilitate proper seating of specimen-insert pairs, inserts were fabricated with matching tapers to their specimen holder counterparts.

For the test shown in Figures 36 and 37, specimen contact load was 0.502 kgf (4.92 N), and a rotation rate of 15 rpm at a 19.05 mm contact radius. This gives a linear speed of 29 mm/sec. Test temperature was 20°C and relative humidity at this temperature was 60% at test time. Test specimen preparation consisted of ultrasonic cleaning of specimens in hexane and acetone followed by sonification in a laboratory detergent solution. To remove residual detergent from the surface several rinses with 10 MΩ de-ionized water were done.

Figure 36 shows frictional results from the wear test. The average frictional output level for the test is 298 mV output (0.135 kgf). Coefficient of friction for this wear test is 0.27 which is consistent with alumina four-ball data run under same conditions with similar cleaning procedures. Figure 37 shows a typical vibration frequency scan for the vibration due to friction. As can be seen on the figure, vibrational levels drop dramatically as frequency is increased. This is to be expected in a system in which severe wear of the specimen does not occur and is consistent with anticipated results.

This result demonstrates the mechanical soundness of the design. High temperature wear data were not available due to the unexpected failure of a ceramic part which was subsequently sent for repair. The furnace and the high temperature capability was separately checked and the results are shown in Figure 32. The system operated as expected.

Furnace Test

RT – 100C	15 min
100C	2 hrs
100 – 250C	30 min
250C	2 hrs
250 – 500C	1 hr
500C	2 hrs
500 – 600C	30 min
600C	2 hrs
600 – 800C	1 hr
800C	4 hrs
800 – 1000C	1 hr

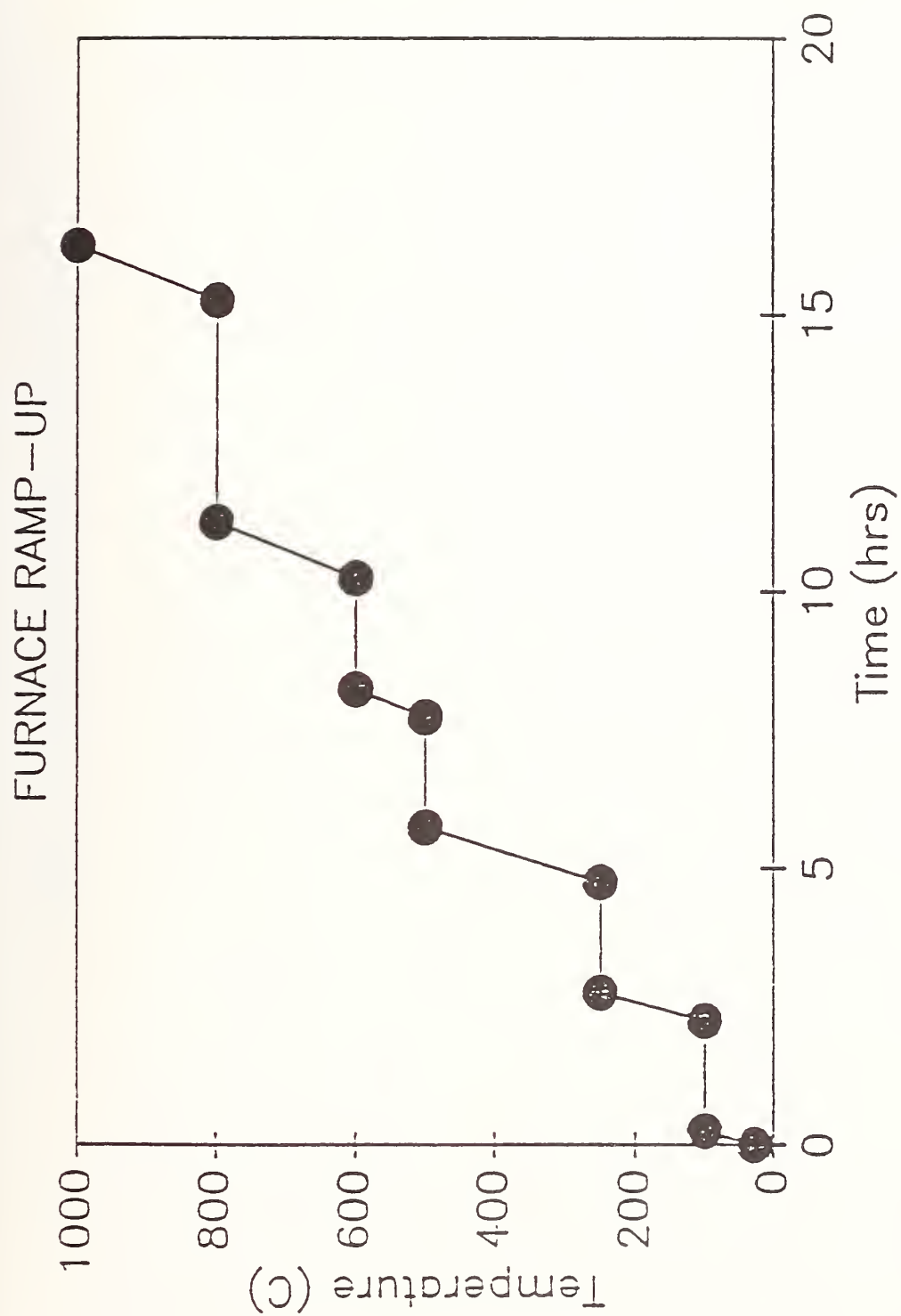Figure 32.   Initial Furnace Testing Ramp Up

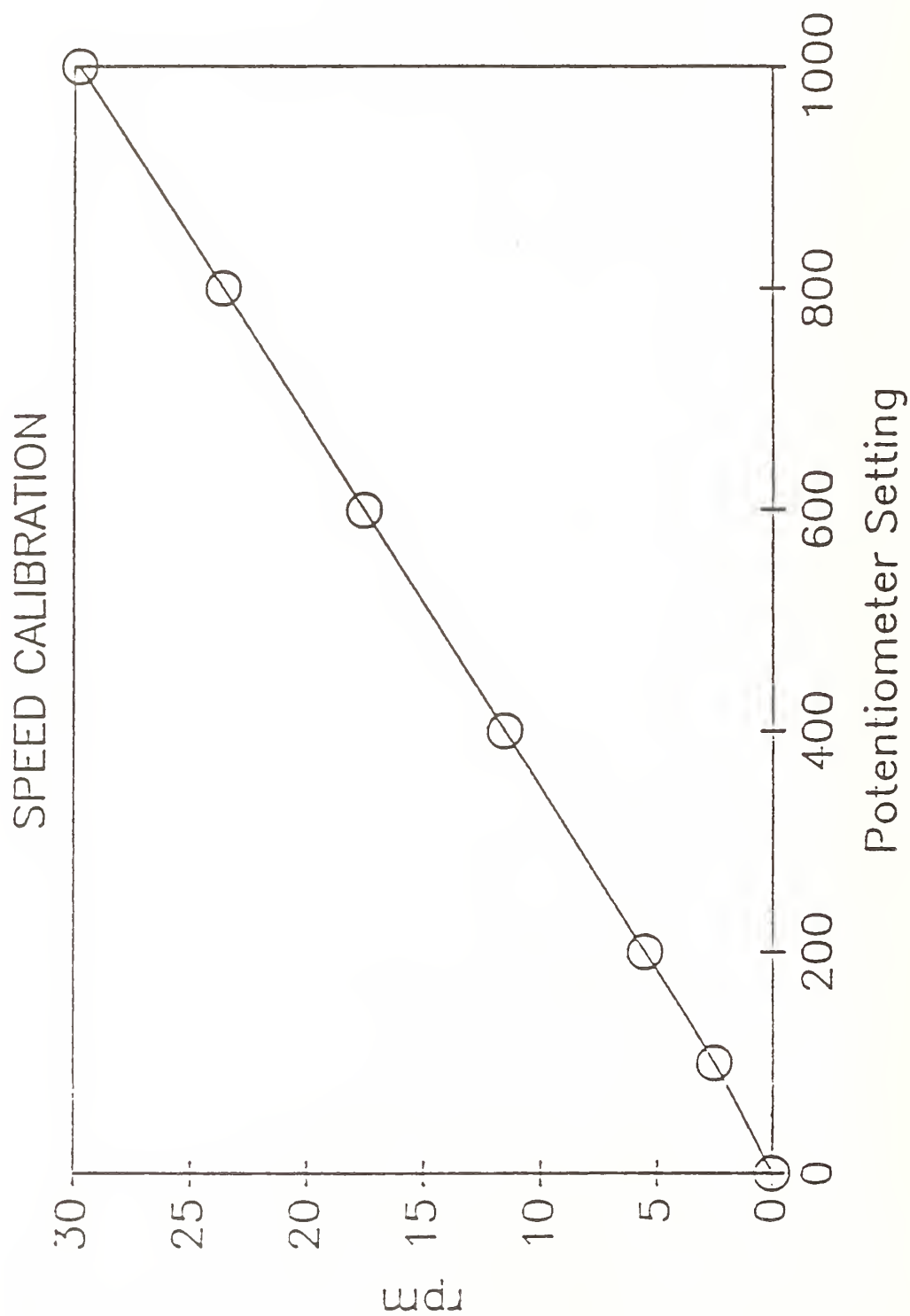Figure 33. Furnace Temperature Ramping Program

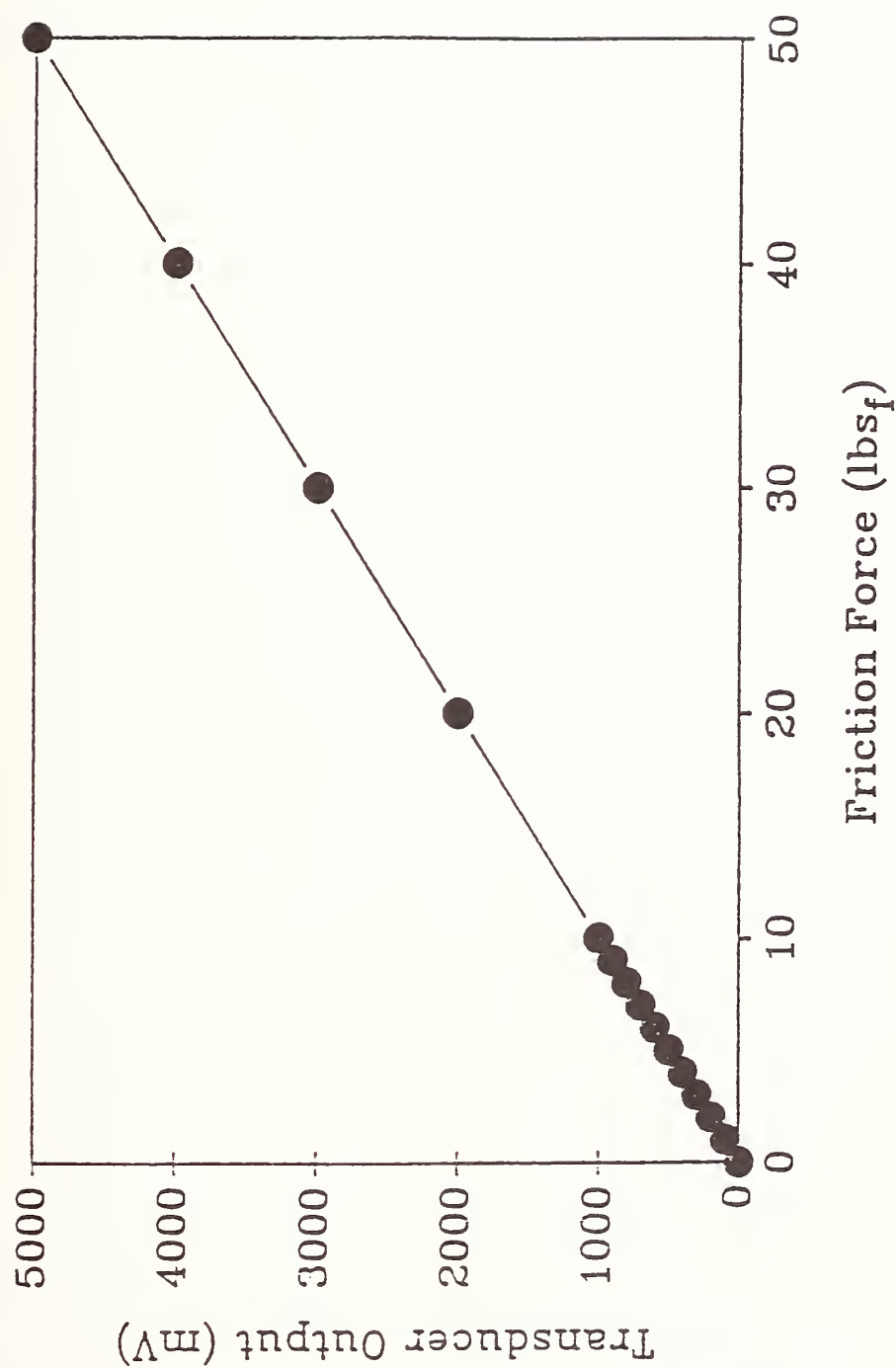Figure 34. Unidirectional Speed Calibration

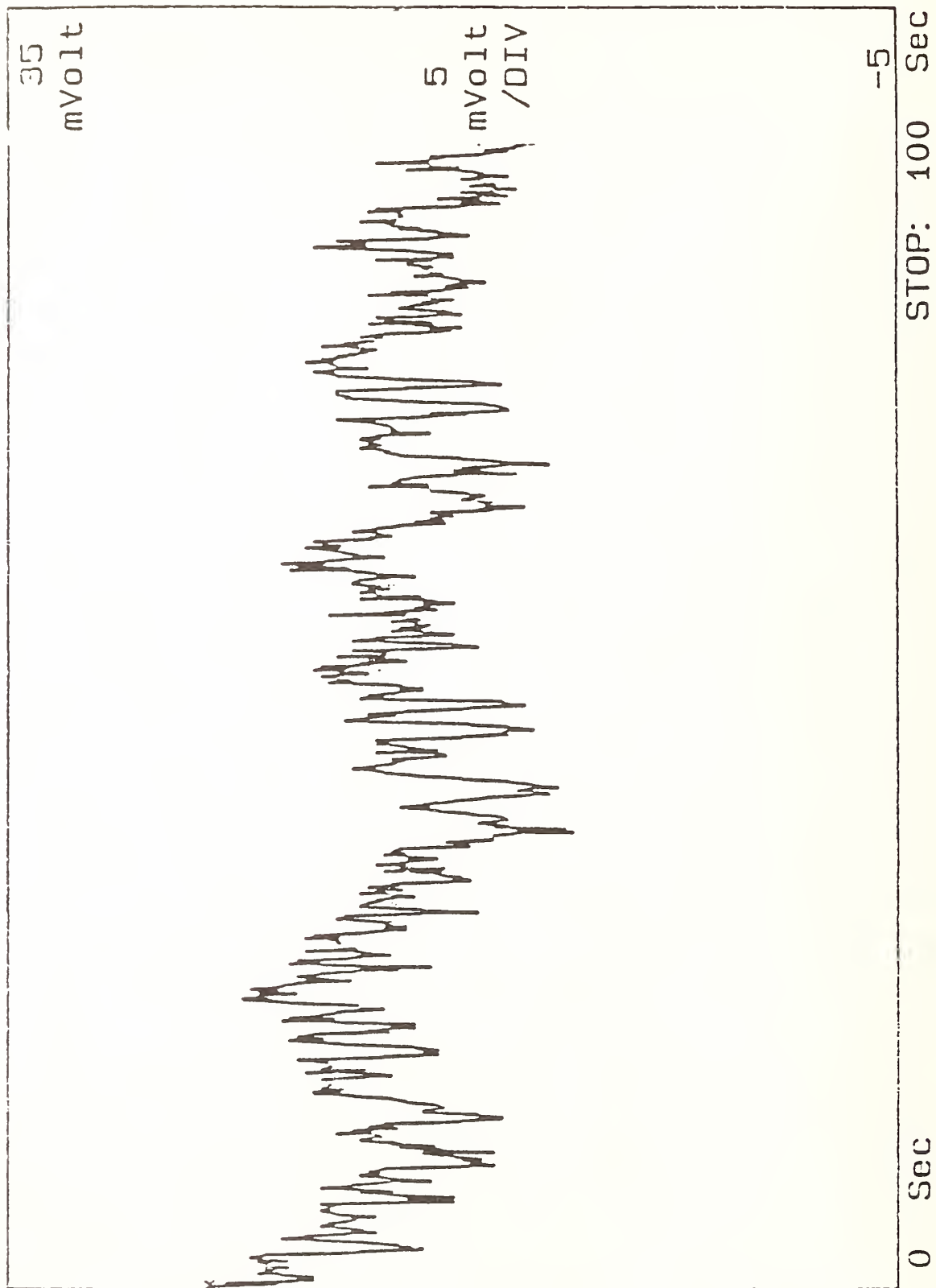Figure 35. Force Transducer Calibration

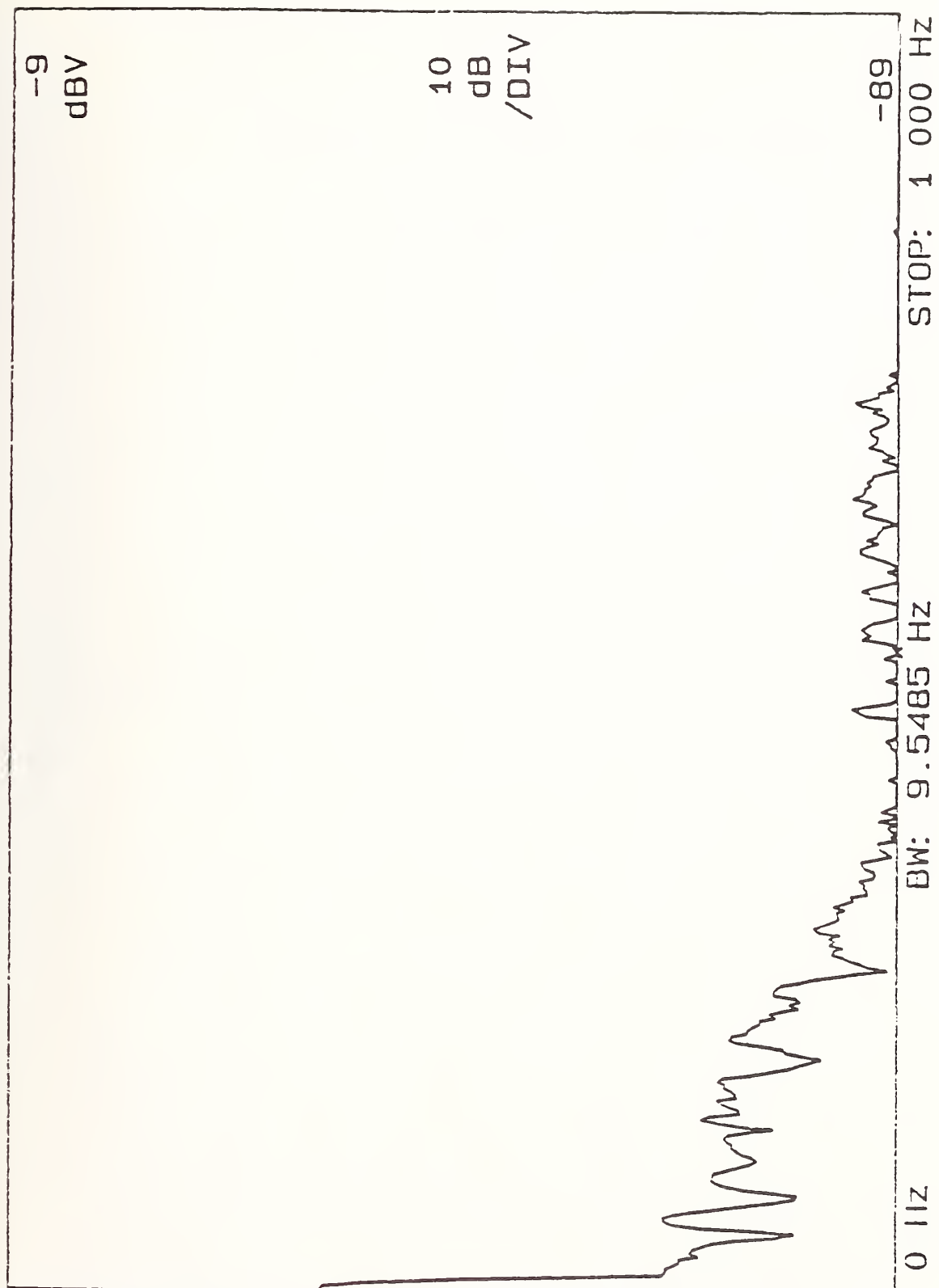Figure 36.   Initial Room Temperature Friction Data

116

Figure 37. Room Temperature Vibrational Friction Transients

Chapter 10

CONCLUSIONS AND RECOMMENDATIONS FOR FUTURE WORK

The design and development of the High Temperature Wear Facility represents a unique task in the field of tribology. In the design of this state-of-the-art tribological test apparatus, several new and novel design techniques were employed in the design of the heat transfer system, the maintenance of alignment and control of vibration, the selection of materials for 1500°C wear tester components, and in mechanical design. This will allow tribological testing of materials over a wide range of temperatures, speeds, and loads.

Because of the unique capabilities of this facility, several programs in engine research will benefit from the availability of the High Temperature Wear Facility. Some of these programs are the automotive gas turbine program, the adiabatic diesel engine program, and the Stirling engine program. However, this facility should not be viewed as a facility which is only useful for the automotive testing industry. The study of the mechanisms of wear of ceramic materials using this apparatus will aid the computer industry in understanding the wear mechanisms in magneto-ceramics, it will help the tool industry in the development of new, highly wear resistant ceramic tools, and it will enable both the high temperature bearing industries and the electronics industry to more fully understand the design of wear resistant tribological components.

Furthermore, in an effort to make the High Temperature Wear Facility more useful, several future modifications should be accommodated. The first of these modifications is to expand the capabilities of this apparatus to include the previously designed reciprocating wear test motions for direct high temperature engine simulation. Also, design expansions to include fretting motions should be implemented, for this will enhance the useability of the facility. As well as these design changes, several other simple design additions can be implemented to enhance the attractiveness of the facility. Modification of the apparatus to allow continuous variance of the contact radius could allow the performance of a tribological test on continuously fresh wear surfaces. This modification is simple and should be implemented in the future. To accent all of the above design capabilities, computer data acquisition, analysis, and control of the High Temperature Wear Facility should be fully explored.

For immediate testing, the use of the High Temperature Wear Facility to develop a model of wear for a ceramic material should be explored. In such a model, the phase transformations due to the tribological contact of test specimens, and the generation of new surface and bulk chemical species due to the interactions of the tribo-surfaces should be examined. In examining these parameters, a more effective understanding of the kinetics and the thermodynamics of the high temperature tribological contact may be possible. Since tribological contact is a highly non-equilibrium occurrence, friction and wear models which incorporate the non-equilibrium thermodynamic transport equation may be useful. If such a model can be formulated, a

major advance in the tribological design of ceramic components will be realized.

REFERENCES

1. Dowson, D., "History of Tribology," NY: Longman, Inc., p. 15.

2. Dowson, D., "History of Tribology," NY: Longman, Inc., p. 23.

3. Dowson, D., "History of Tribology," NY: Longman, Inc., p. 26-37.

4. "Market and Technical Survey of the International High Technology Ceramics Industry," Chemical Hitech, Inc., 15 Avenue Victor Hugo, 75116 Paris, France, 1985.

5. Technological and Economic Assessment of Advanced Ceramic Materials, Vol. 1: Summary and Conclusions, Charles River Associates, Inc., August 1984, p. 26-27.

6. Special Report on Glass Ceramic Composites: Broadening Matrix Technology, Future Tech, No. 13, July 1986, p. 8.

7. Special Report on Glass Ceramic Composites: Broadening Matrix Technology, Future Tech, No. 13, July 1986, pp. 37-38.

8. L. B. Sibley and C. M. Allen, "Friction and Wear Behavior of Refractory Materials at High Sliding Velocities and Temperatures," Wear, 5, 1962, pp. 312-332.

9. L. B. Sibley and C. M. Allen, "Friction and Wear Behavior of Refractory Materials at High Sliding Velocities and Temperatures," Wear, 5, 1962, p. 318.

10. L. B. Sibley and C. M. Allen, "Friction and Wear Behavior of Refractory Materials at High Sliding Velocities and Temperatures," Wear, 5, 1962, p. 319.

11. K. M. Taylor, L. B. Sibley, and J. C. Lawrence, "Development of a Ceramic Rolling Bearing for High Temperature Use," Wear, 6, 1963, pp. 226-240.

12. K. M. Taylor, L. B. Sibley, and J. C. Lawrence, "Development of a Ceramic Rolling Bearing for High Temperature Use," Wear, 6, 1963, pp. 239-240.

13. R. A. Baughman and E. N. Bamberger, "Unlubricated High Temperature Bearing Studies," Transactions of the ASME: Journal of Basic Engineering, June 1963, pp. 265-272.

14. H. M. Dalal, Y. P. Chiu, and E. Rabinowicz, "Evaluation of Hot Pressed Silicon Nitride as a Rolling Bearing Material," ASLE Transactions, 18 (3), 1974, pp. 211-221.

15. J. W. Van Wyk, "Ceramic Airframe Bearings," _Lubrication Engineering_, 31 (11), November 1975, pp. 558-564.

16. J. Blackwell, "The Effects of High Temperature Operation on Rolling Bearing Materials," _Wear_, 56 (1979), pp. 131-138.

17. H. J. Boving, H. E. Hintermann, and G. Stehle, "TiC-Coated Cemented Carbide Balls in Gyro-Application Ball Bearings," _ASLE Preprint_ No. 81-LC-4C-3, 5 pages.

18. B. Bhushan and L. Sibley, "Silicon Nitride Rolling Bearings for Extreme Operating Conditions," _ASLE Preprint_ No. 81-LC-4C-2, 11 pages.

19. J. W. Lucek, L. B. Sibley, and J. W. Rosenleib, "Severe Environmental Testing of Silicon Nitride Rolling Elements," _DCASR Report_ No. N00019-77-C-0551. Final Report for 30 December 1977 -2 March 1979, 83 pages.

20. G. W. Hamburg and W. F. Prusaitis, "Ceramic Mainshaft Roller Bearing Performance in a Gas Turbine Engine," _DTIC Report_ MIPR-AMRDL-75-5, (Grant No. N00140-76-C-404), February 1979, 40 pages.

21. T. M. Yonushonis, "Dry Lubrication of High Temperature Silicon Nitride Rolling Contacts," Final Report for 12 September 1979 - 12 September 1980, _DTIC Report_ No. AT80C040, 78 pages.

22. T. M. Yonushonis, "Solid Lubricated Silicon Nitride Bearings at High Speeds and Temperatures - Phase I," N0019-80-C-0515, _DTIC Report_ No. 82-0S26-012, February 2, 1982, 67 pages.

23. A. O. Weilbach, "High Temperature Bearing and Dry Lubrication Concepts - Phase I," Naval Contract No. N00014-82-C-0248, DARPA Order No. 4477/1-8-82, _DTIC Report_ No. 82-11-12-053, September 1982, 91 pages.

24. Highway Vehicle Systems Contractors Coordination Meeting, Thirteenth Summary Report, October 1977, DOE CONF 771037, UC-96, p. 202.

25. Highway Vehicle Systems Contractors Coordination Meeting, Thirteenth Summary Report, October 1977, DOE CONF 771037, UC-96, p. 202.

26. Highway Vehicle Systems Contractors Coordination Meeting, Thirteenth Summary Report, October 1977, DOE CONF 771037, UC-96, p. 213.

27. G. M. Thur, "Department of Energy Automotive Heat Engine Program," _SAE Technical Paper Series_, No. 780698, August 1978, 9 pages.

28. D. J. Godfrey, "The Use of Ceramics for Engines," Materials & Design, 4, June/July 1983, pp. 759-765.

29. M. E. Woods and I. Oda, "PSZ Ceramics for Adiabatic Engine Components," SAE Technical Paper Series, No. 820429, 1982, Society of Automotive Engineers, Inc., 7 pages.

30. R. H. J. Hannink, M. J. Murray, and M. Marmach, "Magnesia-Partially Stabilized Zirconias (Mg-PSZ) As Wear Resistance Materials," Wear of Materials, 1983, NY; ASME Publications, 1983, pp. 181-186.

31. R. S. Storm, T. W. MacBeth, and G. Flynn, Jr., "Silicon Carbide Components for Diesel Engine Applications," SAE Technical Paper Series, No. 831219, August 8-11, 1983, 9 pages.

32. M. Marmach, et al., "Toughened PSZ Ceramics - Their Role as Advanced Engine Components," The Adiabatic Diesel Engine, SAE SP-543, February 1983, pp. 65-72. (830318)

33. W. Bryzik and R. Kamo, "TACOM/Cummins Adiabatic Engine Program," The Adiabatic Diesel Engine, SAE SP-543, February 1983, pp. 21-46.

34. S. Timoney and G. Flynn, "A Low Friction, Unlubricated SiC Diesel Engine," The Adiabatic Diesel Engine, SAE SP-543, February 1983, pp. 11-20. (830313)

35. J. V. Edwards, "Ceramics and the Swing Beam 2 Stroke Diesel for the Automotive Engine," The Adiabatic Diesel Engine, SAE SP-543, February 1983, pp. 47-54. (830315)

36. R. S. Radovanovic, R. Kamo, and K. F. Dufrane, "Tribological Investigations for an Insulated Diesel Engine," The Adiabatic Diesel Engine, SAE SP-543, February 1983, pp. 73-80. (830319)

37. A. Bayoumi, J. Bailey, and J. S. Stewart, "Comparison of the Wear Resistance of Various Grades of Cemented Carbides that may find Applications in Wood Machining," Wear, 89, 1983, pp. 185-200.

38. G. Dixon, R. N. Wright, and M. Lee, "Processes Involved in the Wear of Cemented Carbide Tools," Wear of Materials, 1983, NY: ASME Publications, 1983, pp. 218-226.

39. Y. Enomoto and K. Fujise, "Observation of wear damage of a hot isostatically pressed alumina cutting tool by cathodoluminescence," Wear, 89, 1983, pp. 107-111.

40. A. K. Cattopadhyay and A. B. Cattopadhyay, "Wear Characteristics of Ceramic Cutting Tools in Machining Steel," _Wear_, 93, 1984, pp. 347-359.

41. C. T. Young, P. C. Becker, and S. K. Rhee, "Performance Evaluation of TiN and TiC/TiN Coated Drills," _Wear of Materials, 1983_, NY: ASME Publications, 1983, pp. 235-242.

42. N. Gane and L. W. Stephens, "The Wear and Fracture Resistance of Ceramic Cutting Tools," _Wear_, 88, 1983, pp. 67-83.

43. T. Karaki and J. Watanabe, "Effect of Frictional Heat on Removal Rate in Mechanochemical Polishing of Crystals Used in Electronics," _Wear of Materials, 1983_, NY: ASME Publications, 1983, pp. 227-234.

44. R. Komanduri, W. Laverty, and M. C. Shaw, "Wear of Abrasives in Simulated Hot Grinding," _Wear of Materials, 1977_, NY: ASME Publications, 1973, pp. 475-481.

45. M. P. Hitchiner, E. M. Wilks, and J. Wilks, "The Polishing of Diamond and Diamond Composite Materials," _Wear_, 94, 1984, pp. 103-120.

46. K. Suzuki and T. Sugita, "Characteristics of Magnesium Oxide Single Crystals Polished with Vibrational Sliding in Water," _Wear of Materials, 1981_, NY: ASME Publications, 1981, pp. 518-524.

47. J. D. Ayers and R. N. Bolster, "Abrasive Wear with Fine Diamond Particles of Carbide-Containing Aluminum and Titanium Alloy Surfaces," _Wear_, 93, 1984, pp. 193-205.

48. V. R. Kangun and R. Z. Tsypkin, "Diamond Honing of Hard Non-Metallic Materials," _Vestnik Mashinostroeniga_, 55 (6), 1975, pp. 66-69.

49. R. Uhrig and N. V. Waubke, "Investigations on the fracture behavior and wearing properties of ceramic flooring material," _Ceramic Forum International_, 60 (9/10), 1983, pp. 357-364.

50. Wallbridge and D. Dowson, "The Wear Characteristics of Sliding Pairs of High Density Polycrystalline Aluminum Oxide Under Both Dry and Wet Conditions," _Wear of Materials, 1983_, NY: ASME Publications, 1983, pp. 202-211.

51. D. Chakravorty, _et al._, "Ceramic Bushing for Glass-Fibre Production," _Materials in Engineering_, 2 (3), 1981, pp. 118-123.

52. A. B. van Groenou, "The Sphere-on-Tape: A Quick Test on Wear of Materials Used in Magnetic Recording," _Wear of Materials, 1983_, NY: ASME Publications, 1983, pp. 212-217.

53. J. Sugishita, _et al._, "Variables Influencing Degradation of SiC Abrasive Papers," _Wear of Materials, 1977_, NY: ASME Publications, 1977, pp. 186-193.

54. H. E. Sliney, "Solid Lubricant Materials for High Temperatures - A Review," _Tribology International_, 15 (5), October 1982, pp. 303-315.

55. H. E. Sliney, "Solid Lubricant Materials for High Temperatures - A Review," _Tribology International_, 15 (5), October 1982, p. 310.

56. D. C. Evans and G. S Senior, "Self-Lubricating Materials for Plain Bearings," _Tribology International_, 15 (5), October 1982, pp. 243-248.

57. R. I. Christy, "Dry Lubrication for Rolling Element Spacecraft Parts," _Tribology International_, 15 (5), October 1982, pp. 262-271.

58. M. N. Gardos, "Self-Lubricating Composites for Extreme Environment Applications," _Tribology International_, 15 (5), October 1982, pp. 273-283.

59. R. R. Paxton, "Carbon, Graphite, and Metal-Bonded Molybdenum Disulfide Solid Lubricant Bearings," _Tribology International_, 15 (5), October 1982, pp. 285-292.

60. K. T. Stevens and M. J. Todd, "parametric Study of Solid Lubricant Composites as Ball-Bearing Gages," _Tribology International_, 15 (5), October 1982, pp. 263-302.

61. S. A. Barber and J. W. Kannel, "A Technique in the Evaluation of Thin, Solid film Lubricants under Combined Rolling and Sliding Contact," _ASLE Transactions_, 26 (4), 1983, pp. 487-492.

62. B. Bhushan and L. B. Sibley, "Silicon Nitride Rolling Bearings for Extreme Operating Conditions," _ASLE Preprint_, No. 81-LC-4C-2, 1981, 10 pages.

63. J. Blackwell, "Effects of High Temperature Operation on Rolling Bearing Materials," _Wear_, 56, 1979, pp. 131-138.

64. M. Connelly and E. Rabinowicz, "Detecting Wear and Migration of Solid-Film Lubricants Using Simultaneous Exoelectron Emission," _ASLE Preprint_, No. 82-AM-2A-1, 1982, 5 pages.

65. S. L. Cosgrove, L. B. Sibley, and C. M. Allen, "Evaluation of Dry Powdered Lubricants at 1000 F in a Modified Four-Ball Wear Machine," _ASLE Transactions_, 2 (2), 1959, pp. 217-224.

66. R. D. Dayton and M. A. Sheets, "Evaluation of Grooved Solid Lubricated Bearings," <u>Air Force Aero-Propulsion Laboratory Technical Report</u>, No. AFAPL-TR-76-76, February 1976, 79 pages.

67. R. L. Fusaro, "Geometrical Aspects of the Tribological Properties of Graphite Fiber Reinforced Polyimide Composites," <u>ASLE Transactions</u>, 26 (2), pp. 209-221.

68. R. L. Fusaro, "Tribological Properties and Thermal Stability of Various Types of Polyimide Films," <u>ASLE Preprint</u>, No. 81-LC-4A-2, 1981, 11 pages.

69. R. L. Fusaro, "Effect of Substrate Surface Finish on the Lubrication and Failure Mechanisms of Molybdenum Disulfide Films," <u>ASLE Transactions</u>, 25 (2), pp. 141-156.

70. R. L. Fusaro, "Polyimides - Tribological Properties and Their Use as Lubricants," <u>NASA Technical Memorandum</u>, No. 82959, November 1982, 28 pages.

71. R. L. Fusaro, "Polyimides Formulated from a Partially Fluorinated Diamine for Aerospace Tribological Applications," <u>NASA Technical Memorandum</u>, No. 83339, April 1983, 26 pages.

72. M. N. Gardos and B. D. McConnell, "Development of a High-Load, High-Temperature, Self-Lubricating Composite - Part I: Polymer Matrix Selection," <u>ASLE Preprint</u>, No. 81-LC-3A-3, 10 pages.

73. M. N. Gardos and B. D. McConnell, "Development of a High-Load, High-Temperature, Self-Lubricating Composite - Part II: Reinforcement Selection, <u>ASLE Preprint</u>, No. 81-LC-3A-4, 8 pages.

74. M. N. Gardos and B. D. McConnell, "Development of a High-Load, High-Temperature, Self-Lubricating Composite - Part III: Additives Selection," <u>ASLE Preprint</u>, No. 81-LC-3A-5, 10 pages.

75. M. N. Gardos and B. D. McConnell, "Development of a High-Load, High Temperature, Self-Lubricating Composite - Part IV: Formulation and Performance of the Best Compositions," <u>ASLE Preprint</u>, No. 81-LC-3A-6, 12 pages.

76. S. Gray, "The Development of Lubricants for High-Speed Rolling Contact Bearings Operating Over the Range of Room Temperature to 1200 Degrees Fahrenheit," Progress Report No. 4, <u>DTIC Technical Report</u>, No. AD-275266, for Contract AF-33(161)-6589, 1961, 46 pages.

77. S. Gray and D. S. Wilson, "The Development of Lubricants for High-Speed Rolling Contact Bearings Operating Over the Range of Room Temperature to 1200 Degrees Fahrenheit," Progress Report No. 3, <u>DTIC Technical Report</u>, No. AD-270994, 1961, 37 pages.

78. L. C. Lipp, J. W. Van Wyk, and F. J. Williams, "Development of Solid Lubricant Compact Bearings for the Supersonic Transport," Lubrication Engineering, 29, March 1973, pp. 108-115.

79. B. Longson, "Lubrication of High Temperature Ceramic Materials," Tribology International, 16 (4), August 1983, pp. 221-225.

80. M. Matsunaga, T. Homma, and A. Tanaka, "Investigation of Vapor Adsorption on Molybdenum Disulfide Surfaces by Auger Electron Spectroscopy," ASLE Preprint, No. 81-LC-4A-1, 6 pages.

81. M. Matsunaga, T. Nakagawa, and M. Tennichi, "The Wear and Friction Behavior of Molybdenum Disulfide Compacts," ASLE Preprint, No. 81-LC-3A-1, 4 pages.

82. M. B. Peterson and R. L. Johnson, "Factors Influencing Friction and Wear with Solid Lubricants," Lubricating Engineering, September-October 1955, pp. 325-331.

83. S. J. Radcliffe and A. A. Parry, "The Dispersion of Life of Bonded MoS_2 Solid Lubricant Coatings," Wear, 56, 1979, pp. 203-212.

84. A. Schlosser, "The Development of Lubricants for High-Speed Rolling Contact Bearings Operating Over the Range of Room Temperature to 1200 Degrees Fahrenheit," Progress Report No. 5, DTIC Technical Report, No. AD-277992, 1962, 36 pages.

85. L. B. Sibley, "Silicon Nitride Elements for High-Speed High-Temperature Applications," AGARD Paper Reprinted from Conference Proceedings, 323, 1982, pp. 5-1 to 5-15.

86. G. H. Baile, et al., "Synopsis of Active SKF Research and Development Programs of Interest to the Aerospace Industry," SKF Report No. AL63M003, Sections 14 and 15, July 1, 1963, pp. 48-57.

87. H. E. Sliney, "An Investigation of Oxidation-Resistant Solid Lubricant Materials," ASLE Proceedings - International Conference on Solid Lubrication, 1971, pp. 259-269.

88. R. W. Raylor, "High Temperature Lubricating Process," U.S. Patent, No. 4,316,921, February 23, 1982.

89. J. W. Van Wyk, "Ceramic Airframe Bearings," Lubrication Engineering, 31 (11), November 1975, pp. 558-564.

90. J. W. Van Wyk, "Bearing Lubrication System," U.S. Patent, No. 3,938,868, February 17, 1976.

91. A. O. Wielbach, "High Temperature Bearing and Dry-Lubrication Concepts," Phase I, Final Report, <u>DTIC Technical Report</u>, No. AD-121386, 1982, 97 pages.

92. T. M. Yonushonis, "Dry Lubrication at High Temperature Silicon Nitride Rolling contacts," <u>DTIC Technical Report</u>, No. AD-A095202, November 1980, 78 pages.

93. T. M. Yonushonis, "Final Report Solid Lubricated Nitride Bearings at High Speed and Temperature - Phase 1," <u>DTIC Technical Report</u>, No. AD-A114848, Report No. AT-82D002, February 1982, 67 pages.

94. C. W. Moore, R. L. Brandon, III, and J. P. Smyly, "Bearings," <u>U.S. Patent</u>, No. 3,284,144, November 8, 1966.

95. A. Zacherl, "Air-Supported Bearing for Turbine Engines," <u>U.S. Patent</u>, No. 4,184,720, January 22, 1980.

96. C. W. Lai, "Lubrication System for Stainless Steel Die Casting," M.S. Thesis, The Pennsylvania State University, Department of Chemical Engineering, November 1974, 140 pages.

97. W. Min, "Kinetic Studies of Vapor-Deposited Films on Hot Surfaces," M.S. Thesis, The Pennsylvania State University, Department of Chemical Engineering, August 1980, 93 pages.

98. Neville deGovea Pinto, "High Temperature Vapor Phase Deposition Studies for Organic Liquid Lubricants," M.S. Thesis, The Pennsylvania State University, Department of Chemical Engineering, November 1982, 102 pages.

99. W. H. Gitzen, <u>ed.</u>, <u>Alumina as a Ceramic Material</u>, 1970, American Ceramic Society, Columbus, Ohio, p. 5.

100. W. H. Gitzen, <u>ed.</u>, <u>Alumina as a Ceramic Material</u>, 1970, American Ceramic Society, Columbus, Ohio, p. 5.

101. C. F. Bersch, "Properties of Ceramics for Structural and/or High Temperature Use: Need for Control, Measurement, and Compilation," in Wachtman, T. B., Jr., <u>Mechanical and Thermal Properties of Ceramics</u>, NBS Special Publication 303, May 1969, pp. 13-18.

102. C. F. Bersch, "Properties of Ceramics for Structural and/or High Temperature Use: Need for Control, Measurement, and Compilation," in Wachtman, T. B., Jr., <u>Mechanical and Thermal Properties of Ceramics</u>, NBS Special Publication 303, May 1969, p. 16.

103. J. E. Hines, Jr., "Delta Alumina Formation During the Abrasive Wear of Polycrystalline Alumina," Wear of Materials, 1979, NY: American Society of Mechanical Engineers, 1979, pp. 540-550.

104. J. E. Hines, Jr., "Delta Alumina Formation During the Abrasive Wear of Polycrystalline Alumina," Wear of Materials, 1979, NY: American Society of Mechanical Engineers, 1979, pp. 550.

105. Benzig, et al., Friction and Wear Devices, 2nd Edition, American Society of Lubrication Engineers, 458 pages.

106. Enomoto, Y. and Fujise, K., "Observations of a hot, isostatically pressed alumina cutting tool by cathodoluminescence," Wear, 89, 1983, p. 110.

107. Munro, R. G., "Temperature Considerations in the Study of Surfaces using a Four-Ball Wear Apparatus," J. Appl. Phys., Vol. 57, No. 11, 1 June 1985, p. 4952.

108. Burton, R. A., "Thermal Deformation in Frictionally Heated Contact," Wear, 59, 1980, p. 7.

109. Winer, W. O., "A Review of Temperature Measurements in EHD Contacts,"

110. Earles, S. W. E., Hayler, M. G., and Powell, D. G., "A Comparison of Surface Temperature Theories and Experimental Results for High Speed Dry Sliding," ASLE Transactions, 14, p. 136.

111. Wallace, F. J., et al., "Thermal Barrier Pistons and Their Effect on the Performance of Compound Diesel Engine Cycles," SAE Technical Paper Series, No. 830312, Warrendale, PA: Society of Automotive Engineers, 1983, p. 3.

112. Schilling, Automotive Engine Lubrication.

113. SAE Progress in Technology Series PT-27, p. 41.

114. Bird, R. B., Stewart, W. E., and Lightfoot, E. N., Transport Phenomena, NY: John Wiley & Sons, Inc., 1960, p. 393.

115. Perry, R. H., Chilton, C. H., and Kirkpatrick, S.D., Chemical Engineers' Handbook, 5th Edition, NY: McGraw Hill Book Co., pp. 23-38.

116. H. S. Cheng, API-MTI - Gas Bearing Design Course, Chapter 5: Hydrostatic Thrust Bearings, 1966, Mechanical Technology Incorporated, Personal copy received from author.

117. Perry, R. H., Chilton, C. H., and Kirkpatrick, S. D., *Chemical Engineers' Handbook*, 4th Ed., NY: McGraw Hill Book Co., 1969, pp. 23-31 to 23-40.

Appendix A

A Review of Wear Test Configurations

A REVIEW OF WEAR TEST CONFIGURATIONS

Introduction

Wear testing of materials is one of the most diverse fields known to engineering. Throughout the tribologcal testing community, many wear test configurations exist. Since the choice of wear test configurations is fundamental to wear tester design and development, it is fortunate that many tribologists, more ceramic scientists, metallurgists, materials scientists, and engineers have similar wear test configurations. This review will attempt to classify some of the major wear test configurations and point out strengths and weaknesses in each of the configurations.

Wear test configurations may be categorized as follows: Class 1) Point and multiple point contacts, Class 2) Line and multiple line contacts, and Class 3) Area and multiple area contacts. Within each of these classes, a wide range of motions might be implemented. For instance, tests in which a sliding motion, a rolling motion, or a mixture of rolling or sliding motions could be performed. A reciprocating motion, a vibratory motion, or unidirectional motion could be utilized in a tribological tester.

Presented below is a summary of several test configurations in each of the three major classifications. A schematic of each of the wear test configurations is given in conjunction with an explanation of the strengths and weaknesses of each configuration. For a more complete listing of wear test configurations, Friction and Wear

<u>Devices</u>,[1] published by the American Society of Lubrication Engineers,

provides a summary of over 230 different wear test devices.

Class #1 - Point and Multiple Point Contacts

A.   Single Point Contacts

   1)   Ball on Ball Contact
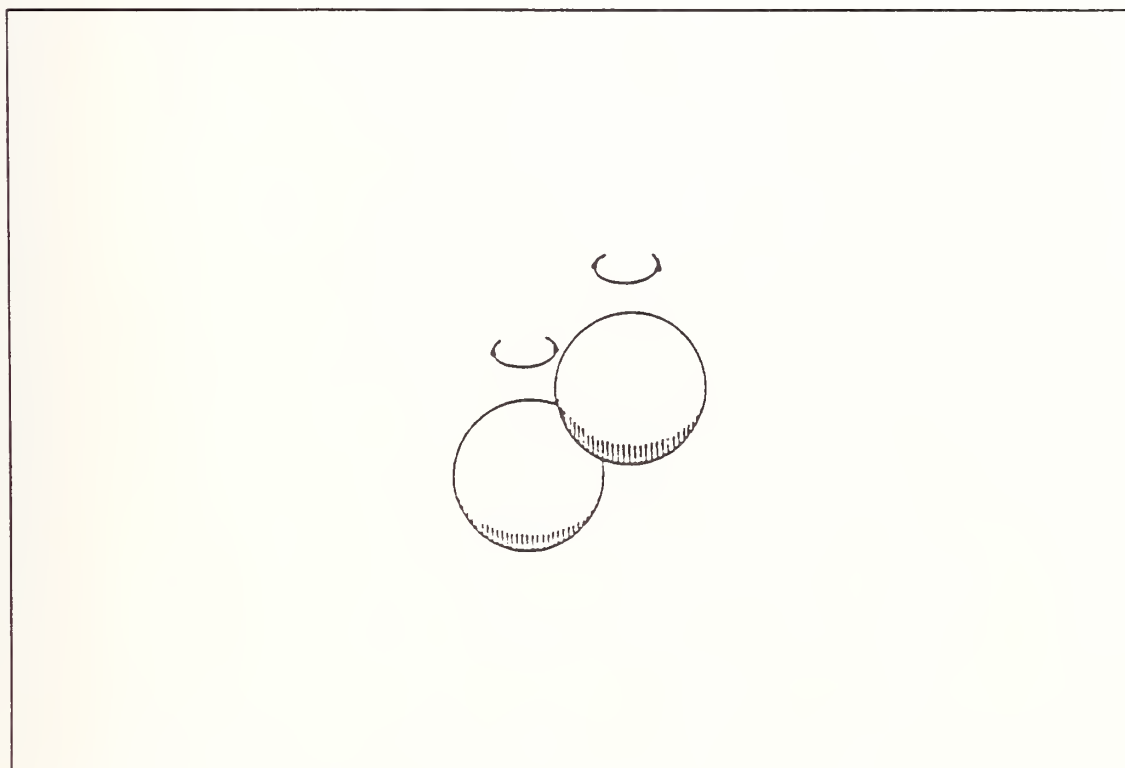
Figure 38.   Two-Ball Contact

   In this configuration, 2 balls contact each other as shown in

Figure 38.   Both balls may rotate in either direction to simulate a

wide variety of sliding and rolling contact ranges as well as different

slide/roll ratios.

Strength: For metallic samples, it is reasonably easy to get well machined, well finished metallic balls for testing. The configuration is simple, and a wide range of rolling or sliding contacts is possible.

Limitation: At high loads, unless a very hefty and precise alignment system is employed, contact misalignment may occur.

2)   Ball on Flat/Ball on Disk Configuration
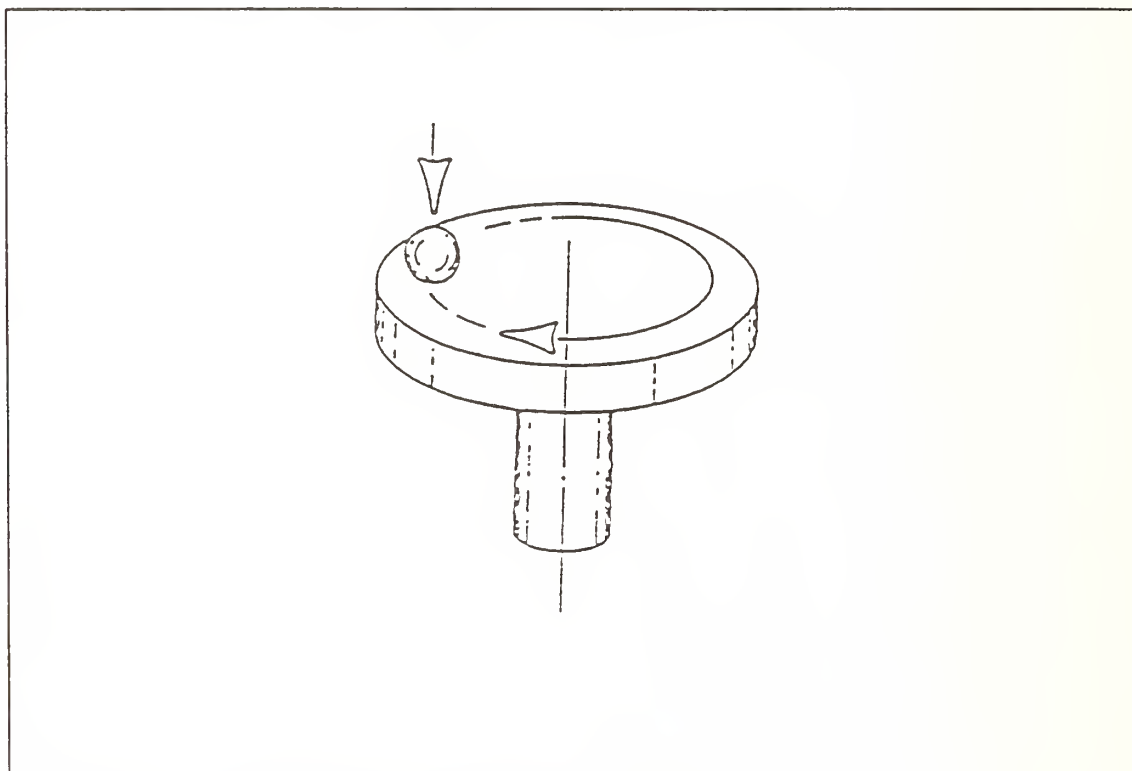
Figure 39. Ball on Flat/Ball on Disk Configuration

In this configuration, a ball is contacted with a rotating disk in an off center position. Normally the radius of contact may be varied to vary linear speed for a given rotation rate. Also, the possibility exists for continuously varying the contact radius and conducting a test in which fresh surface on the rotating flat is always contacted.

Strength: A wide range of linear speeds is usually possible by changing the contact radius at a given speed.

Limitation: For new materials, samples for the rotating disk specimen may be difficult to obtain.

3) Ball on Ring Configuration
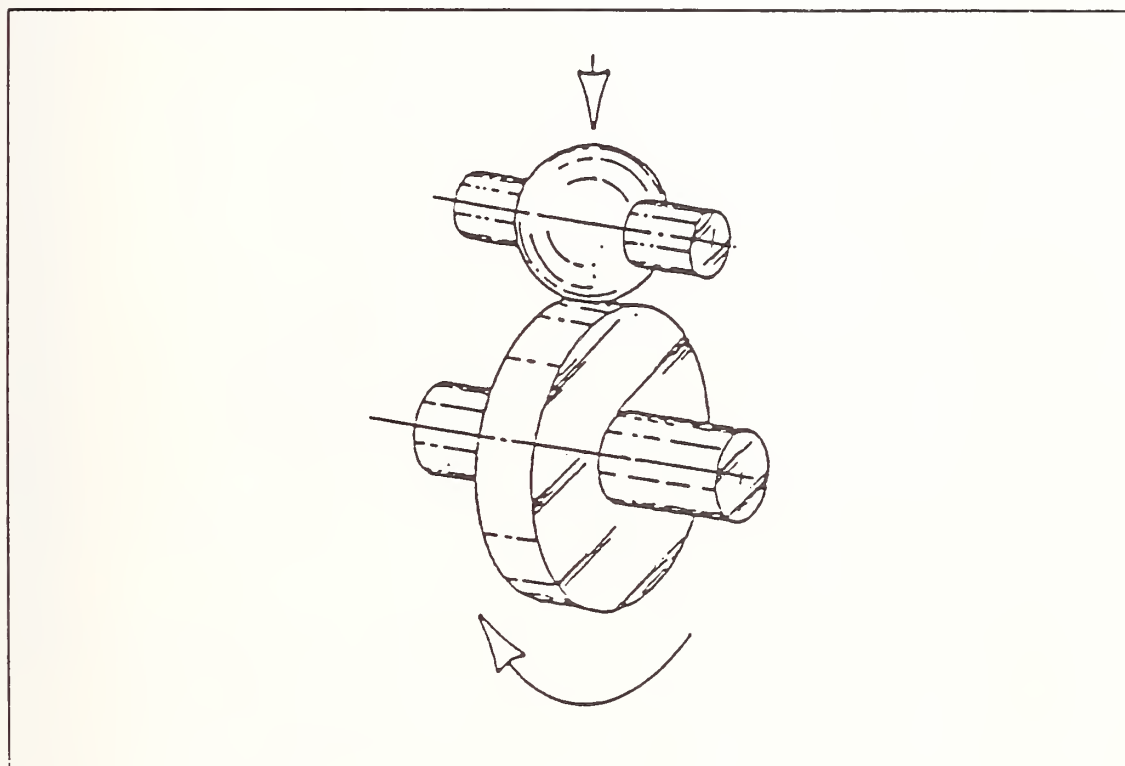
Figure 40. Ball on Ring Configuration

In this configuration a ball is loaded against a rotating ring. The ring turns and causes slip between the ball and the ring.

Strength: A wide range of linear speeds is possible by changing the rpm rate of the ring.

Limitation: Stub mounted ball bearings are difficult to find

and/or manufacture in large quantities. Therefore, a large number of tests should be performed per ball specimen.

4)   Ball on Cylinder Configuration
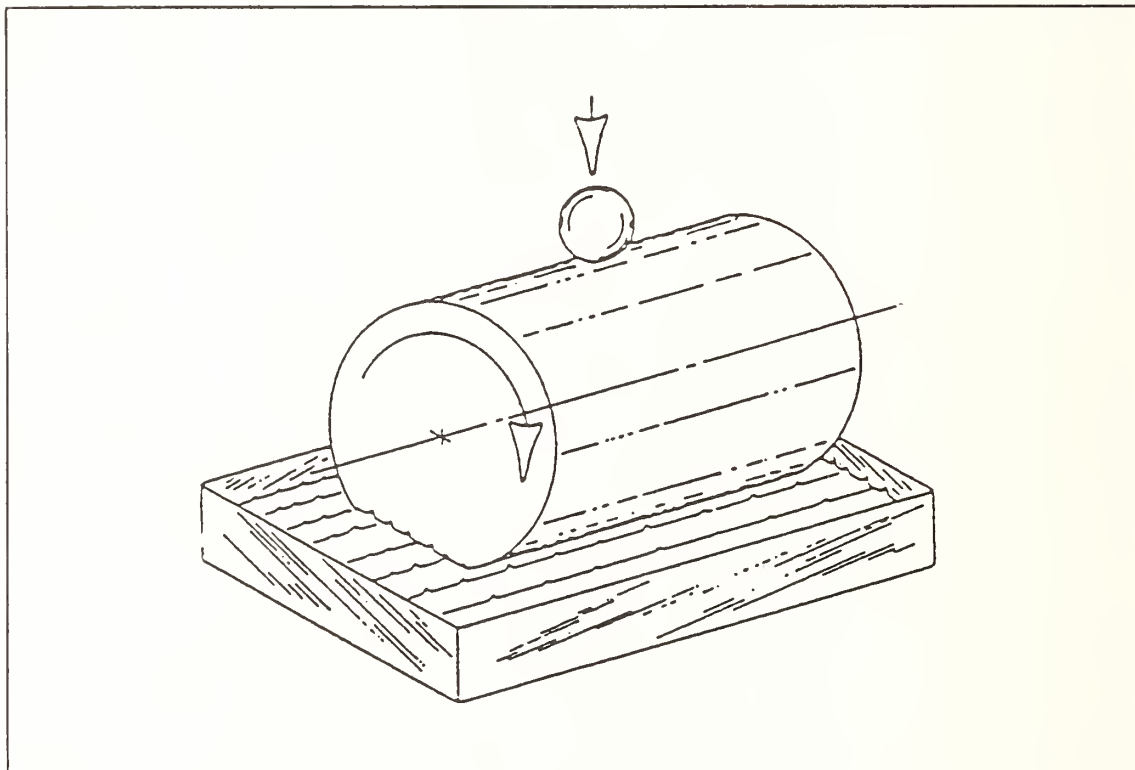
Figure 41.   Ball on Cylinder Configuration

In this configuration, a ball is loaded against a rotating rod or cylinder. The cylinder is partially immersed in a lubricant test bath if lubrication studies are desired.

Strength: For conventional materials, ball stock and rod stock are common shapes. For new materials, the rod stock is very common.

Limitation: Analyses of wear tracks by SEM or other methods are difficult because of the bulkiness of the cylinder specimen. For new materials ball stock may be expensive.

5)   Pin-on-Disk - Rim Loaded
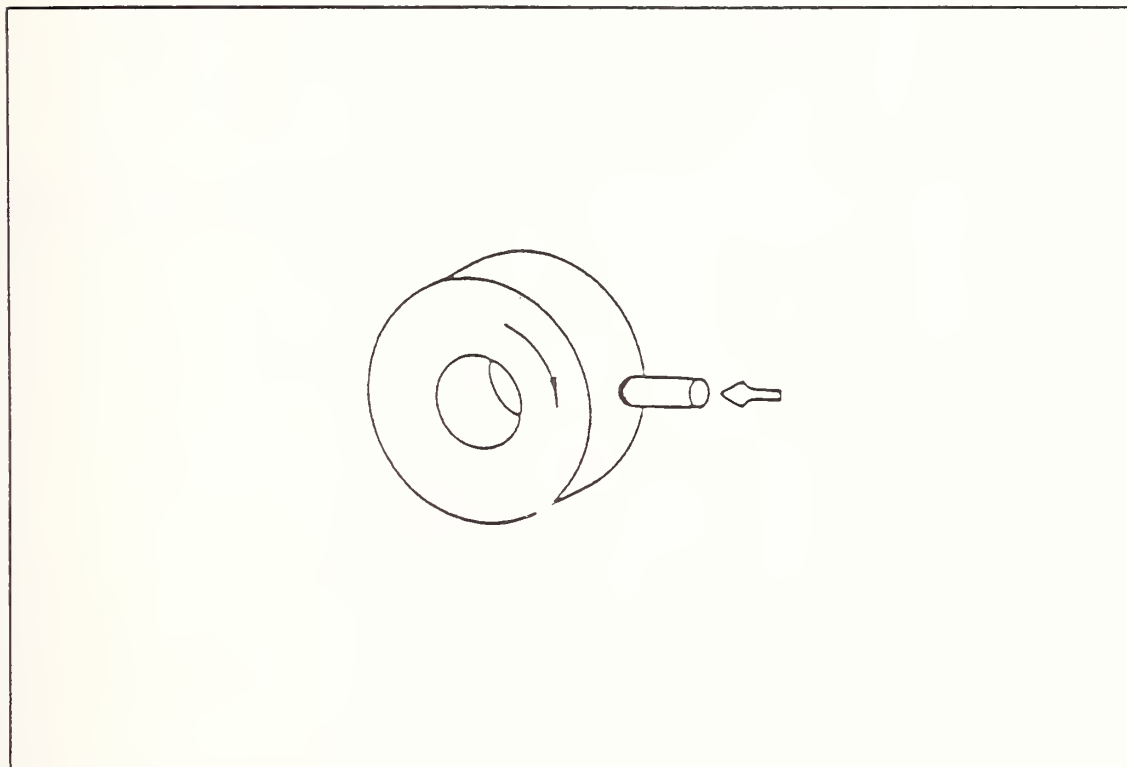
Figure 42.   Pin-on-Disk - Rim Loaded

This configuration consists of a hemispherically tipped pin that contacts a rotating disk on the curved rim face.   Note that the configuration would be quite similar to configuration #4 - Ball on Cylinder Configuration if a) the cylinder was very short and, if b) the ball surface was replaced by a hemisphere on the end of a piece of rod stock.

Strength: Almost any material can be obtained in either a disk configuration or a rod stock shape.   Pins can be machined from rod stock and contact pressures for a given load can be varied by changing the curvature of the hemispherical tip.

Limitation: It is desirable to vary the radius of contact to vary linear speed given rotation rate. This cannot be done with a rim loaded pin-on-disk configuration.

6)   Pin-on-Disk - Face Loaded
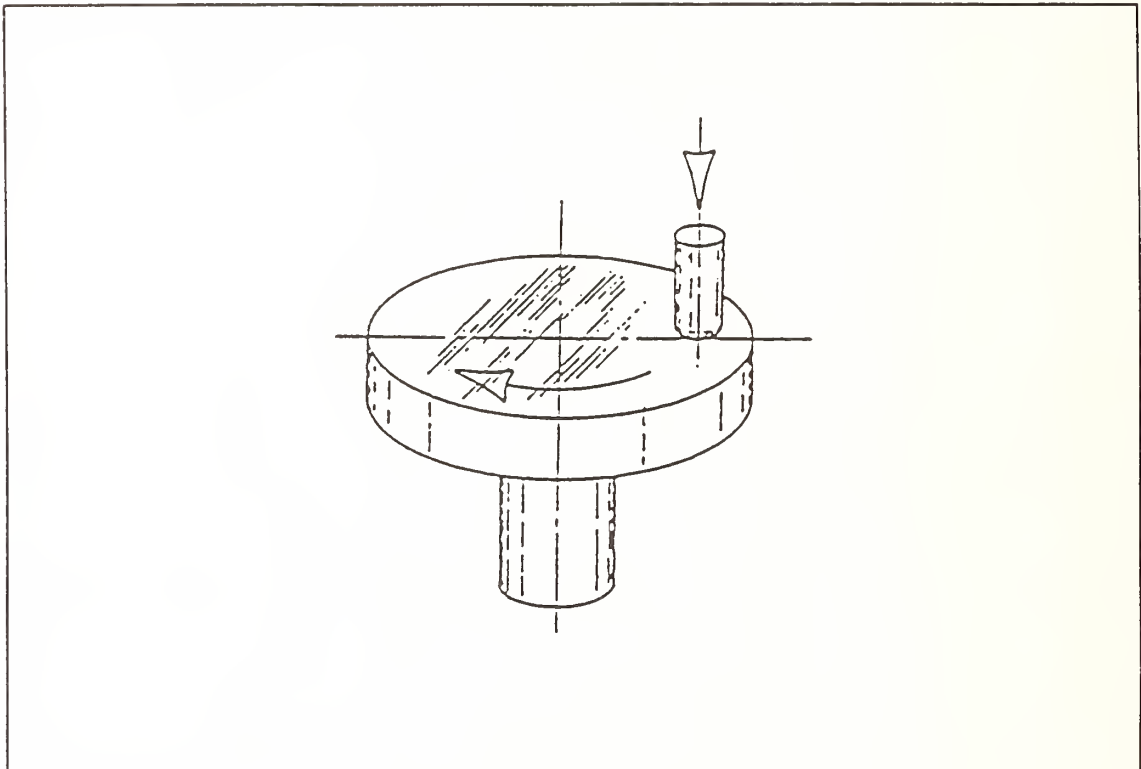
Figure 43.   Pin-on-Disk - Face Loaded

A face loaded pin-on-disk configuration consists of a hemispherically tipped pin contacting the flat face of a rotating disk.

Strength: The following parameters can be varied. 1. For a given loading on disk, the curvature of the pin tip can be changed to vary contact pressure. 2. For a given revolution rate, the linear speed of the pin vs. disk surface may be varied by changing the contact radius.

As in the rim loaded pin-on-disk configuration, both types of samples are relatively easy to obtain for new materials.

Limitation: Mounting of the disk do avoid slip may be difficult.

7) Pin-on-Disk - Non-rotating Configurations
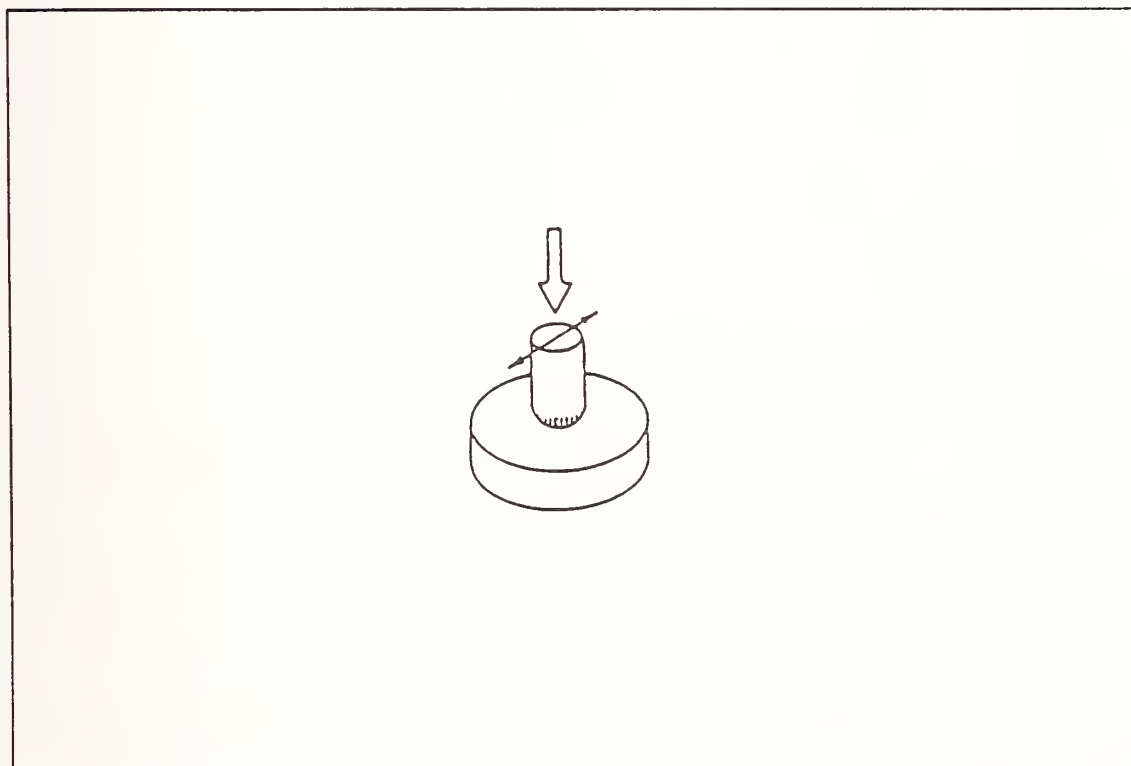
Figure 44A. Pin-on-Disk - Fretting Motion
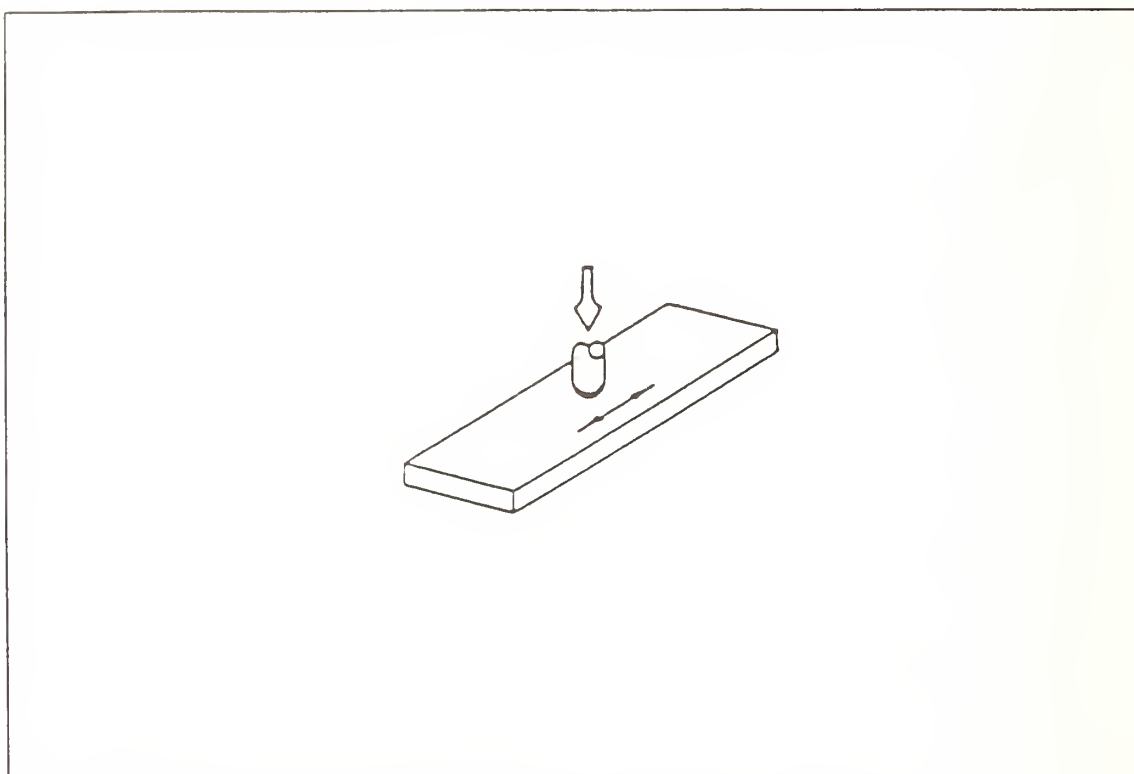
Figure 44B.   Pin-on-Disk - Reciprocating Motion

These configurations are similar to the pin-on-rotating-disk

configuration with the exception that 1) The "disk" is not necessarily

circular, and 2) The disk does not rotate. A distinction has been

made between testers that test very high frequency - low amplitude

motions which induce a fretting/fatigue type of wear versus testers

which test at larger amplitudes and lower frequencies to test

reciprocating wear. Practically, design of testers to facilitate these

motions may be quite different.

8)   Cylinder on Disk Rim Configuration
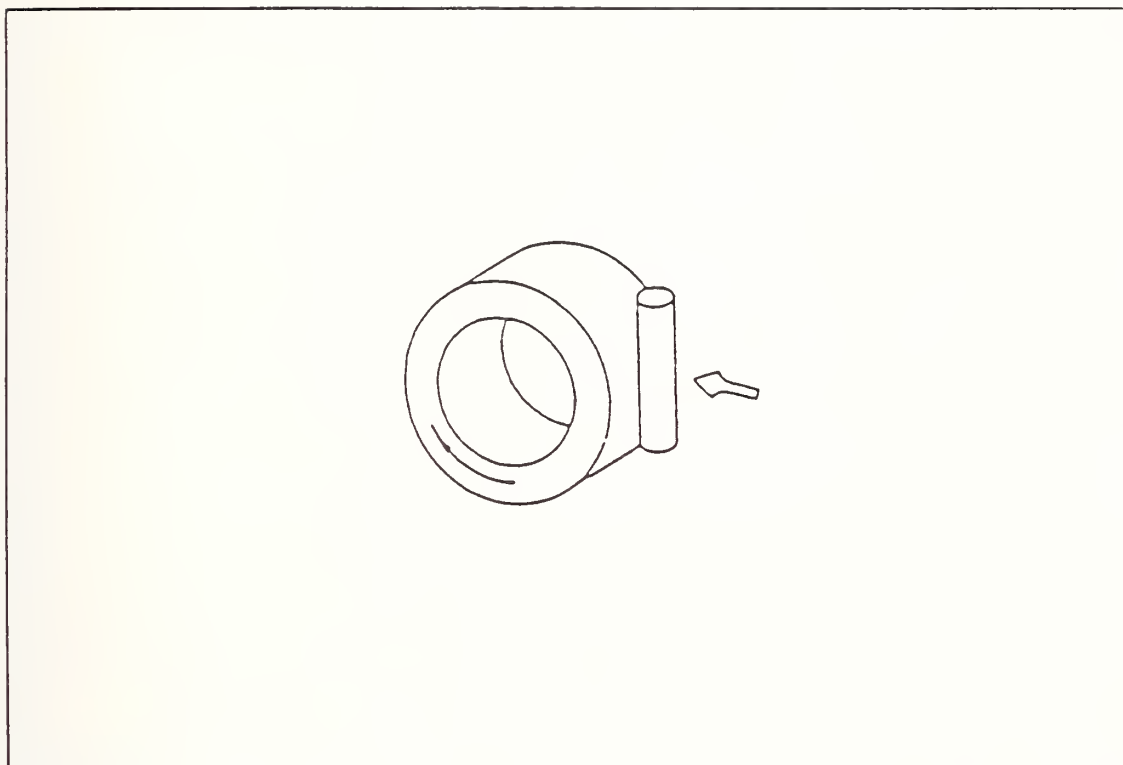
Figure 45.   Cylinder on Disk Rim Configuration

In this configuration, a cylinder or rod is loaded against the edge of a rotating disk as shown in Figure 45.

Limitation: Perfect vertical alignment of cylinder needs to be maintained.   If this is not maintained, a line contact is formed rather than a point contact.   (In the extreme case, if the cylinder were horizontal, a line contact would develop across the entire rim of the disk.)

9)   Crossed Cylinder Devices
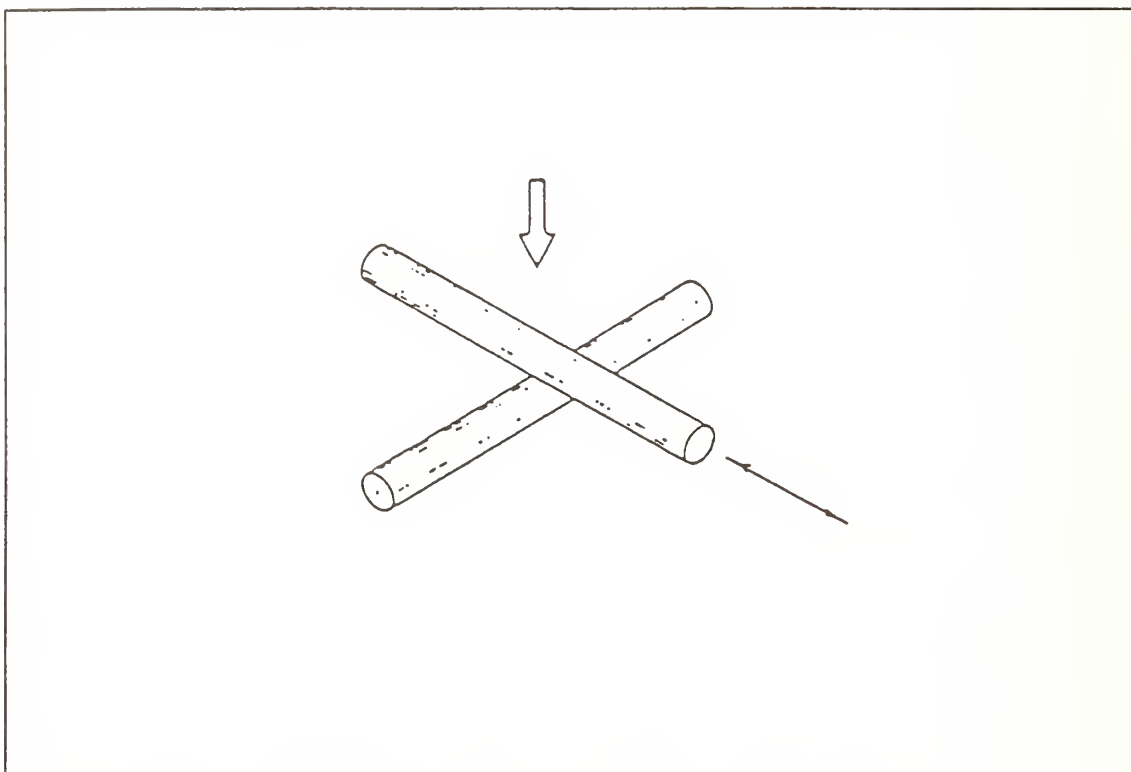
Figure 46A.   Crossed Cylinder Device - Reciprocating Cylinder
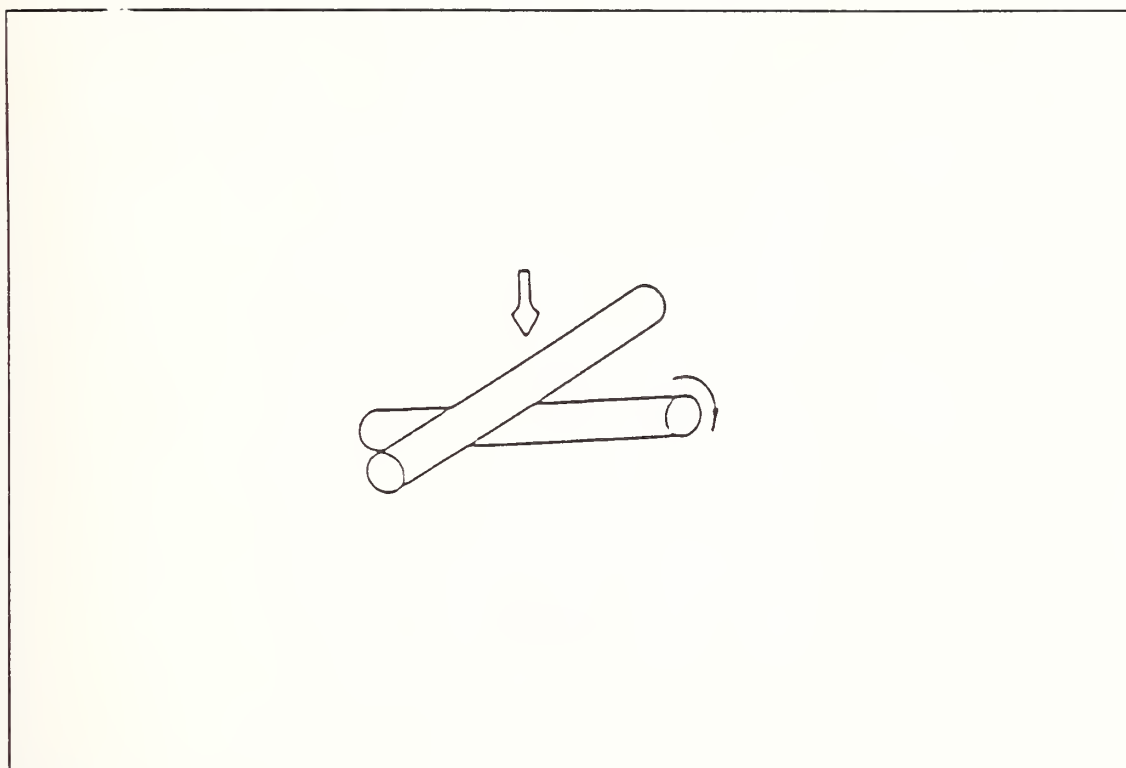
Figure 46B.   Crossed Cylinder Device - Rotating Cylinder

These configurations have the same basic limitations as that of configuration #8 - cylinder on disk rim configuration. In fact, if the disk could be viewed as a short cylinder we have the same configuration as the configurations 46A and 46B.

B) Multiple Point Contacts

Many multiple point contact testers exist. For the sake of brevity, a few of the major multiple point contacts are presented below along with a brief summary of the strengths and limitations of each configuration.

10)   Four-Ball Wear Test Configuration
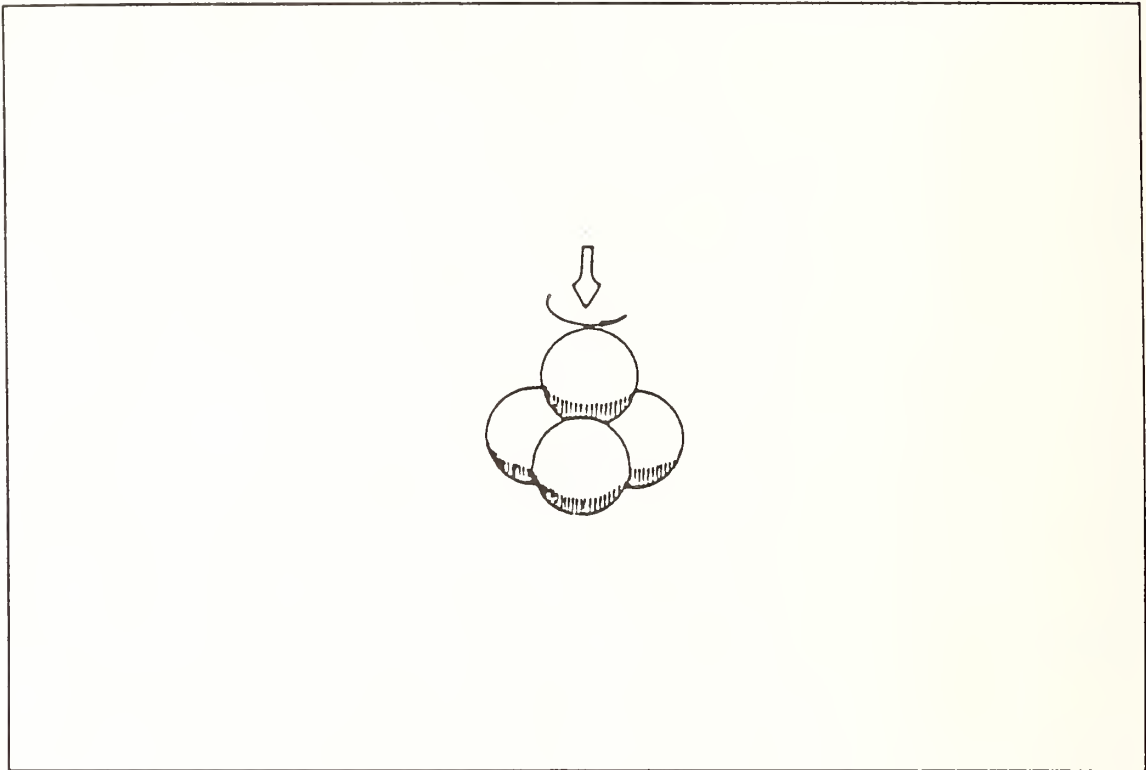
Figure 47A.   Four-Ball Wear Test Configuration

This configuration consists of 3 lower balls which are held stationary and an upper ball which is loaded against it and rotated is a commonly used wear tester for boundary lubrication.

Strengths: By nature, this test is a self-aligning wear test. It is widely used throughout the lubricant industry for testing lubricants under boundary lubrication. A common variation this configuration is the ball on 3-flat configuration in which 3 flats are arranged at the contact points of Figure 47A and thus a tetrahechal configuration is preserved. Figure 47B gives a general schematic of this configuration.
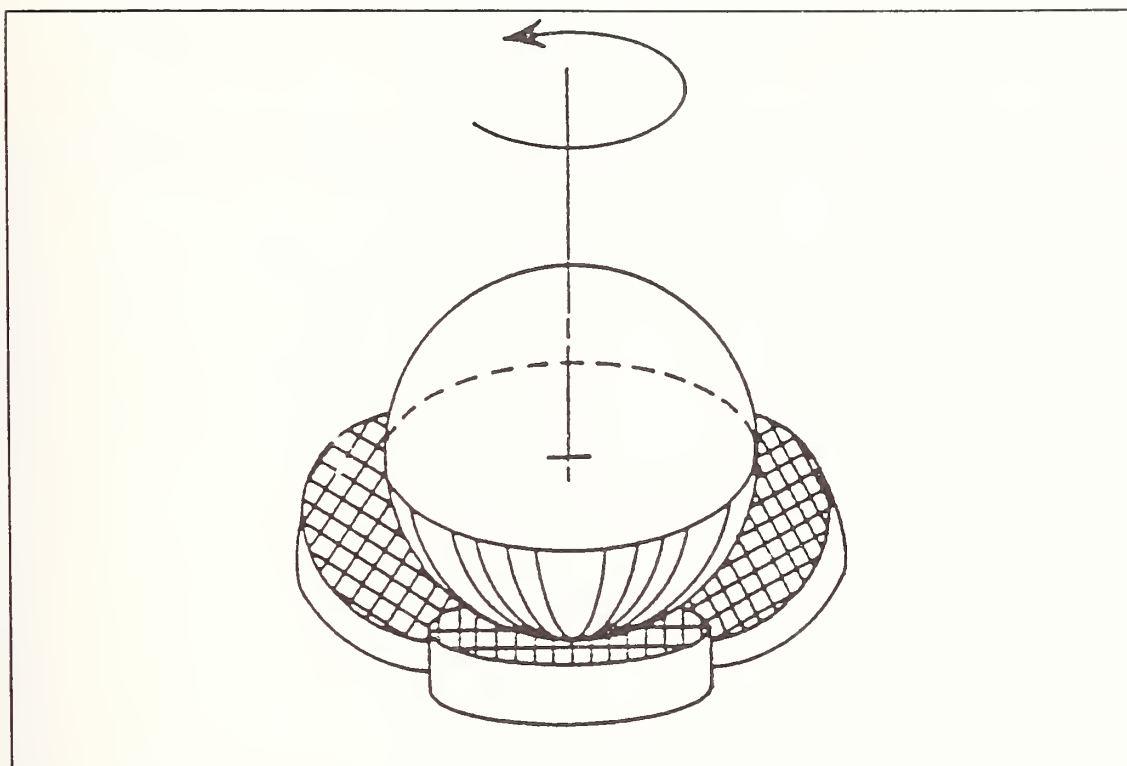
Figure 47B. Ball on 3-Flat Configuration

Limitation: A four-ball tester does not possess the capability of large linear speeds unless a very high rotational speed are possible. For new materials, ball bearings may be expensive to machine. Contact pressures are high, even at low loads.
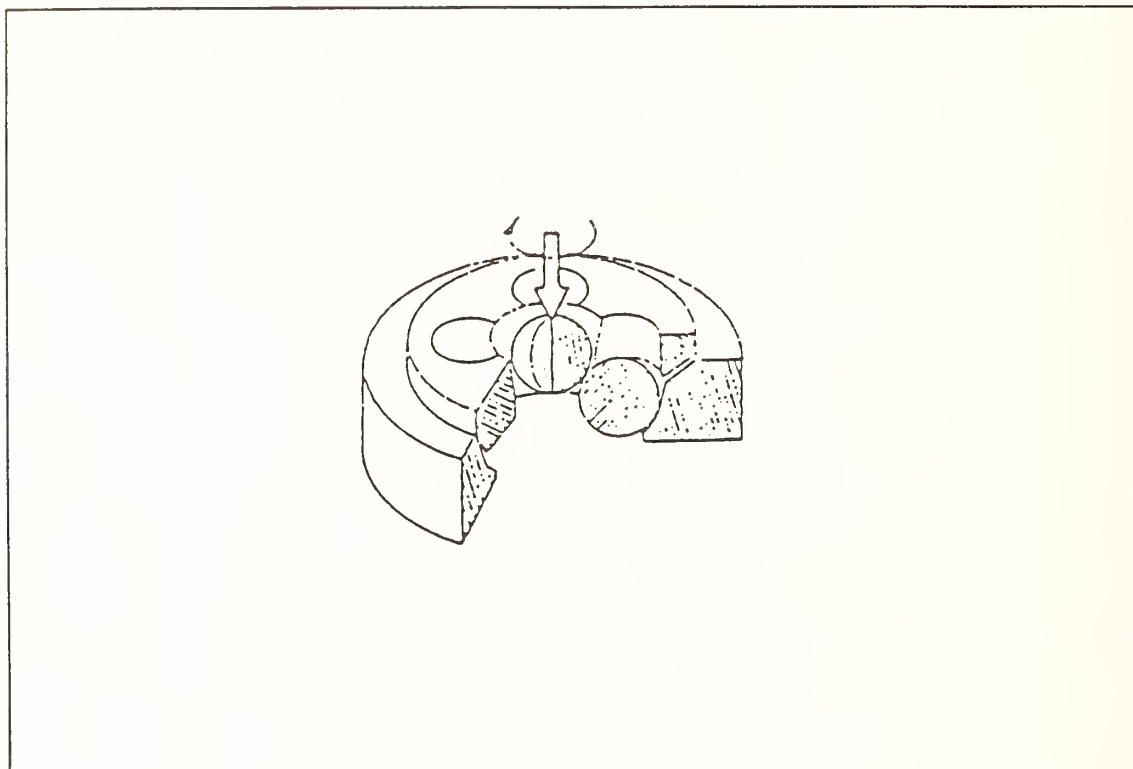
11) Five Ball Wear Test Configuration

Figure 48. Five Ball Wear Test Configuration

In this configuration, 4 lower balls are separated by a separator and the upper ball is loaded against them and rotated. The lower balls are free to roll and thus a simulated bearing contact is formed. A reference where this type of configuration was used in Zaretsky, E.V., Parker, P.J., and Anderson, W.J., "Component Hardness Differences and Their Effect on Bearing Fatigue," ASME Trans. Journal of Lubrication Technology, January, 1967, p. 47.

12) Multiple Pin-on-Disk Configurations
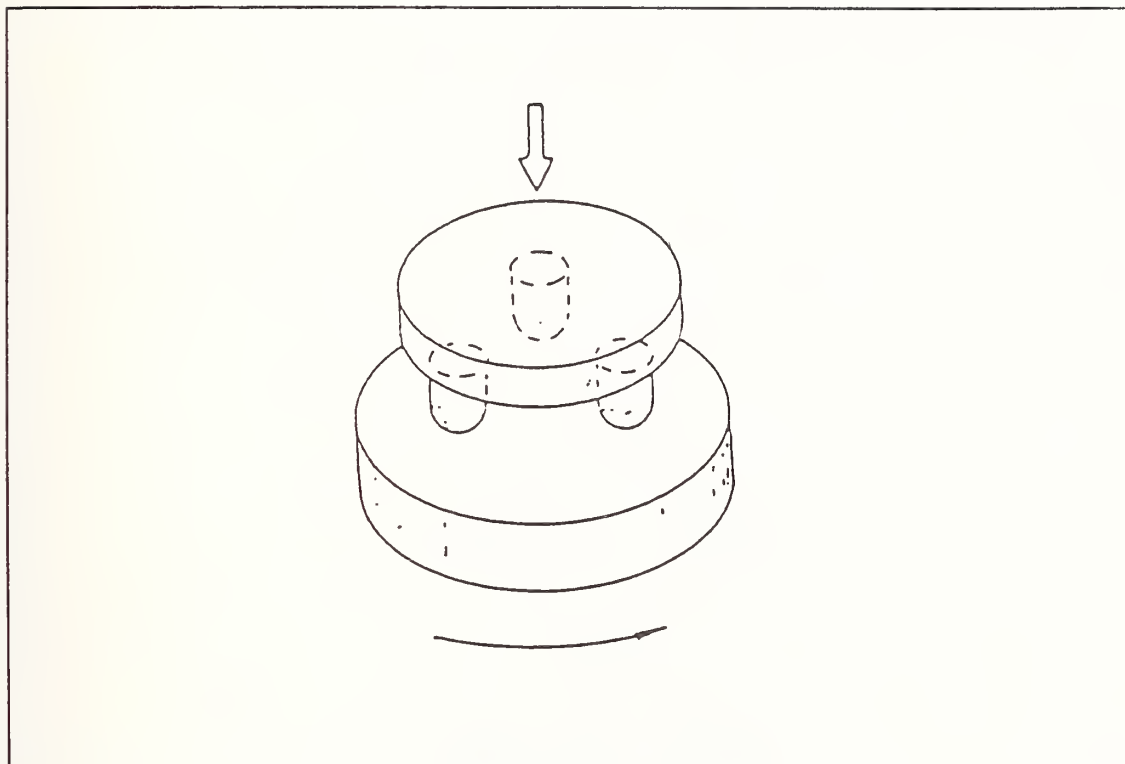
Figure 49. Multiple Pin-on-Disk Configuration

Multiple pin-on-disk configurations have the same strengths and limitations as single pin-on-disk configurations with the following exception. In a configuration such as above a load applied along the central axis of rotation does not cause uneven deflection of the disk at very high loads.

Class #2 - Line and Multiple Line Contacts

A.   Line Contacts

13) Disk Rim on Disk Rim

Figures 50A and 50B show two different views of this type of configuration.
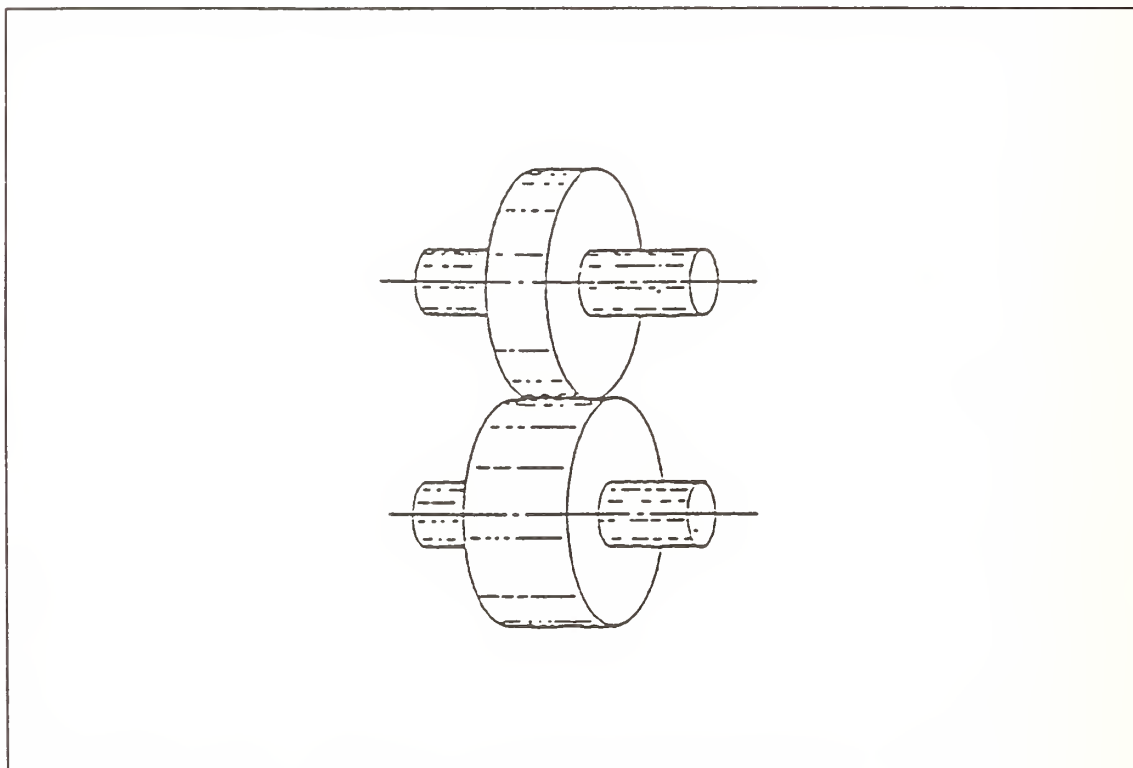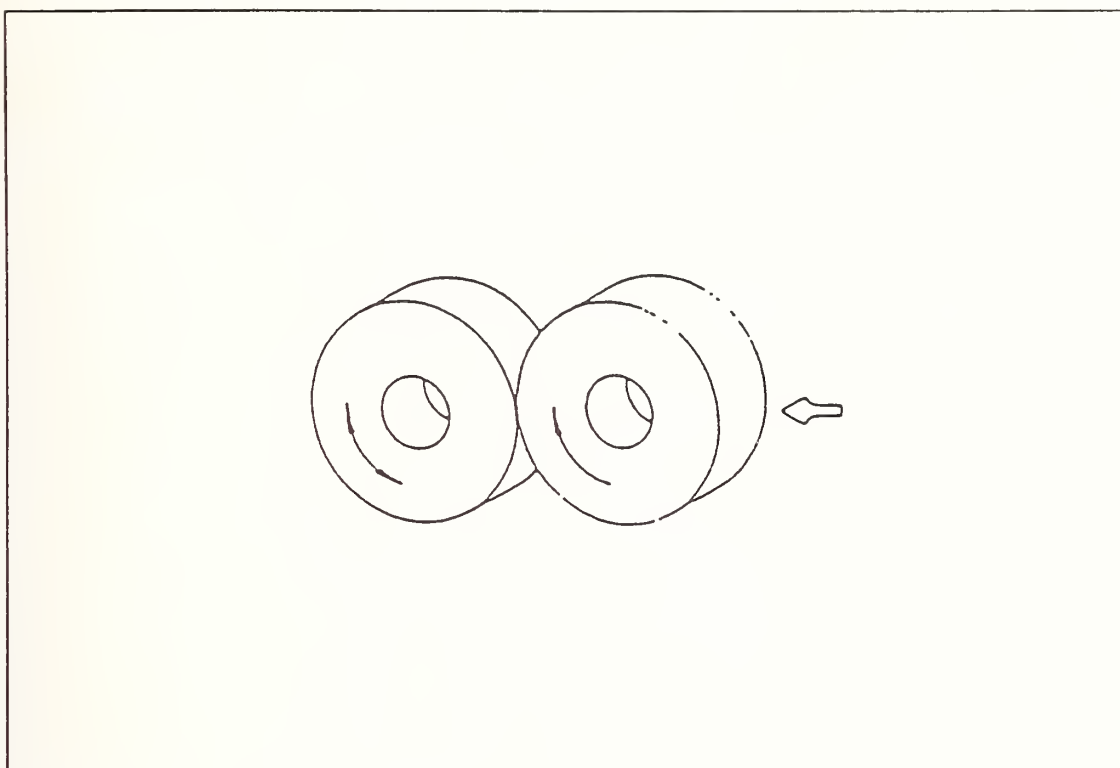

Figure 50A.   Disk Rim on Disk Rim

Figure 50B. Implementation #2 Disk Rim on Disk Rim

Configurations of this type are commonly used to simulate pure sliding and combinations of rolling and sliding which might occur in tooth friction for gears. The configuration tries to simulate fatigue, gear wear and scoring by changing the slip to roll ratio for a given speed.
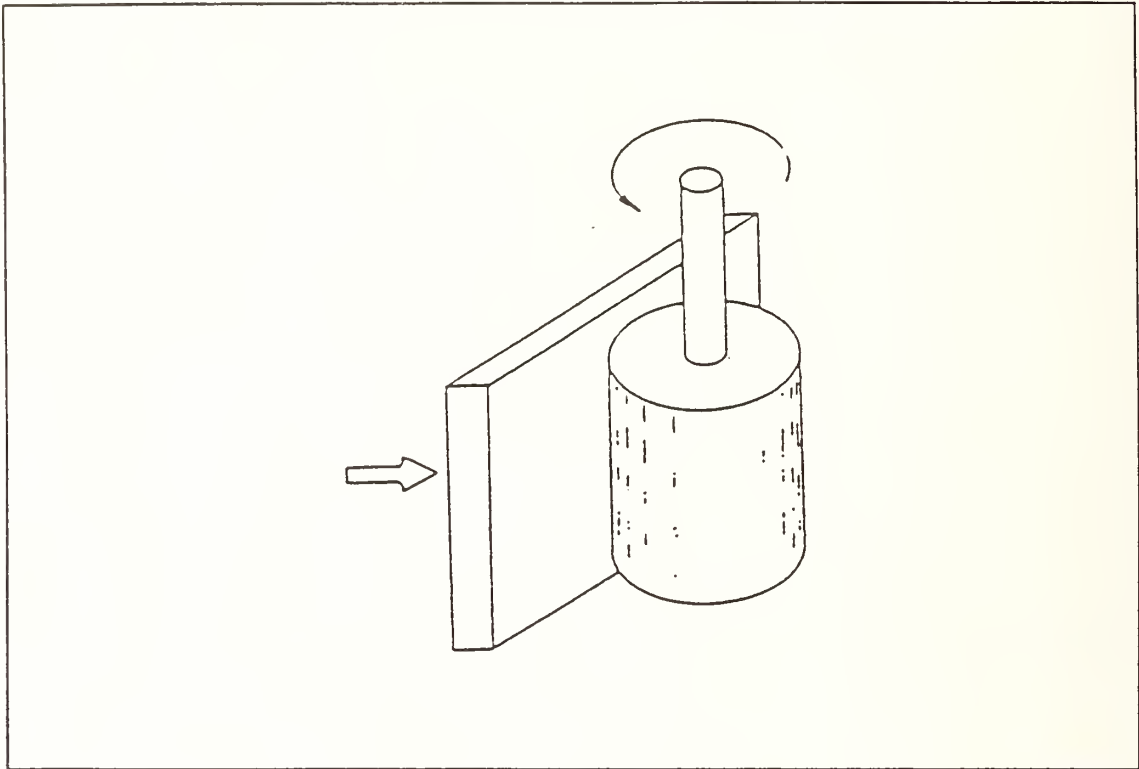
14) Rotating Cylinder on Plate Configuration

Figure 51. Rotating Cylinder on Plate Configuration

Configurations of this type are commonly used. They are commonly
used in the testing of lubricants under boundary lubrication. Since a
line contact is larger than a single point contact, more wear debris is
generated under the same conditions and wear monitoring of a
configuration such as this becomes possible. Careful vertical
alignment of the rotating cylinder should be maintained in order to
prevent the tendency of the plate to twist. This would skew frictional
force measurements.
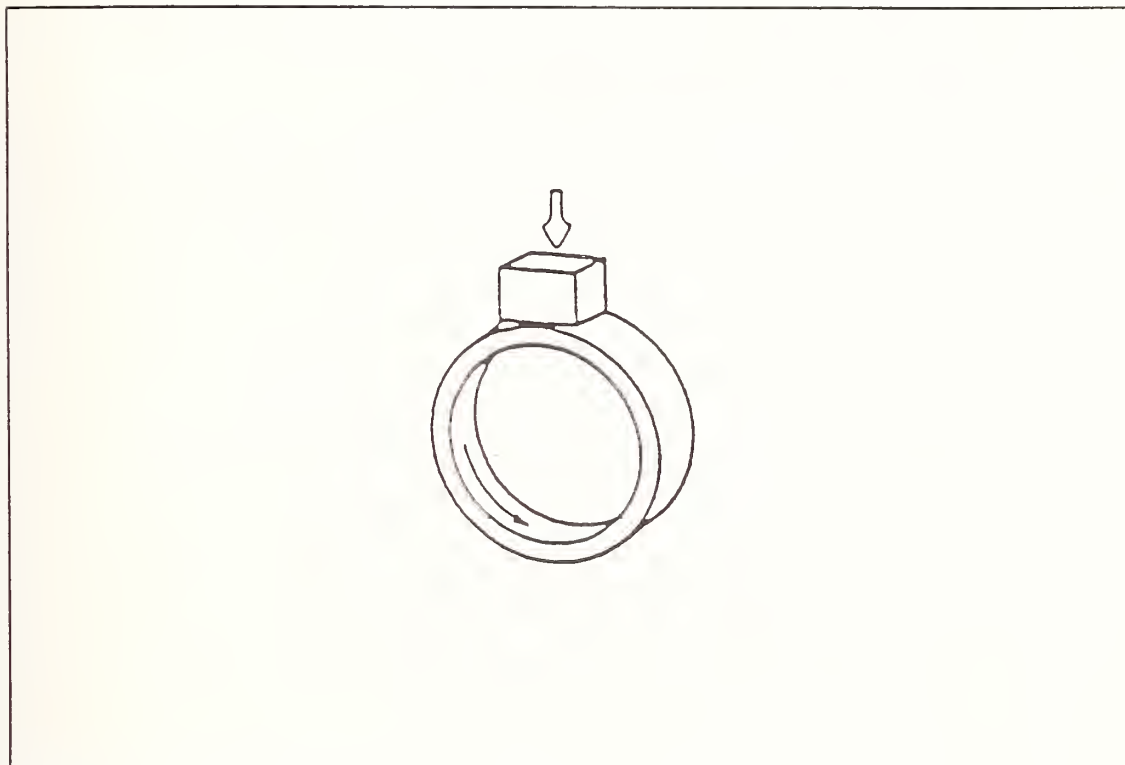
15) Ring-on-Block Configuration

Figure 52. Ring-on-Block Configuration

The ring on block configuration is one of the most common
configurations for a line contact. In this configuration, a ring is
contacted with a steel block that is loaded against it. This
configuration is commonly used throughout the tribological world for
general sliding friction and continuous wear measurement. Lubrication
studies can be done by immersing the ring and block in lubricant or by
suspending a drop of lubricant on the bottom of the ring. The
advantage of the latter is that continuous collection of the wear
debris in the oil droplet is possible.

Limitations: If the block is not maintained in perfect alignment, odd shaped wear scars result.

B. Multiple Line Contacts

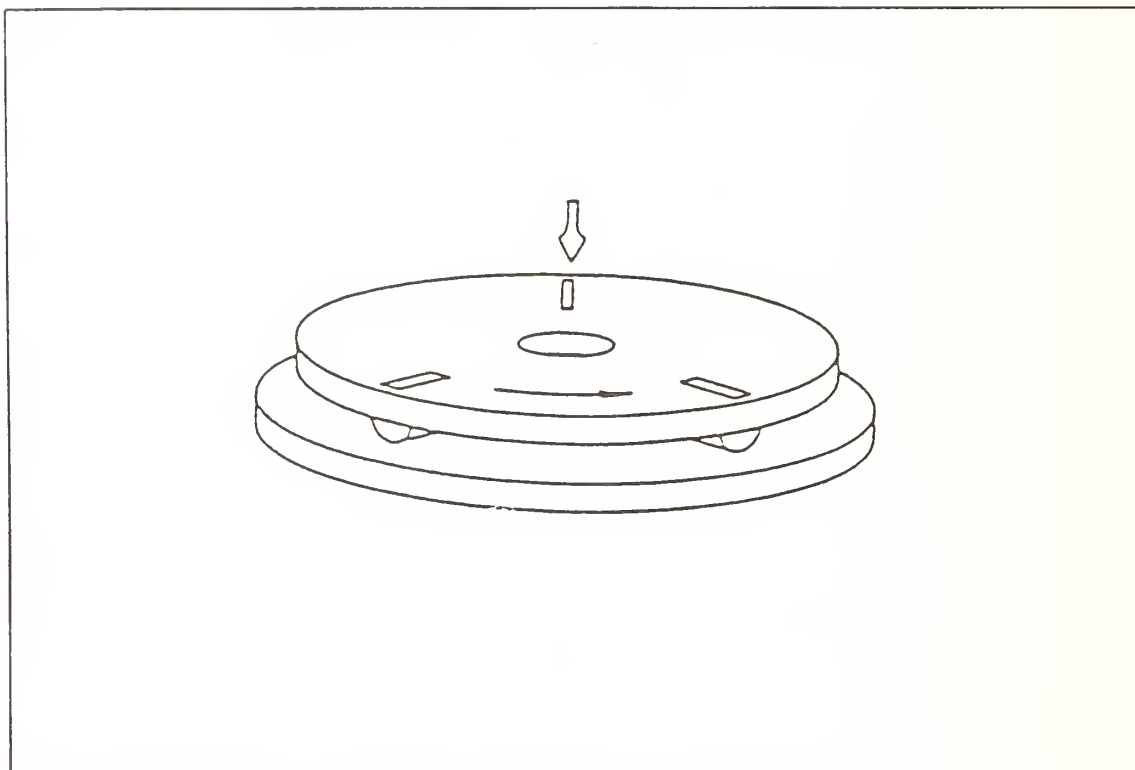16) Three Pellet on Disk Configuration

Figure 53. Three Pellet on Disk Configuration

In this configuration 3 short cylinders, or pellets contact a disk on their curved surfaces. Thus 3 lines of contact are formed. This configuration, originally designed for solid lubrication [see Lavik, M.T., "High Temperature Solid Dry Film Lubrication," WADC Technical Report 57-455, Part III, 1959][2], would probably be a poor design for

metal pellets because wear debris that is generated in one contact

could be trapped in another contact thus causing 3-body wear.
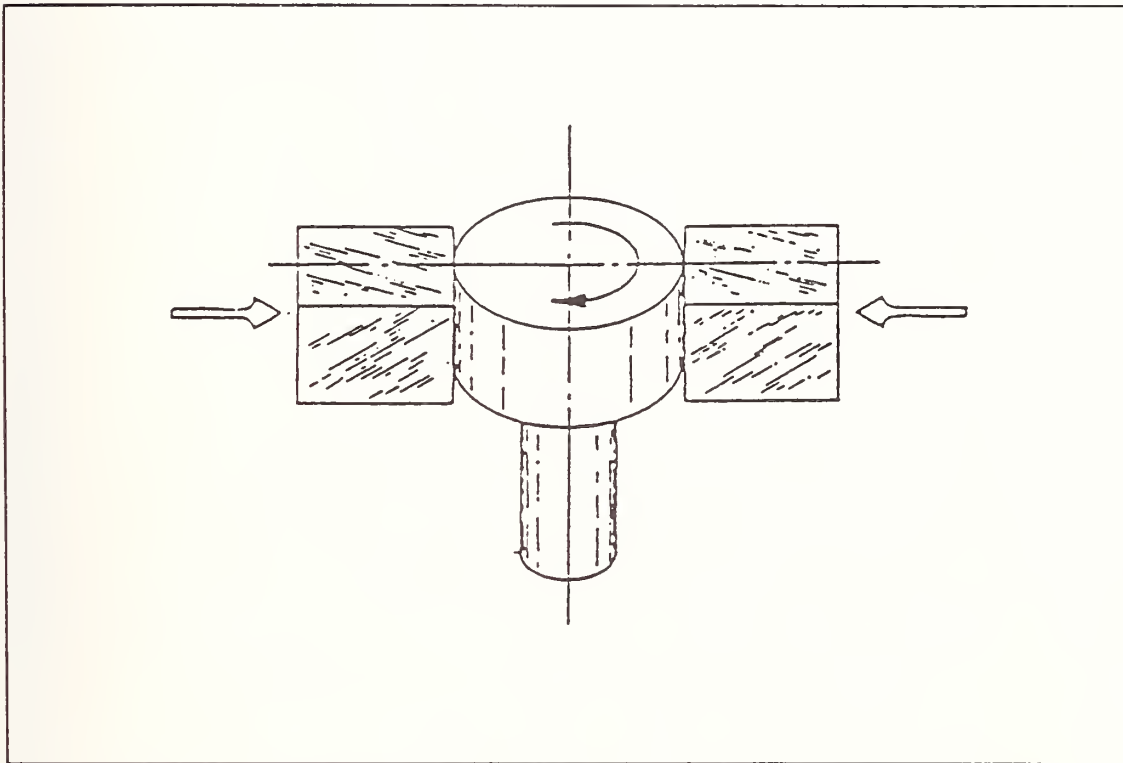
   17)   Ring on 2 Block Configuration

Figure 54.   Ring on 2 Block Configuration

In this configuration, two blocks are loaded against a rotating

disk and two line contacts are formed.   Friction is determined by

transfer of torque from the cylinder to the blocks.   Continuous wear

measurement may be obtained by continuously measuring the positioning

of the blocks.

Class #3 - Area Contacts

Many different area contacts have been devised. A brief summary
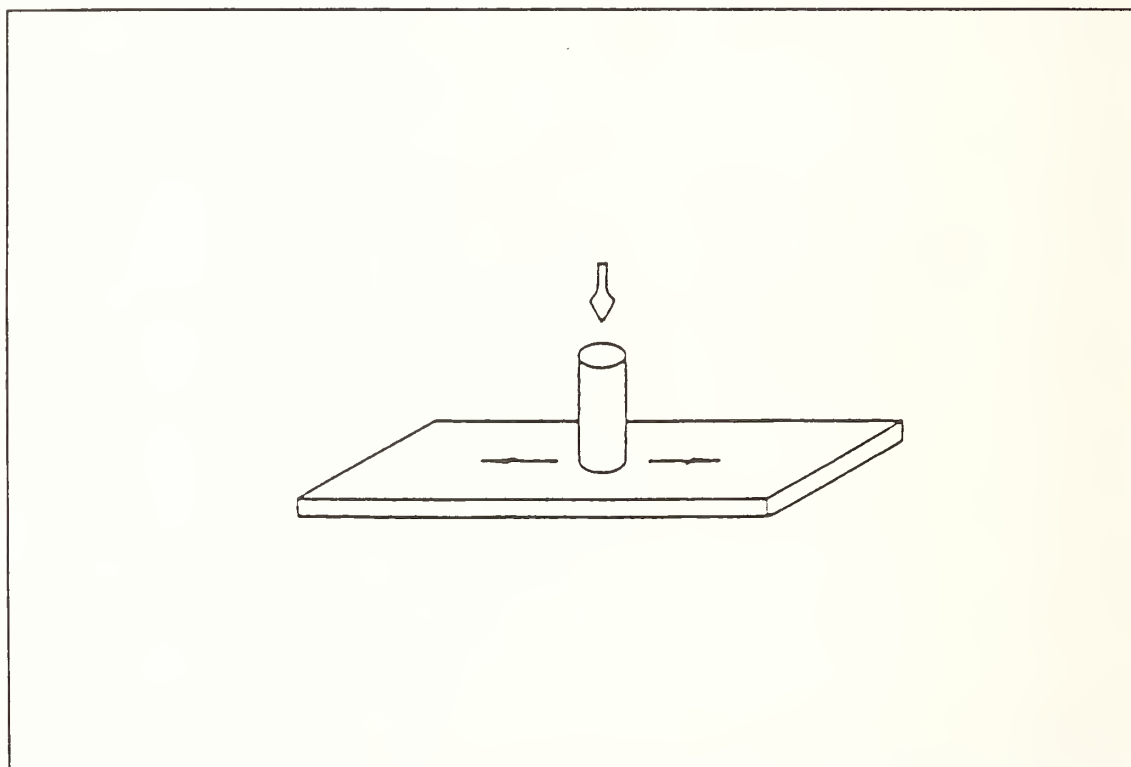of a few of these area contacts follows.

18) Pellet/Slider on Plate

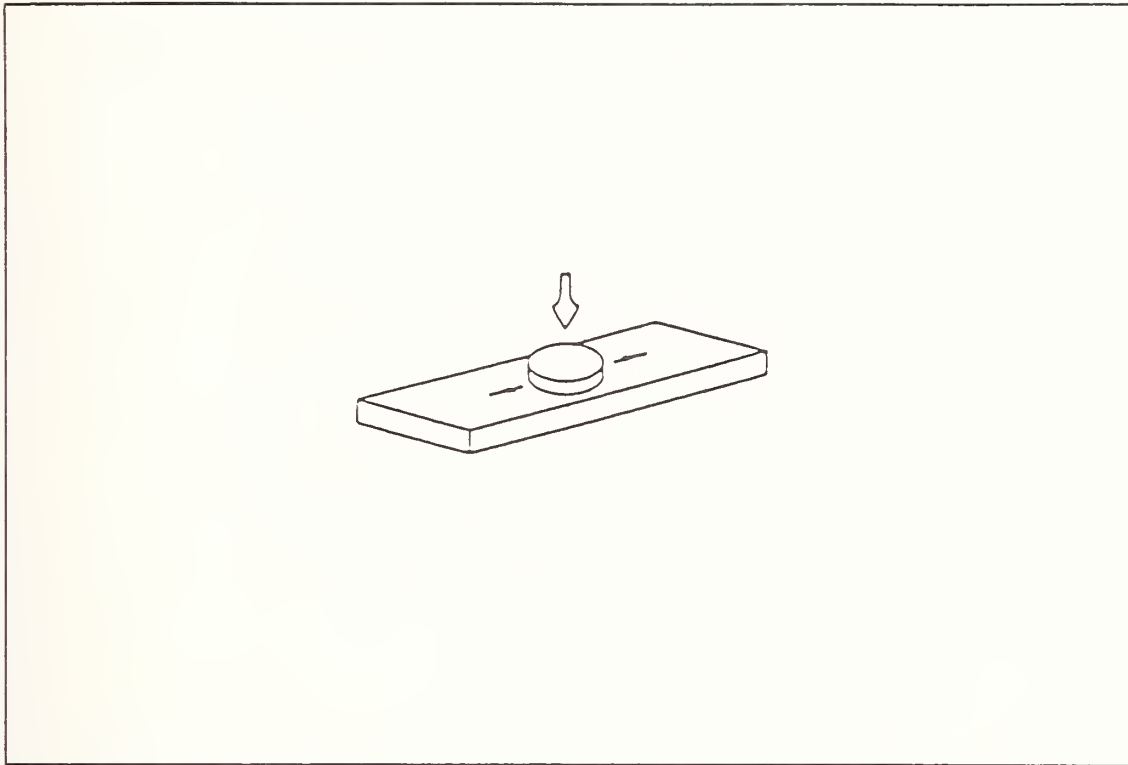Figure 55A.   Pellet on Reciprocating Plate

Figure 55B.   Slider on Reciprocating Plate

This configuration is quite similar to the pin-on-disk
reciprocating motion configuration (44B) with the following change:
Instead of a curved surface at the tip of the pin, a flat machined
surface is used in the testing. This allows the contact area to be a
circular area rather than a "point" contact.
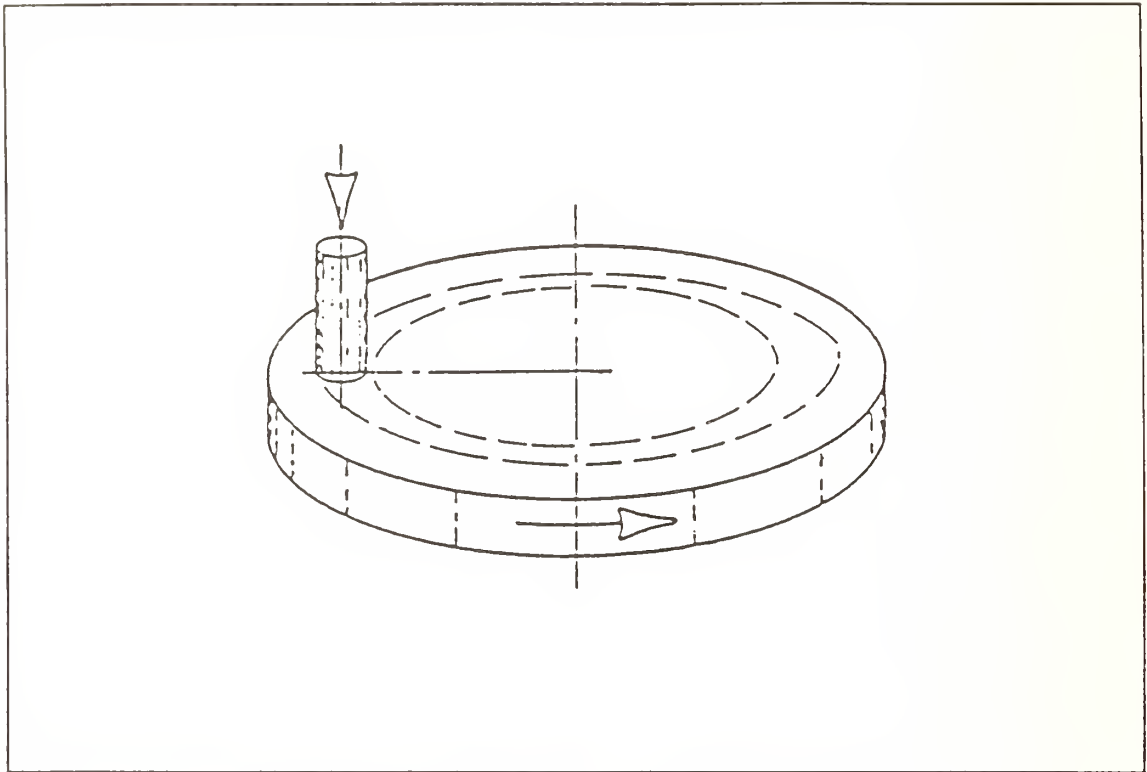
19) Pellet on Disk Configuration

Figure 56. Pellet on Disk Configuration

This configuration is similar to configuration #43 - Face loaded pin-on-disk except that a flat has been machined on the disk end rather than a surface of curvature.

Conclusions

Many different configurations exist and are widely used throughout
the tribological testing community. Each configuration is suitable to
a fixed range of conditions, speeds, loads, and environments.
Different configurations lend themselves more easily to different types
of analyses. For example, large cylinders do not usually lend
themselves easily to SEM analysis but are easily analyzed with an
optical microscope. It would be convenient to have a wear tester that
has the capability to test a number of different configurations.
Obviously, no one tester could test all configurations under all
conditions. Such a tester could test no one configuration well.
However, in certain systems, not much is lost in adding some
variability. For instance, let us look at the face loaded pin-on-disk
configuration: If we allow the variability to replace a ball for the
pin, then we have a ball-on-disk configuration. If we have the
capability to machine the pin end to a flat, then we have an area
contact -a button-on-disk contact. If the contact radius can be varied
for a given rpm rate we can test different linear speeds for these
contacts.

If possible, such an approach should be taken in wear tester
design. This approach allows specimen variability without the cost or
sacrifice. If certain new materials come only in certain specimen
shapes, these shapes need to be utilized. It is necessary, whenever
possible, to accommodate such shapes in a wear tester. Therefore, for

the High Temperature Wear Facility, a ball-on-disk/flat - pin-on-

disk/flat configuration has been chosen.

1.   Benzig, et al., Friction and Wear Devices, 2nd ed., American
      Society of Lubrication Engineers, 1976, 458 pages.

2.   Lavik, M.T., "High Temperature Solid Dry Film Lubrication," WADC
      Technical Report 57-455, Part III, 1959.

Appendix B

Development of Finite Difference Equations for

High Temperature Wear Facility Furnace Design

<u>SUMMARY OF EQUATIONS AND BOUNDARY CONDITIONS</u>

Steady State Energy Transport Equation

$$\frac{1}{r}\frac{\partial}{\partial r}(rq_r) + \frac{\partial}{\partial z}(q_z) = 0$$

$$q_z = -k_{eff}\frac{\partial T}{\partial z}$$

$$q_r = -k_{eff}\frac{\partial T}{\partial r}$$

$$k_{eff} = k_{eff}(T)$$

Boundary Conditions

@ $r = 4$, $0 \leq z \leq 3$, $T = 1500°C$

@ $0 \leq r \leq 4$, $z = 3$, $T = 1500°C$

@ $4 \leq r \leq 10$, $z = 0$, $\frac{\partial T}{\partial z} = 0$

@ $r = 0$, $3 \leq z \leq 9$, $\frac{\partial T}{\partial r} = 0$

@ $r = 10$, $0 \leq z \leq 9$, $q_r = h(T_{wall} - T_{room})$

@ $0 \le r \le 10$, $z = 9$, $q_z = h(T_{wall} - T_{room})$

T_{room} = constant

h = constant

$T_{wall} = T_{wall}(r,z)$

Boundary Conditions Summarized

$$q_z = h(T_{wall} - T_{room})$$

$q_r =$
$h(T_{wall} - T_{room})$

$\dfrac{\partial T}{\partial r} = 0$

T = 1500

T = 1500
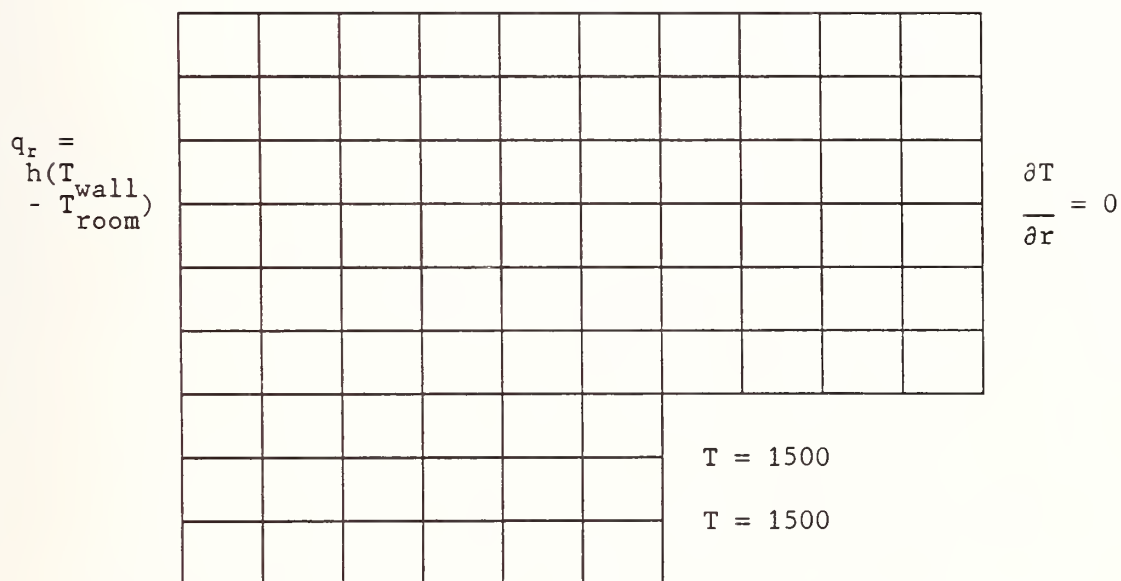
$$\frac{\partial T}{\partial z} = 0$$

Case I k_{eff} = constant

$$\frac{1}{r}\frac{\partial}{\partial r}\left(r\frac{\partial T}{\partial r}\right) + \frac{\partial}{\partial z}\left(\frac{\partial T}{\partial z}\right) = 0$$

or, in an alternate form

$$\frac{1}{r}\frac{\partial T}{\partial r} + \frac{\partial^2 T}{\partial r^2} + \frac{\partial^2 T}{\partial z^2} = 0$$

Note: At $r = 0$ $\partial T/\partial r$ <u>must</u> be zero, or the finite difference equation would blow up to infinity. This is one of our boundary conditions.

Now finite difference equations for internal grid points and for each boundarycan be developed. The figure below marks out each type of boundary and internal grid point.

II

III   I

1500°C
V
1500°C

IV
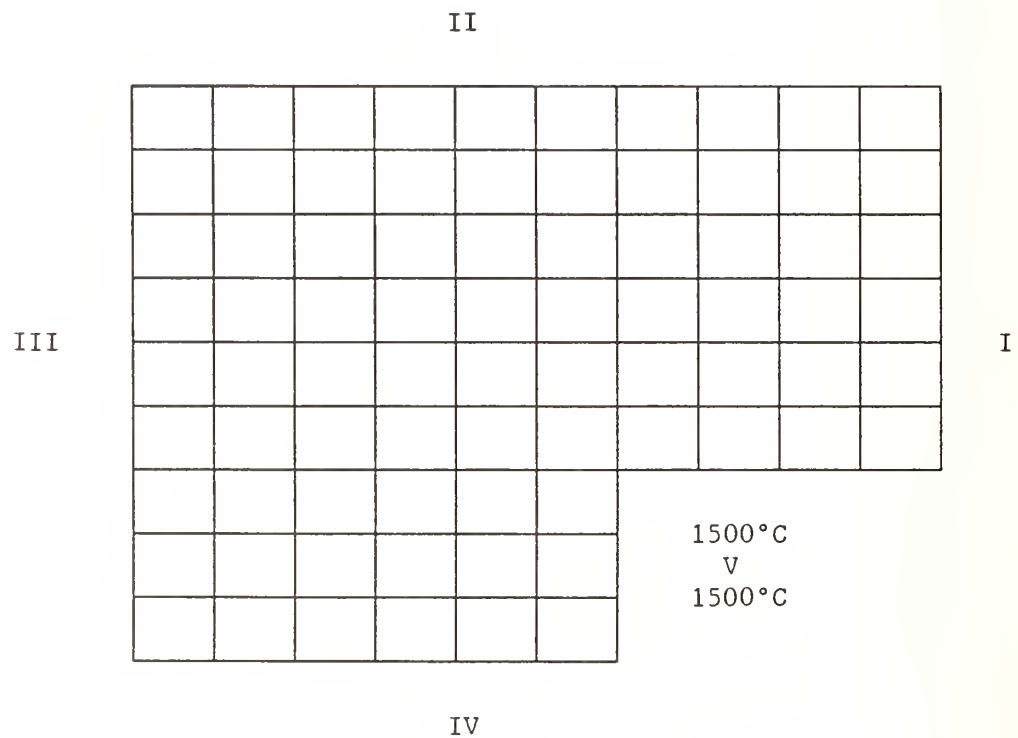
Each of the regions I, II, III, IV, V, and internal node points will
have different finite difference equations.

Internal finite difference equation:

Grid points

$$(i, \ j + 1)$$

$$(i + 1, \ j) \qquad (i, \ j) \qquad (i - 1, \ j)$$

$$(i, \ j - 1)$$

$$\frac{\partial^2 T}{\partial r^2} = \frac{1}{\Delta r^2} \ (T(i - 1, \ j) \ -2T(i, \ j) + T(i + 1, \ j)$$

$$\frac{\partial T}{\partial r} = \frac{1}{2\Delta r} \ (T(i - 1, \ j) + T(i + 1, \ j)$$

$$r = (i - 1)\Delta r$$

$$\frac{\partial 2T}{\partial z^2} = \frac{1}{\Delta z^2} \ (T(i, \ j - 1) - 2T(i, \ j) + T(i, \ j + 1))$$

$$2 \leq i \leq M - 1 \qquad \text{in this particular region}$$
$$2 \leq j \leq N - 1$$

Finite difference equation:

$$T(i+1,j)] \frac{1}{2(i-1)\Delta r^2} [T(i-1,j) + T(i+1,j)] + \frac{i}{\Delta r^2} [T(i-1,j) - 2T(i,j) +$$

$$+ \frac{1}{\Delta z^2} [T(i, j-1) - 2T(i, j) + T(i, j+1)] = 0$$

or, gathering like terms and solving for T(i, j) we have

$$T(i, j) = \frac{1}{2 \left[\frac{1}{\Delta z^2} + \frac{1}{\Delta r^2} \right]} \left[\frac{1}{\Delta r^2} \frac{2i - 1}{2(i-1)} \{T(i-1, j) + T(i+1, j)\} + \frac{1}{\Delta z^2} \{T(i, j-1) + T(i, j+1)\} \right]$$

Region I Finite Difference Equation

$$\frac{\partial T}{\partial r} = 0 \text{ is the governing equation}$$

Expressing $\partial T/\partial R$ in finite difference form:

Grid points for region I

$$(i, j + 1)$$

$$(3, j) \qquad (2, j) \qquad (1, j) \qquad\qquad \text{Region I Grid Points}$$

$$(i, j - 1)$$

Since this is a special boundary, expand about Taylor series to obtain
a finite difference equation ($O\Delta r^2$ error) to give:

$$\frac{\partial T}{\partial r} = \frac{1}{\Delta r} \left[-\frac{3}{2} T(1,j) + 2T(2,j) - \frac{1}{2} T(3,j) \right] = 0$$

where j ranges from Y to N.

If $\Delta r \neq 0$ solving for T(1, j) we have

$$\boxed{T(i, j) = \frac{4}{3} T(2, j) - \frac{1}{3} T(3, j)}$$

Region III Finite Difference Equation

Governing differential heat transfer equation at wall

$$-k_{eff} \frac{\partial T}{\partial z} \bigg|_{wall} = h(T_{wall} - T_{room})$$

Expressing $\dfrac{\partial T}{\partial z}\bigg|_{wall}$ in finite difference form.

Grid points for Region II:

<div align="center">Region II Grid Points</div>

$\bullet$ (i+2, N) $\bullet$ (i+1, N) $\bullet$ (i, N) $\bullet$ (i-1, N)

$\bullet$ (i+2, N-1) $\bullet$ (i+1, N-1) $\bullet$ (i, N-1) $\bullet$ (i-1, N-1)

Again, this is a special boundary, expand the Taylor series about this boundary to obtain a finite difference equation with order of error of $\Delta z^2 (O\Delta z^2)$.

This gives the equation

$$\frac{\partial T}{\partial z} = \frac{1}{\Delta z}\left[\frac{3}{2} T(i, N) - 2T(i, N-1) + \frac{1}{2} T(i, N-2)\right]$$

If we substitute this directly into the governing differential heat transfer equation we have:

$$-\frac{k_{eff}}{\Delta z}\left[\frac{3}{2} T(i, N) - 2T(i, N-1) + \frac{1}{2} T(i, N-2)\right] = h(T(i, N) - T_{room})$$

Solving for T(i,N) we have

$$
T(i,N) = \cfrac{1}{\dfrac{3}{2} + \dfrac{h\Delta z}{k_{eff}}} \left[2T(i,\ N-1) - \frac{1}{2} T(i,\ N-2) + \frac{h\Delta z}{k_{eff}}\ T_{room} \right]
$$

$i = 1$ to M

Region III Finite Difference Equation

Governing differential heat transfer equation at wall:

$$
-\ k_{eff}\ \frac{\partial T}{\partial r}\bigg|_{wall} = h(T_{wall} - T_{room})
$$

Expressing $\dfrac{\partial T}{\partial r}\bigg|_{wall}$ in finite difference form, we obtain:

Grid points for Region III:

Region	• (m, j+1)	• (m-1, j+1)
III	• (m, j)	• (m-i, j)
Grid		
Points	• (m, j-1)	• (m-1, j-1)

Performing Taylor series expansions about Region III grid points, we obtain $(0\Delta r^2)$:

$$\frac{\partial T}{\partial r} = \frac{1}{\Delta r}\left[\frac{3}{2} T(m, j) - 2T(m - 1, j) + \frac{1}{2} T(m - 2, j)\right]$$

Substituting into the governing finite difference equation and solving for $T(m, j)$ we obtain:

$$T(m, j) = \frac{1}{\frac{3}{2} + \frac{h\Delta r}{k_{eff}}}\left[2T(m -1, j) - \frac{1}{2} T(m -2, j) + \frac{h\Delta r}{k_{eff}} T_{room}\right]$$

$j = 1$ to N

Region IV Finite Difference Equations

Governing equation for this region:

$$\frac{\partial T}{\partial z} = 0$$

Grid Points for Region IV:

$(i+1, i)$ $(i, 1)$ $(i-1, 1)$ $(i-2, 1)$

$(i+1, 0)$ $(i, 0)$ $(i-1, 0)$ $(i-2, 0)$

Region IV Grid Points

Using the Taylor series to obtain an order Δz^2 error approximation for

$$\frac{\partial T}{\partial z}$$

we obtain:

$$\frac{\partial T}{\partial z} = \frac{1}{\Delta z}\left[-\frac{3}{2}T(i,\ 0) + 2T(i,\ 1) - \frac{1}{2}T(i,\ 2)\right]$$

Plugging this into the governing equation for this region:

$$T(i,\ 0) = \frac{4}{3}T(i,\ 1) - \frac{1}{3}T(i,\ 2)$$

i ranges from X to M

Region V Finite Difference Equation

Governing Equation:

$$T = 1500°C$$

Grid Points

. . . . .
(X,Y)   (X-1,Y)   (X-2, Y) ... (1, Y)   (0, Y)

.
(X, Y-1)

.
.
.

.
(X, 1)

.
(X, 0)

Finite difference form:

$T(X, j) = 1500 \qquad j = 0, 1, \ldots, Y - 1, Y$

$T(i, Y) = 1500 \qquad i = 0, 1, \ldots, X - 1, X$

Summary of finite difference equations for k_{eff} = constant case:

Internal Grid Points

$$T(i, j) = \cfrac{1}{+ \cfrac{1}{\Delta z^2} + \cfrac{1}{\Delta r^2}} \left[\frac{1}{\Delta r^2} \; \frac{\sigma i - 1}{\sigma(i-1)} \; (T(i-1, j) + T(i+1, j)) \right.$$

$$\left. \frac{1}{\Delta z^2} \; (T(i, j - 1) + T(i, j + 1)) \right]$$

Region I

$$T(1, j) = \frac{4}{3} T(2, j) - \frac{1}{3} T(3, j)$$

$$j = y, y+1, \ldots , N-2, N-1, N$$

Region II

$$T(i, N) = \frac{1}{\frac{3}{2} + \frac{h\Delta z}{k_{eff}}} \left[2T(i, N-1) - \frac{1}{2} T(i, N-2) + \frac{h\Delta z}{k_{eff}} T_{room} \right]$$

$$i = 1, 2, \ldots , M-2, M-1, M$$

Region III

$$T(M, j) = \frac{1}{\frac{3}{2} + \frac{h\Delta r}{k_{eff}}} \left[2T(M-1, j) - \frac{1}{2} T(M-2, j) + \frac{h\Delta r}{k_{eff}} T_{room} \right]$$

$$j = 1, 2, \ldots , N-2, N-1, N$$

Region IV

$$T(i, 0) = \frac{4}{3} T(i, 1) - \frac{1}{3} T(i, 2)$$

$$i = x, \; x+1, \; \ldots \ldots \; , \; M-2, \; M-1, \; M$$

Region V

$$T(X, j) = 1500, \; j = 0, 1, \ldots Y - 1, Y$$

$$T(i, Y) = 1500, \; i = 0, 1, \ldots X - 1, X$$

To solve the finite difference grid use the following procedure:

1. Use the equations above to write one and only one finite difference equation for each node point. Note that at intersections of regions I and II, II and III, III and IV, IV and V, and V and I, two equations for boundary conditions could be written. Use only one boundary condition for each of these points.

2. Once you have gotten one equation for each of the P node points, solve all of the linear equations simultaneously for the temperatures at the node points.

3. Change the finite difference grid size and re-iterate from Step 1 until temperatures at the outer shell do not change appreciably with changing grid size.

Example:

For the grid given on page 3 of this appendix:

1. There are 98 nodes in the finite element grid. Thus we would need to write 98 finite element analysis equations.

2. Solve 98 simultaneous linear equations using some technique to solve these equations (such as matrix inversion or diagonalization).

3. Increase the number of grid points and re-solve the equation. If the outer shell temperatures have changed appreciably, increase the number of grid points and re-iterate.

Case II $k_{eff} = k_{eff}(T)$

All boundary conditions (Regions I - V) remain the same as in Case I except that in any equation where keff is used it is to be evaluated at a node under inspection.

The Steady State Heat Transport Equation becomes

$$+ \frac{1}{r} \frac{\partial}{\partial r} \quad r \; k_{eff} \quad \frac{\partial T}{\partial r} \quad + \quad \frac{\partial}{\partial z} \; k_{eff} \quad \frac{\partial T}{\partial z} \; = 0$$

$$\frac{\partial}{\partial z} k_{eff} \frac{\partial T}{\partial z} + k_{eff} \frac{\partial}{\partial z} \frac{\partial T}{\partial z} = 0$$

Further expanding we have

$$\frac{\partial}{\partial T} k_{eff} \frac{\partial T}{\partial r}^2 + k_{eff} \left[\frac{1}{r} \frac{\partial T}{\partial r} + \frac{\partial^2 T}{\partial r^2} \right] +$$

$$\frac{\partial}{\partial T} k_{eff} \frac{\partial T}{\partial z}^2 + k_{eff} \frac{\partial^2 T}{\partial z^2} = 0$$

Analysis of this equation and solution proceeds in the same manner as in Case I <u>except</u> that now since k_{eff} is a function of T iteratively solve the P finite element equations until 1) The temperatures and the k_{eff}'s for each node do not change, i.e., (estimate k_{eff}'s calculate T's use calculated T's to re-estimate k_{eff}'s, etc.).

Appendix C

Gas Bearing Design Calculation for the

High Temperature Wear Facility

High Temperature Wear Facility Gas Bearing Design Calculation Using
the RPI-MTI Gas Bearing Design Course*
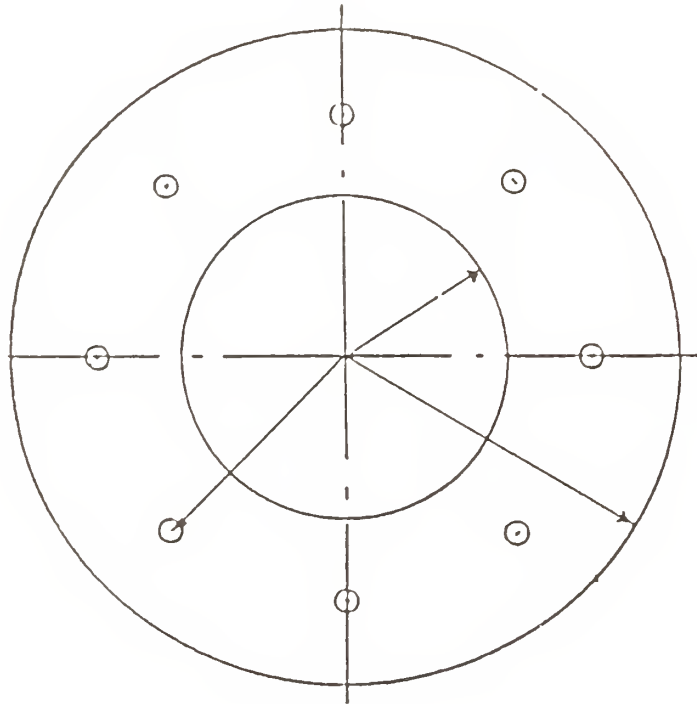
R_o is the outer radius of the hydrostatic thrust bearing

R_i is the inner radius of the hydrostatic thrust bearing

R_c is the radius of hole centers

For all of the design charts to be given, it is assumed that R_c =
$\sqrt{R_o \times R_i}$. This gives a maximum of load carrying capabilities with a
minimum of gas flow.

---

*Personal copy of RPI-MTI Gas Bearing Design Course received from H.S.
Cheng, Northwestern University, Chapter 5, Hydrostatic Thrust
Bearings, by H. S. Cheng was used in this calculation.

For the design given, there are four dimensionless input
parameters:

They are:

1. The ratio of outer to inner radius R_o/R_i

2. Supply Pressure Ratio P_s/P_a

    where P_s = supply pressure

    P_a = pressure of the surrounding atmosphere

3. Restrictor Coefficient

$$\Lambda_s = \frac{6\mu \ n \ a^2 \ \sqrt{RT}}{P_s \ C^3 \ \sqrt{1 + \delta^2}}$$

where μ = gas viscosity

   n = number of feeder holes

   a = orifice radius

   R = ideal gas constant

   T = absolute temperature

   P_s = supply pressure

   C = film thickness

and $\delta = \pi a^2/\pi c d$ = ratio of orifice area to inherent restriction

area.

For inherently compensated bearings $\delta = \infty$.

4. Feeder Hole Volume Ratio:

$$\frac{n \ V_i}{\pi(R_o^2 - R_i^2)C}$$

where n = number of feeder hole

V_i = volume of a single hole

C = film thickness

Outputs from Design Charts (MTI, 1966)

Dimensionless load:

$$W = \frac{W}{\pi(R_o^2 - R_i^2) \ (p_s - p_a)}$$

W = real axial loading of system

Dimensionless stiffness:

$$K = \frac{1 + \delta^2}{1 + \frac{2}{3}\delta^2} \ \frac{K}{\frac{1}{C} \ \pi(R_o^2 - R_i^2) \ (p_s - p_a)}$$

Dimensionless mass flow:

$$G_t = \frac{6\mu \ RT}{\pi \ C^3 \ p_s^2} \ G$$

Dimensionless damping coefficient:

$$B = \frac{B}{\mu R_o \left(\dfrac{R_o}{C}\right)^3}$$

Dimensionless angular stiffness:

$$K_A = \frac{1 + \delta^2}{1 + \dfrac{2}{3}\delta^2} \; \frac{K}{\dfrac{1}{C}\pi(R_o{}^2 - R_i{}^2) R_o{}^2 (p_s - p_a)}$$

Dimensionless mass flow:

$$G_t = \frac{6\mu \, RT}{\pi \, C^3 \, p_s{}^2} \, G$$

Dimensionless damping coefficient:

$$B = \frac{B}{\mu R_o \left(\dfrac{R_o}{C}\right)^3}$$

Dimensionless angular stiffness:

$$K_A = \frac{1 + \delta^2}{1 + \dfrac{2}{3}\delta^2} \; \frac{K_A}{\dfrac{1}{C}\pi(R_o{}^2 - R_i{}^2) R_o{}^2 (p_s - p_a)}$$

Dimensionless angular damping:

$$B_A = \frac{B_A}{\mu \; R_o{}^3 \; \left(\dfrac{R_o}{C}\right)^3}$$

The Design Given in Figure 57 will be Approximated by an Annular
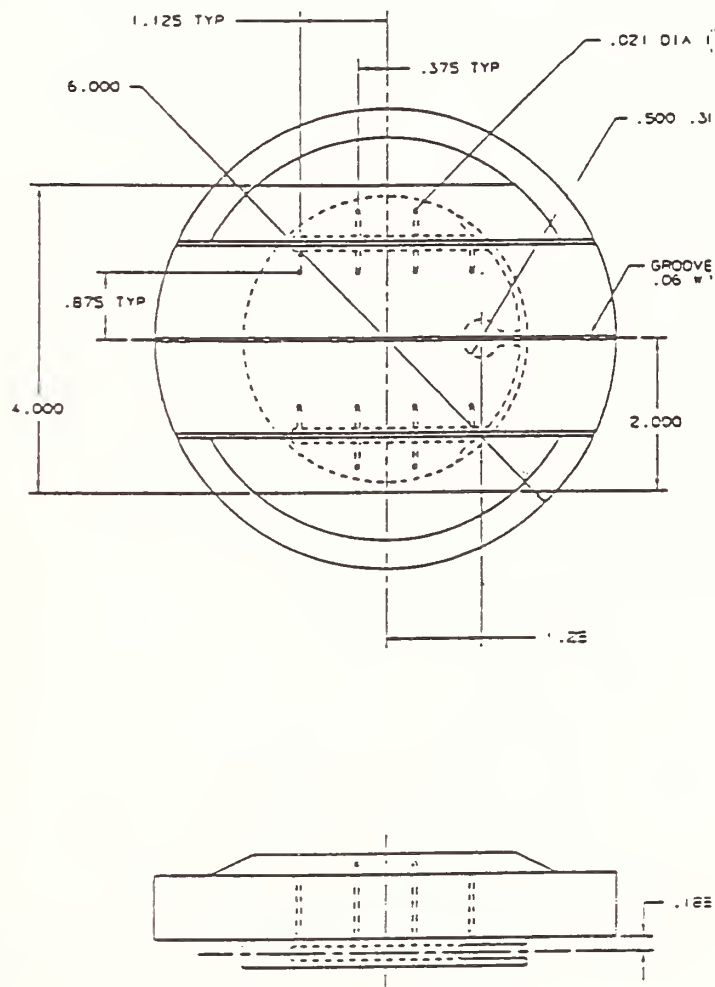
Bearing as Illustrated in Figure 58

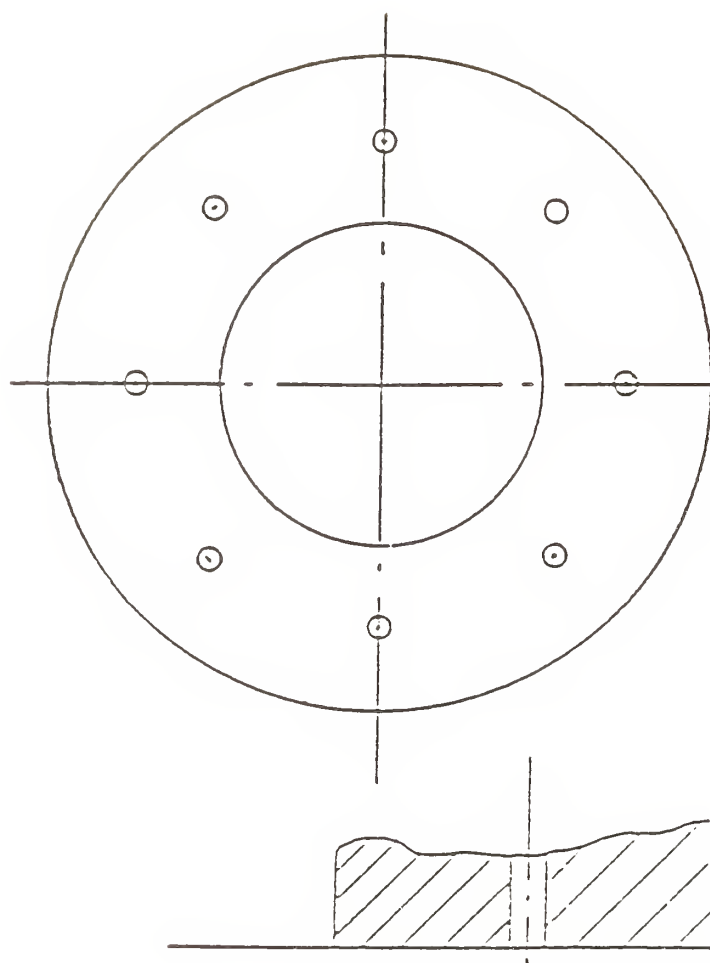Figure 57. Hydrostatic Bearing Design Surface

Figure 58. Hydrostatic Supply Surface Approximation

Because the bearing has straight slots we will assume that the following approximation can be made

R_o - R_i = the distance between the two air channels as shown in Figure 58 and R_i = the shortest distance between a hole and a slot.

If this is done

$R_i \approx 1/2"$

R_o - $R_i \approx 1.25"$

so

$\frac{R_o}{R_i} = 3.5$

$R_o \approx 1.75"$

$\sqrt{R_o \times R_i} = R_c$

Use design charts for R_o/R_i = 3.0, because this is the closest design chart for our purposes.

We want to design for maximum stiffness so we will use Figure 5.3.13 from the MTI Gas Bearing Design Course is shown in Figure 59.

$$\Lambda_s = \frac{6\mu n \sigma^2 \sqrt{RT}}{p_s C^3 \sqrt{1+\delta^2}}$$

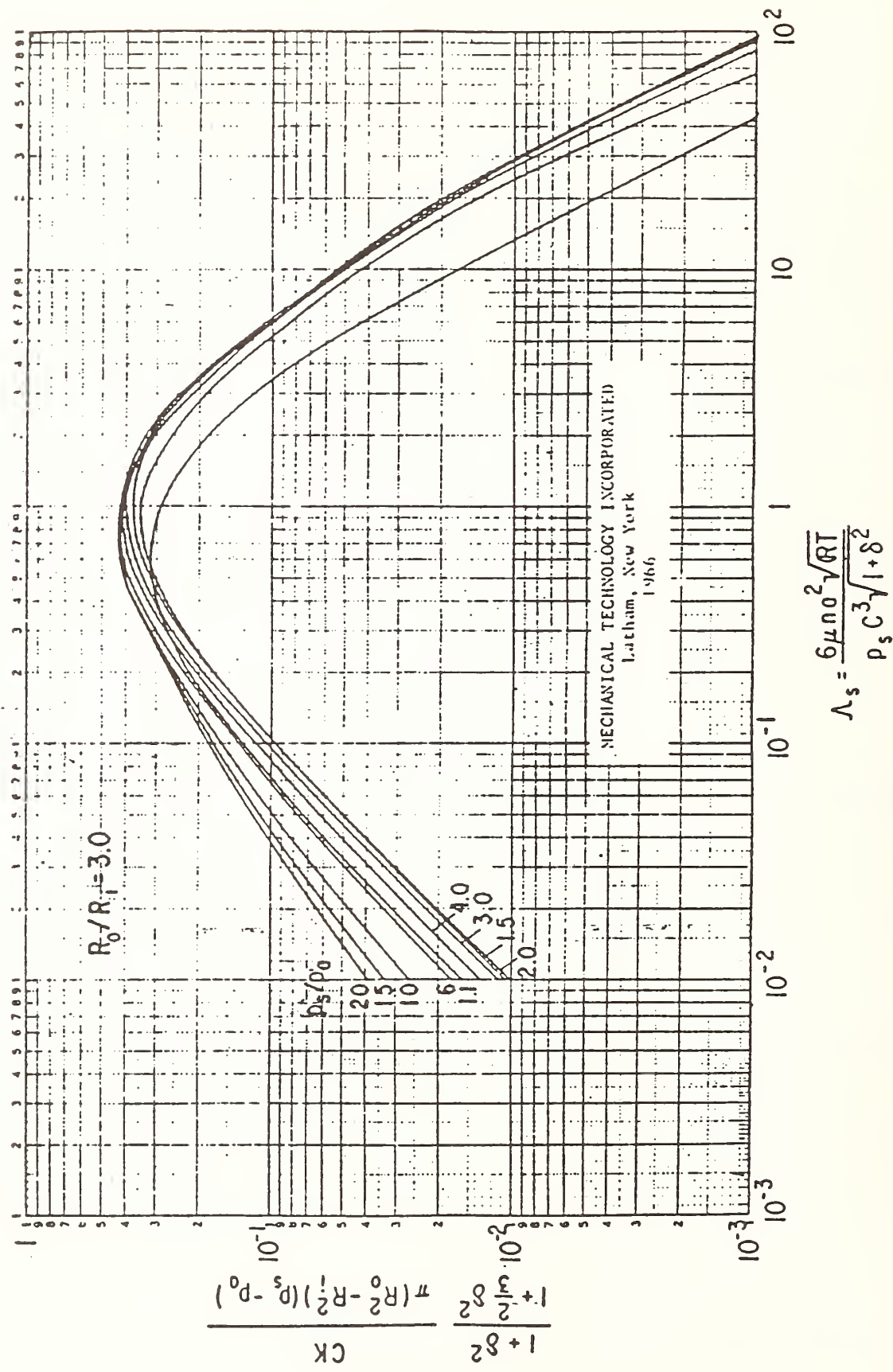MECHANICAL TECHNOLOGY INCORPORATED
Latham, New York
1966

Figure 59. Fig. 5.3.13-MTI Gas Bearing Design Course

Assume that the maximum supply pressure is going to be about 120 psia and the ambient pressure will be 14.696 psia. Therefore for the supply pressure ratio

$$\frac{120 \text{ psig}}{14.696 \text{ psia}} \approx 8 = p_s/p_a$$

For anything above $p_s/p_a \approx 4$ the maximum $\Lambda_s \approx 0.9$

and

$$\frac{1 + \delta^2}{1 + \frac{2}{3} \delta^2} \quad \frac{C \, K}{\pi (R_o^2 - R_i^2)(p_s - p_a)} \approx 0.4$$

To find load carrying capacity Figure 5.3.5 of the MTI Gas Bearing Design Course is used assuming a $p_s/p_a = 6.0$ or $p_s = 88.176$ psia or close to 90 psia and $\Lambda_s = 0.9$. This is shown in Figure 60. From the Chart:

$$\frac{W}{\pi (R_o^2 - R_i^2)(p_s - p_a)} = 0.27$$

use $R_i = 0.5''$

$R_o = 1.5''$

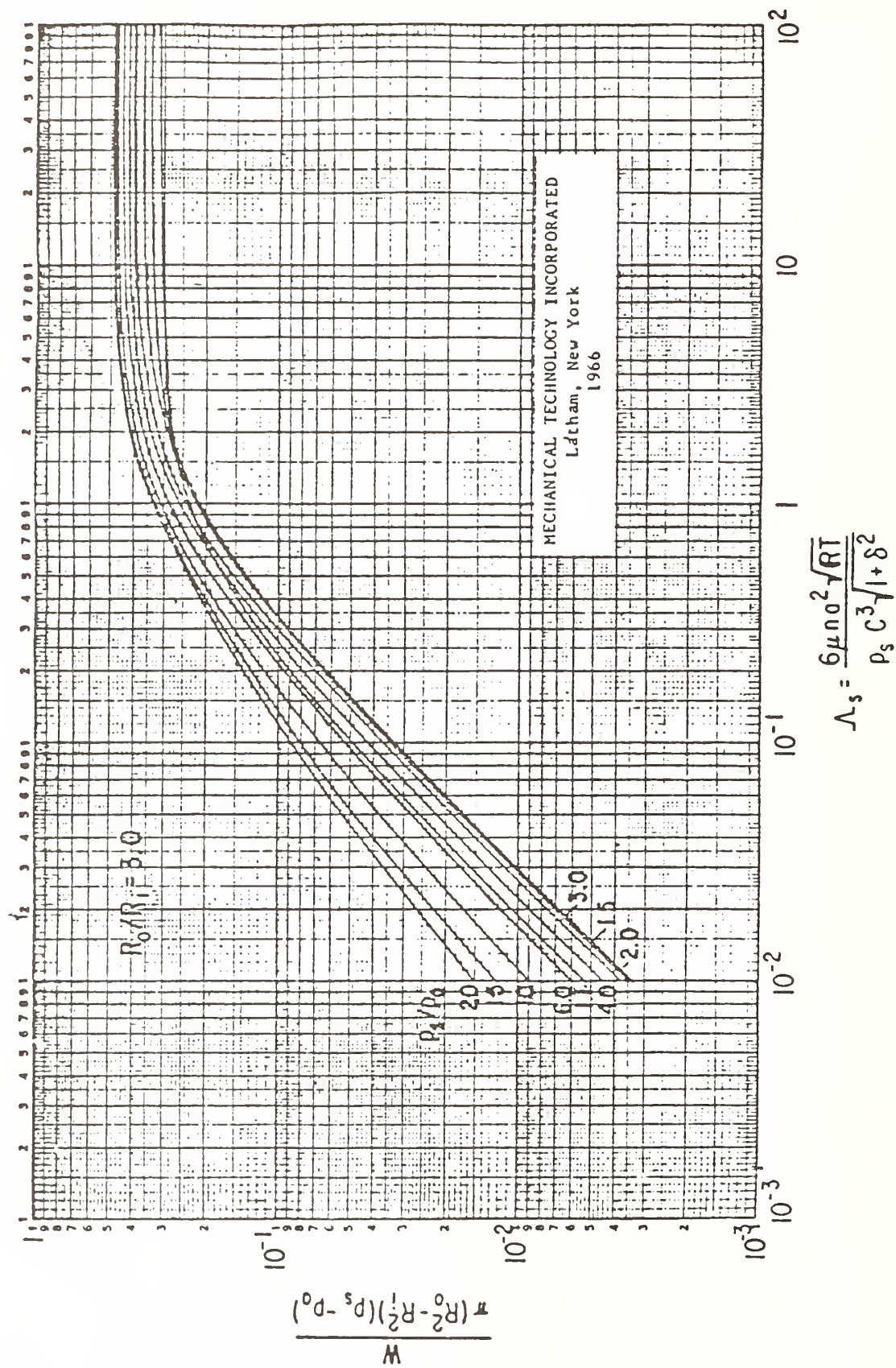$p_s = 88.176$ psia

$p_a = 14.696$ psia

Figure 60.   Fig. 5.3.5-MTI Gas Bearing Design Course

Plugging in the numeric values for R_o, R_i, p_s, and p_a we have:

$$\frac{W}{\pi(1.5^2 - 0.5^2)\ (88.176 - 14.696)} = 0.27$$

> W = 124.65 lbs thrust
> or
> 56 Kg

Therefore we have a load of 56 Kg.

Now a look at stiffness:

$$\frac{1 + \delta^2}{1 + \dfrac{2}{3}\delta^2} \quad \frac{C\ K}{\pi(R_o^2 - R_i^2)\ (p_s - p_a)} \approx 0.4$$

For an inherently compensated bearing $\delta = \infty$

Therefore $\quad \dfrac{1 + \delta^2}{1 + \dfrac{2}{3}\delta^2} = \dfrac{3}{2}$

therefore

$$K = \frac{(0.4) \times \frac{2}{3} \times \pi \times (R_o{}^2 - R_i{}^2)(p_s - p_a)}{C}$$

and we have set $R_o \approx 1.5"$

$$R_i \approx 0.5"$$

$$p_s \approx 88.176 \text{ psia}$$

$$p_a \approx 14.696 \text{ psia}$$

To choose C we want the smallest possible thickness and it is suggested that as a minimum film thickness to choose 0.5×10^{-3} or 0.0005" as an estimate.

$$C = 0.5 \times 10^{-3} \text{ in}$$

therefore the stiffness may be given by

$$K = 0.4 \times \frac{2}{3} \times \pi \times (1.5^2 - 0.5^2) \frac{(88.176 - 14.696)}{0.5 \times 10^{-3}}$$

$$\boxed{K = 246,233 \text{ lb}_f/\text{in}}$$

Estimate of the resonant freqeuncy of the specimen holder

1) Total weight of the specimen holder

Assume 2 1/2" diameter by 12" length ceramic rods + 1, 4" x 6" x 15" block of Carborundum's Hexoloy sintered alpha silicon carbide which has a density of 3.1 g/cm^3 or 3100 kg/m^3

$$\frac{3100 \text{ kg}}{\text{m}^3} \times \frac{2.2046226 \text{ lb}}{\text{kg}} \times \left[\frac{0.3048 \text{ m}}{1 \text{ ft}^3} \right]^3$$

$$193.52668 \frac{\text{lb}}{\text{ft}^3}$$

total volume

$$2(\pi \times (1/4)^2 \times 12)$$

$$+ (4 \times 6 \times 1.5)$$

$$40.7 \text{ in}^3 \times \frac{1 \text{ ft}^3}{(12) \text{in}^3}$$

$$= 0.0235604 \text{ ft}^3$$

total mass is 4.559568 lb$_m$

$$4.559568 \text{ lb}_m \times \frac{32.174 \text{ ft}}{\text{sec}^2} \times \frac{1 \text{ lb}_f}{\frac{32.174 \text{ lb}_m \text{ ft}}{\text{sec}^2}}$$

$$4.559568 \text{ lb}_f \text{ x } \frac{\sec^2}{386.088 \text{ in}}$$

$$M = 1.180966 \text{ x } 10^{-2} \text{ lb } \frac{\sec^2}{\text{in}}$$

so,

$$[N \text{ cps}]_{\text{resonant axial vibration}} = \frac{1}{2\pi} \quad \frac{K}{M}$$

K is in lb/in = 246,233 lb_f/in

and M is in lb $\sec^2$/in = 1.180966 x 10^{-2} lb_f $\sec^2$/in

$$N = \frac{1}{2\pi} \quad \frac{246{,}233 \text{ lb}_f/\text{in}}{1.180966 \text{ x } 10^{-2} \text{ lb}_f \sec^2/\text{in}}$$

$$N = 726 \text{ Hz}$$

Therefore we get some sort of resonance frequency about

700 Hz which could hinder the performance of the bearing system.

Dimensionless bearing flow:

Given that $\Lambda s \approx 0.9$, use Figure 5.3.9 of the MTI Gas Bearing Design Course to obtain the dimensionless flow parameter. Figure 5.3.9 is shown in Figure 61.

Given the assumption that

$$p_s/p_a = 6$$

we get that

$$\frac{6\mu\ RT}{\pi\ p_s{}^2\ C^3}\ G = 0.54$$

$$G\left[\frac{lb\ sec}{in}\right] = \frac{\pi\ C^3\ p_s{}^2}{6\mu\ RT}\ x\ 0.54$$

where μ is viscosity in lb sec/in^2 (0 Argon)

(The viscosity of argon at room temperature is 0.022 cp)

R is in in^2/sec^2 °R

$$\mu\ \frac{lb\ sec}{in^2} = 0.022\ cp\ x\ \frac{2.0886\ x\ 10^{-5}\ lb_f\ sec}{ft^2\ cp}\ x\ \frac{1\ ft^2}{144\ in^2}$$
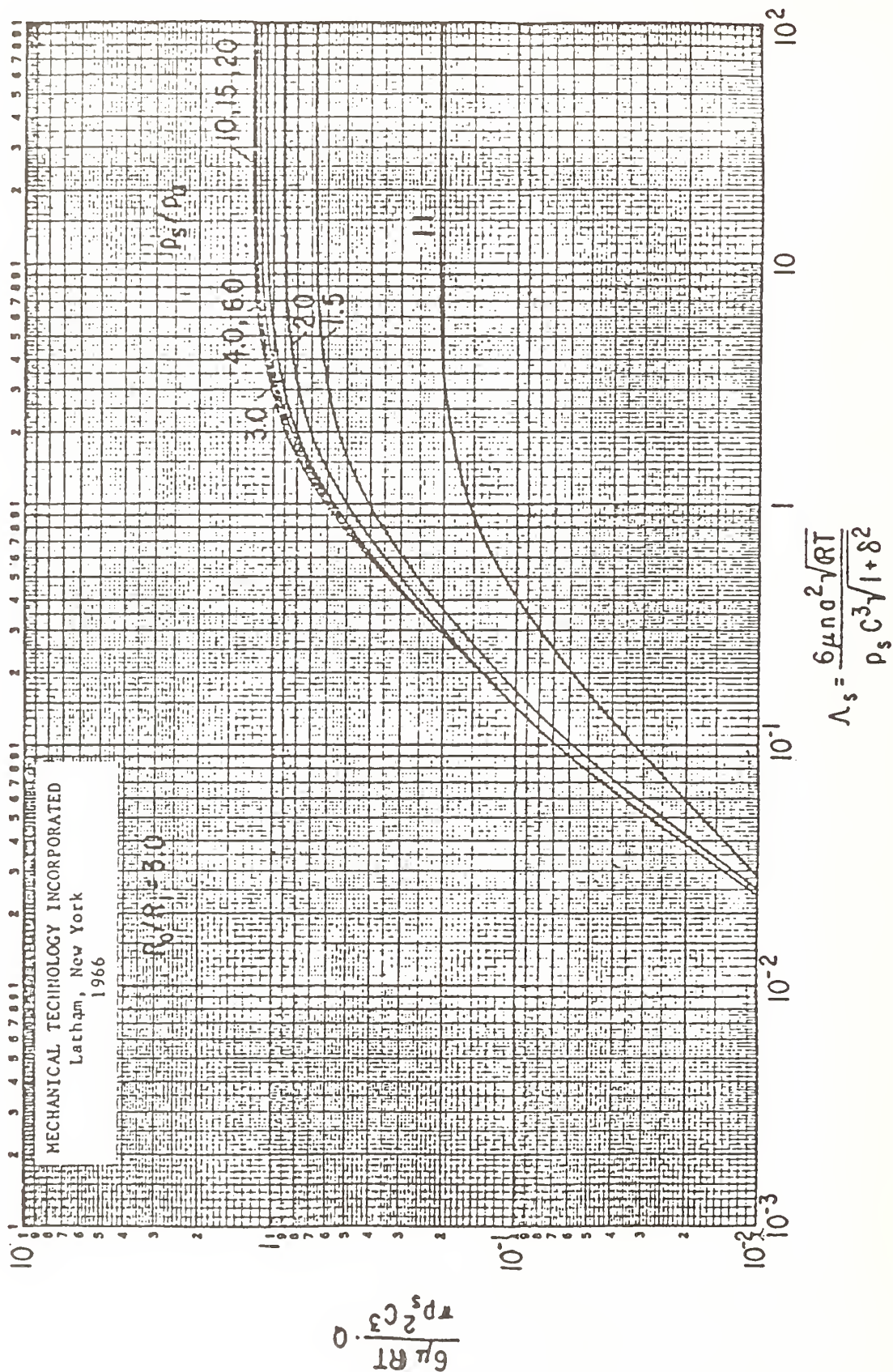
Figure 61.   Fig. 5.3.9-MTI Gas Bearing Design Course

$$\mu = 3.1909167 \times 10^{-9} \; \frac{lb_f \; sec}{in^2}$$

$$C = 0.5 \times 10^{-3} \; in$$

$$T = 68°F = 527.59°R$$

Ideal gas constant, R

$$\frac{1.9872 \; BTU}{lb \; mol \; °R} \times \frac{lb \; mol \; Ar}{39.944 \; lb_{Ar}} = 4.974965 \times 10^{-2} \; \frac{BTU}{lb \; °R}$$

To convert to the proper units of

$$R \; in \quad \frac{in^2}{sec^2 \; °R}$$

a factor of 8.6051×10^6 $\left[R_1 \; \dfrac{BTU}{lb \; °R} \right] = R \left[\dfrac{in^2}{sec^2 \; °R} \right]$

$$R \left[\frac{in^2}{sec^2 \; °R} \right] = 1.7935246 \times 10^5 \; \frac{in^2}{sec^2 \; °R}$$

Recalling

$$G \; \frac{lb \; sec}{in} = \frac{\pi \; C^3 \; p_s^2}{6\mu \; RT} \times 0.54$$

$$G = \frac{\pi (0.5 \times 10^{-3})^3 \ M^3 \ \times \ (88.176)^2 \ \frac{lb_f^2}{in^2}}{6 \times 3.1909167 \times 10^{-9} \ \frac{lb_f \ sec}{in^2} \ 1.7935246 \times 10^5 \ \frac{in^2}{sec^2 \ °R} \ 527.59°R} \ \times 0.54$$

$$G \ \frac{lb_f \ sec}{in} \ = \ 9.1008891 \times 10^{-7} \ \frac{lb_f \ sec}{in}$$

$$G(scfm) \ = \ 2.8696969 \times 10^5 \ \times \ G \ \frac{lb_f \ sec}{in}$$

$$\boxed{G(scfm) \ = \ 0.2611679 \ (scfm)}$$

Now, calculate the number of gas supply holes necessary for the bearing. From the gas supply course:

$$nd \ = \ \frac{P_s \ C^2}{6\mu \ \sqrt{RT}} \ \Lambda s$$

where n = number of supply holes

d = diameter

Plugging in the proven values we have:

$$nd \ = \ \frac{88.176 \ \frac{lb_f}{in^2} \ \times \ (0.5 \times 10^{-3})^2 \ in^2}{6 \times 3.1909167 \times 10^{-9} \ \frac{lb_f \ sec}{in^2} \ \sqrt{RT}} \ \times \ 0.9$$

where $R = \dfrac{17935246 \times 10^5 \ in^2}{sec^2 \ °R}$ and $T = 527.59°R$

$nd = 1.0652812 \times 10^{-1}$ in

$nd = 0.1065281$ in

If we assume that $d = 0.025$, then we find that $n = 4$ from flow calculations. However, from geometric considerations a minimum number of holes is necessary.

Figure 5.3.19 of the MTI Gas Bearing Design Course gives a procedure for finding the minimum number of holes. This chart is shown in Figure 62.

$$\epsilon = \frac{1}{2} \ \ell n \ \frac{R_o}{R_i} = \frac{1}{2} \ \ell n \ 3 = 0.5493061$$

$$D = 2 \ \sqrt{R_o R_i} = 2 \ \sqrt{1.5 \times 0.5} = 1.7320508$$

$$\frac{1}{\epsilon D} = 1.0510538$$
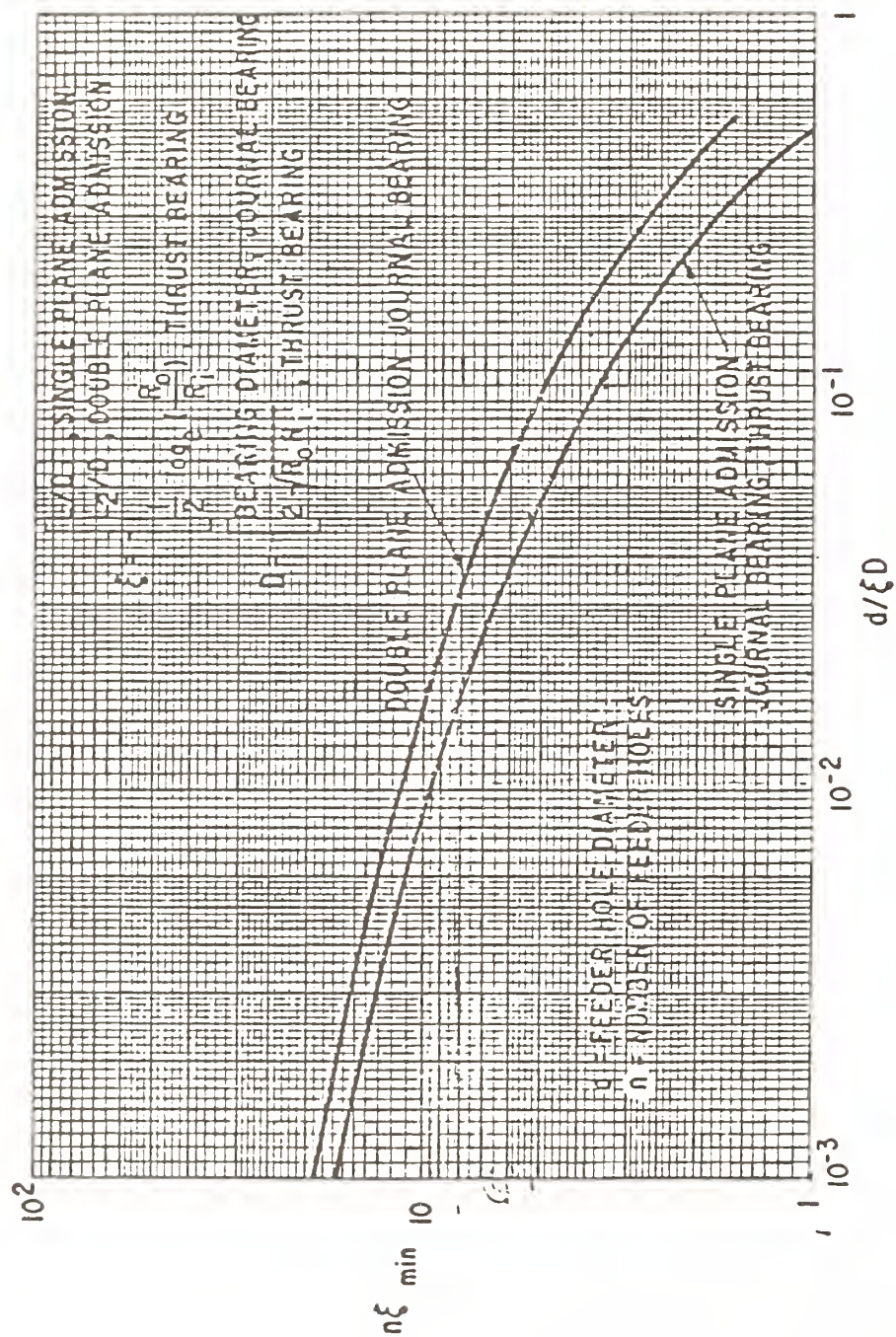
therefore $\dfrac{d}{\epsilon D} = 0.026$

Figure 62. Fig. 5.3.19-MTI Gas Bearing Design Course

From Figure 62.

$$n \, \epsilon_{min} = 8 \qquad\qquad n_{min} = 14$$

If we decrease hole size to 0.0125"

we need 8.5 holes $\approx$ 9 holes

$$\frac{d}{\epsilon D} = 0.0131382 \qquad\qquad n \, \epsilon_{min} = 9$$

and $n = 16$

If we increase hole to size 0.05"

then $n \, \epsilon_{min} \approx 6.1$ $\qquad\qquad n_{min} = 11$

Calculation of failure load.

$$\epsilon = \frac{W}{CK}$$

$$C = 0.5 \times 10^{-3} \text{ in}$$

$$K = 246{,}233 \text{ lbf/in}$$

$$W = 124.65 \text{ lbs} = 52 \text{ kg}$$

$\epsilon = 1.01$

If $\epsilon > 0.4$ the bearing will lock up.

However, at 20 kg = 44.09 lb

$\epsilon = 0.35$

This is a safe operating range. If we plug in $\epsilon = 0.4$ we find that

0.4 x C x K = 49 lbs

Therefore, the bearing should not be subjected to much more than area 22 kg.

Parameter sheet:

$R_i \approx 1/2''$

$R_o - R_i \approx 1.25''$

$R_o \approx 1.75$

$\dfrac{R_o}{R_i} = 3.5$

say that R_o = 1.5

R_i = 0.5

$$\frac{R_o}{R_i} = 3$$

maximum supply pressure 88.176 psia, 73.48 psig (5 scfm)

Λs = 0.9

W_{cap} = 56 kg, 124 lbs

K = 246,233 lbf/in

C = 0.5 x 10^{-3} in

$N_{resonance\ vibration\ frequency}$ = 726 cps

mass flow rate

$$G = 9.1008891 \times 10^{-7} \frac{lbf\ sec}{in} = 0.2611679\ scfm$$

diameter of feeder holes 0.050"

minumum number is 11

Bearing designed for 20 holes

if we look at range that bearing can handle and avoid lock up

$$\epsilon = \frac{W}{CK}$$

where ϵ = 0.4 to 0.5 (max)

therefore the very maximum that the bearing should be subjected to avoid lock up is 28 kg load.

but

22 is a better safe estimate.

U.S. DEPT. OF COMM. **BIBLIOGRAPHIC DATA** **SHEET** *(See instructions)*	1. PUBLICATION OR REPORT NO. NIST/SP-755	2. Performing Organ. Report No.	3. Publication Date September 1988

4. TITLE AND SUBTITLE

THE DESIGN AND CONSTRUCTION OF A STATE-OF-THE-ART HIGH TEMPERATURE TRIBOMETER

5. AUTHOR(S)

Jeffrey P. Yellets , Stephen M. Hsu, and E. Erwin Klaus

6. PERFORMING ORGANIZATION *(If joint or other than NBS, see instructions)* NATIONAL INSTITUTE OF STANDARDS AND TECHNOLOGY (formerly NATIONAL BUREAU OF STANDARDS) U.S. DEPARTMENT OF COMMERCE GAITHERSBURG, MD 20899	7. Contract/Grant No. 8. Type of Report & Period Covered Final

9. SPONSORING ORGANIZATION NAME AND COMPLETE ADDRESS *(Street, City, State, ZIP)*

SAME AS ITEM #6 ABOVE.

10. SUPPLEMENTARY NOTES

Library of Congress Catalog Card Number: 88-600579

☐ Document describes a computer program; SF-185, FIPS Software Summary, is attached.

11. ABSTRACT *(A 200-word or less factual summary of most significant information. If document includes a significant bibliography or literature survey, mention it here)*

High temperature ceramic tribology is one of the fastest growing and least understood areas in tribology. The need to understand the mechanisms of friction and wear for ceramic materials is critical. Ceramic materials are being utilized to tool development, bearing design, materials development for low-heat-rejection diesels, automotive gas turbines, Stirling engines, and aerospace applications. The development of a ceramics industry capable of manufacturing high technology wear resistant ceramics is essential in the United States, for if we do not develop such an industry, we will lose a substantial market to an already rapidly growing foreign market.

This effort describes the design, development, and construction of a unique, state-of-the-art, ultra-high temperature tribometer for the mechanistic study of novel ceramic materials. An overview of ceramic tribology is included in this work as well as a review of many common wear test configurations. The final designs and the construction of the High Temperature Wear Facility is presented in this work. Recommendations for future work on high temperature mechanisms of ceramic materials and the tribological testing of such materials are presented at the conclusion of this work.

12. KEY WORDS *(Six to twelve entries; alphabetical order; capitalize only proper names; and separate key words by semicolons)*

ceramic(s); construction; design; high temperature; tribology; tribometer

13. AVAILABILITY	14. NO. OF PRINTED PAGES
☒ Unlimited ☐ For Official Distribution. Do Not Release to NTIS ☒ Order From Superintendent of Documents, U.S. Government Printing Office, Washington, D.C. 20402. ☒ Order From National Technical Information Service (NTIS), Springfield, VA. 22161	212 15. Price